NASA TECHNICAL NOTE

NASA TN D-5778

LATERAL VIBRATION CHARACTERISTICS OF THE 1/10-SCALE APOLLO/SATURN V REPLICA MODEL

by Ellwood L. Peele, H. Wayne Leonard, and Sumner A. Leadbetter

Langley Research Center
Hampton, Va. 23365

NATIONAL AERONAUTICS AND SPACE ADMINISTRATION • WASHINGTON, D. C. • APRIL 1970

1. Report No.	2. Government Accession No.	3. Recipient's Catalog No.
NASA TN D-5778		

4. Title and Subtitle

LATERAL VIBRATION CHARACTERISTICS OF THE 1/10-SCALE APOLLO/SATURN V REPLICA MODEL

5. Report Date: April 1970

6. Performing Organization Code:

7. Author(s)
Ellwood L. Peele, H. Wayne Leonard, and Sumner A. Leadbetter

8. Performing Organization Report No.: L-6736

10. Work Unit No.: 124-08-13-04-23

9. Performing Organization Name and Address
NASA Langley Research Center
Hampton, Va. 23365

11. Contract or Grant No.:

13. Type of Report and Period Covered: Technical Note

12. Sponsoring Agency Name and Address
National Aeronautics and Space Administration
Washington, D.C. 20546

14. Sponsoring Agency Code:

15. Supplementary Notes

16. Abstract

A 1/10-scale replica model of the Apollo/Saturn V vehicle has been tested to determine its free-free lateral vibration characteristics. Several simulated propellant loadings were investigated for each of three model configurations simulating the first-stage, second-stage, and third-stage burns. Tests were conducted in both the pitch and yaw directions. A one-dimensional lumped-parameter analysis employing the transfer-matrix method was used to calculate the uncoupled natural modes and frequencies of the system. Analytical parameter studies were conducted to investigate the effects of engine flexibility, liquid slosh, and decreased stiffness due to ineffective skin on the modal behavior of the system.

17. Key Words (Suggested by Author(s))
Saturn V model vibration
Lateral vibration

18. Distribution Statement
Unclassified – Unlimited

19. Security Classif. (of this report)	20. Security Classif. (of this page)	21. No. of Pages	22. Price*
Unclassified	Unclassified	86	$3.00

*For sale by the Clearinghouse for Federal Scientific and Technical Information
Springfield, Virginia 22151

LATERAL VIBRATION CHARACTERISTICS OF THE 1/10-SCALE APOLLO/SATURN V REPLICA MODEL

By Ellwood L. Peele, H. Wayne Leonard,
and Sumner A. Leadbetter
Langley Research Center

SUMMARY

A 1/10-scale replica model of the Apollo/Saturn V vehicle has been tested to determine its free-free lateral vibration characteristics. Several simulated propellant loadings were investigated for each of three model configurations simulating the first-stage, second-stage, and third-stage burns. Tests were conducted in both the pitch and yaw directions. A one-dimensional lumped-parameter analysis employing the transfer matrix method was used to calculate the uncoupled natural modes and frequencies of the system. Analytical parameter studies were conducted to investigate the effects of engine flexibility, liquid slosh, and decreased stiffness due to ineffective skin on the modal behavior of the system.

For modes in which the model responds as a beam, the analysis predicts the behavior with reasonable accuracy. The presence of large concentrated masses such as contained liquids or concentrated structural and subsystem masses tends to limit the number of modes which the analysis can be expected to produce. Branch masses which possess resonant frequencies near structural resonant frequencies can impair experimental definition of the structural resonant frequency. Likewise, the existence of shell modes in the primary structure makes experimental definition of higher mode shapes and frequencies difficult. The one-dimensional analysis cannot predict radial or shell response; therefore, for applications requiring knowledge of the shell behavior, analyses which include two- or three-dimensional motions are required.

INTRODUCTION

Analytical representations of the dynamics of complex launch-vehicle structures involve many idealizations and simplifying assumptions. Thus, at some point in the vehicle development, analytical methods and procedures proposed for determining the launch-vehicle dynamic behavior must be verified. Verification is usually obtained by comparing the experimental data from full-scale ground tests of the vehicle, and ultimately flight data, with the predictions of the analysis.

Dynamic models have been used in investigations of aeroelastic stability phenomena (see, for example, refs. 1 to 3) and it is natural to extend the concept to replica models of launch vehicles. Utilizing a 1/5-scale model, the concept was applied to the Saturn I launch vehicle as reported in references 4 to 9. This work verified the premise that the overall dynamic characteristics of large, complex vehicles can be accurately, economically, and quickly determined through model tests. Confidence in the use of dynamic models was further advanced by data obtained during scaled model studies of an operational Air Force launch vehicle, as reported in references 10 and 11.

Confidence in launch-vehicle analyses is enhanced by good correlation of these analyses with model experimental data. Also, areas of applicability and limitations of analytical models can be determined effectively early in the launch-vehicle development cycle through such correlations. One method of analyzing liquid-propellant launch vehicles is to represent the launch vehicle as a beam with attached spring-mass components. Simplicity and ease of application make this representation attractive in studies in which overall dynamic characteristics are desired – for example, in control-system stability investigations. When such a representation is verified by correlation with experimental data, parametric studies to assess the effects of shear deformation, rotatory inertia, and slosh can be performed efficiently. This analytical approach, however, has one important limitation in that it has no provision for the inclusion of shell-type modes.

Experimental and analytical studies of the dynamic response characteristics of the Apollo/Saturn V launch vehicle have been conducted with scale models. The models employed were: A 1/40-scale dynamic model of the launch vehicle, launch platform, and umbilical tower; and a 1/10-scale structural replica model of the launch vehicle.

The purposes of the model construction, test, and analysis program were: (1) To advance the state of the art in model construction; (2) to provide structural dynamics data to organizations responsible for full-scale analysis, design, and test prior to availability of full-scale test data; (3) to provide information on the practical limits of scaling; and (4) to provide experimental vibration data for evaluation of vibration analyses. Results from the 1/40-scale dynamic-model program are reported in references 12 to 14. The longitudinal dynamic characteristics of the 1/10-scale replica model are given in reference 15.

The purpose of this paper is to present the results of a combined experimental and analytical study of the pitch and yaw vibration characteristics of the 1/10-scale replica model of the Apollo/Saturn V launch vehicle for simulated flight times ranging from lift-off through third-stage burnout. These results help to establish the areas of applicability of the one-dimensional lumped-parameter representation of a typical launch-vehicle structure.

SYMBOLS

A	area
a_{ref}	acceleration at reference station, divided by gravitational acceleration
C	integration constant
$c_1, c_2, \ldots$	flexibility influence coefficients
d	suspension-cable separation distance (see fig. 4)
E	Young's modulus
$[e]_i$	transfer matrix for ith elastic beam
f	frequency
G	shear modulus
g	structural damping coefficient
h	amplitude of total bending and shear deformation
I	area moment of inertia of cylindrical shell
$\{I\}$	column matrix each element of which is unity
$I_{0,i}$	second moment of ith concentrated mass about its own center of gravity
$i = \sqrt{-1}$	
K	form factor for shear deformation
l_i	length of ith elastic beam element
M	bending moment
M_{gh}	normalized generalized mass

M_t	total mass of configuration
$\overline{M}_{gg}$	nondimensional generalized mass
$m(x)$	mass distribution
m_{gh}	generalized mass corresponding to gth and hth modes
m_i	ith concentrated mass
$\left[m(\omega)\right]_i$	transfer matrix for ith concentrated mass
R	radius of cylindrical shell
r_i	offset of the ith concentrated mass
t	time
$\left[U(\lambda)\right]$	transfer matrix
$\left[\overline{U}(\lambda)\right]$	reduced-order transfer matrix
V	transverse shear
X	deflection function
x	Cartesian coordinate
x/L	dimensionless longitudinal coordinate of configuration I
x'/L'	dimensionless longitudinal coordinate of configuration II
x''/L''	dimensionless longitudinal coordinate of configuration III
y	lateral displacement
$\{Z\}$	state vector
$\{\overline{Z}\}$	reduced-order state vector

α	incremental bending deformation
β	incremental shear deformation
δ	tangential deviation
ϵ	neutral-axis offset
θ	neutral-axis offset angle, $\sin^{-1}\left(\frac{\epsilon}{R}\right)$
λ	frequency parameter
ξ	dummy variable
ρ	mass density
$\left[\sigma(\omega)\right]$	collapsed transfer matrix
$\left[\bar{\sigma}(\omega)\right]$	reduced-order transfer matrix
τ	skin thickness
ϕ	slope of the bending deformation
ω	circular frequency

Subscripts:

a	analytical
B	branched beam
g	gth mode
h	hth mode
i	ith mass location
j	jth mass location

l	last mass in chain of transfer matrices
0	first mass in chain of transfer matrices
p	pitch
R	root end of branched beam
T	free end of branched beam
y	yaw

Matrix notation:

$[\ ]$	square or rectangular matrix
$\{\ \}$	column matrix
adj$[\ ]$	adjoint matrix

A superscript T denotes a transpose matrix.

Dots over symbols denote differentiation with respect to time.

APPARATUS AND TEST PROCEDURE

Model Description

A complete description of the 1/10-scale Apollo/Saturn V model, the design philosophy, typical problems encountered in the fabrication along with their solutions, and a discussion of associated test equipment are presented in reference 16. The model description presented in this paper will, therefore, be brief and will illustrate only the general model configuration. All nomenclature used in discussing the model components will be the same as that for the full-scale counterparts.

The complete model, shown photographically in figure 1 and schematically in figure 2, consists of the S-IC, S-II, and S-IVB stages, the instrument unit (IU), and the Apollo payload with its launch escape system (LES). All main, load-carrying structures of the model are essentially geometrically scaled. However, the model payload differs significantly from full-scale hardware. For example, the model Apollo command module (CM) and service module (SM) retain only general external dimensions, longitudinal mass

distribution, and bending stiffnesses as scaled quantities. The simulated lunar module (LM) has only the correct mass, center of mass, mass moments of inertia, and simulated truss work for attachment of the LM to the adapter structure. The payload dimensions, inertias, and stiffness and mass distributions were scaled from the CM, SM, LM, and Saturn LM adapter (SLA) concepts existing at the time the model was constructed and are, therefore, not representative of any flight configuration.

The calculated cross-sectional area distribution of the models is given in figure 3 and measured mass characteristics of the three configurations tested are given in table 1. A discussion of the method used in calculating the model stiffness from the cross-sectional area plot is given in a subsequent section. The three configurations are defined numerically in the order in which they occur in flight. Configuration I consists of the complete model, configuration II is the model with the S-IC stage removed, and configuration III is the model with both the S-IC and S-II stages removed. In flight, the LES is not jettisoned until the S-II engines reach full thrust. Therefore an additional subconfiguration, representing the vehicle immediately following the S-IC staging, was studied.

Liquid Propellant Simulation

Onboard liquids in the three booster stages were simulated as follows: liquid oxygen (lox) in all stages and the RP-1 fuel in the first stage were simulated with water; the liquid hydrogen (LH_2) in the second and third stages was simulated with small, hollow styrene plastic beads. Proper control of the water and bead levels then permitted representation of the correct propellant weight; however, some deviation from full-scale mass distribution occurred as a result of differences in specific gravity between water (1.0) and RP-1 (0.80) and lox (1.14).

Suspension System

Two-cable suspension systems of the type described in reference 17 and depicted schematically in figure 4 were used to support the models and to provide simulated free-free restraint. The configuration under test was mounted on a cradle at its base and two vertical cables were connected to the cradle so that the plane of the cables passed through the model center line normal to the direction of excitation. Tipover stability was provided by horizontal restraint cables connecting the support cables to the model at a point above the center of gravity of the configuration. The tension in the horizontal cables, and thus the stabilizing force, was controlled by adjustment of the cable terminal separation distance, designated d in the sketches. The cables were steel, composed of seven 19-wire strands, and were 5/16 inch in diameter. All rigid-body frequencies ($f < 1.0$ Hz) were much lower than the lowest structural frequency ($f = 8.6$ Hz) for all tests. Force application points for the various tests are also shown in figure 4.

TABLE I.- MEASURED MASS DATA FOR 1/10-SCALE SATURN V MODEL

Model section	c.g., $\frac{x}{L}$	Configuration I							Configuration II							Configuration III						
		Struct. mass, kg	Fuel and lox loading						Struct. mass, kg	Fuel and lox loading						Struct. mass, kg	Fuel and lox loading					
			100 percent		50 percent		0 percent			100 percent		50 percent		0 percent			100 percent		50 percent		0 percent	
			c.g., $\frac{x}{L}$	Mass, kg	c.g., $\frac{x}{L}$	Mass, kg	c.g., $\frac{x}{L}$	Mass, kg		c.g., $\frac{x}{L}$	Mass, kg	c.g., $\frac{x}{L}$	Mass, kg	c.g., $\frac{x}{L}$	Mass, kg		c.g., $\frac{x}{L}$	Mass, kg	c.g., $\frac{x}{L}$	Mass, kg	c.g., $\frac{x}{L}$	Mass, kg
Payload:																						
LES	0.946	3.96							3.96													
Command module	.894	3.02							3.02							3.02						
Service module	.861	22.39							22.39							22.39						
LM and adapter	.788	14.96							14.96							14.96						
Instrument unit	.761	1.66							1.66							1.66						
S-IVB:																						
S-IVB hydrogen			0.705	18.4	0.705	18.4	0.705	18.4		0.705	18.4	0.705	18.4	0.705	18.4		0.705	18.4	0.686	9.19	0	0
S-IVB tanks	.692	7.32							7.32							7.32						
S-IVB lox			.655	88.0	.655	88.0	.655	88.0		.655	88.0	.655	88.0	.655	88.0		.655	88.0	.648	44.0	0	0
Aft structure	.622	4.75							4.75							4.75						
J-2 engine	.615	1.42							1.42							1.42						
Support cradle	.588															4.3						
S-II:																						
S-II hydrogen			.514	70.8	.514	70.8	.514	70.8		.514	70.8	.486	35.4	0	0							
S-II tanks	.482	23.61							23.61													
S-II lox			.431	344.7	.431	344.7	.431	344.7		.431	344.7	.421	172.4	0	0							
Aft structure	.392	13.03							13.03													
J-2 engines	.384	23.61							23.61													
Support cradle	.358								4.3													
S-IC:																						
Lox tank	.259	20.35	.262	1343	.227	671.3	0	0														
Inter tank	.181	14.32																				
Fuel tank	.120	10.04	.109	607.8	.086	303.9	0	0														
Aft structure	.045	47.31																				
F-1 engines	.011	40.28																				
Support cradle	.021	6.92																				

Configuration mass totals

Configuration	Propellant loading, percent	Mass, kg
I	100	2371.7
	50	1756.1
	0	780.9
II	100 + LES	649.9
	100	645.9
	50	438.2
	0	230.4
III	100	170.2
	50	117.0
	0	63.8

Instrumentation

The instrumentation of the 1/10-scale Saturn V model was designed to provide continuous electronic signals to define the dynamic response of the model to sinusoidal force inputs. The instrumentation system provided a means of monitoring exciter inputs and transducer output signals, recording these signals for subsequent in-depth analysis, and performing simple onsite data analysis. The locations of primary transducers for sensing responses of the models to the induced excitation are shown in figure 5. The primary transducers used in the test program were Kistler Model 303 servo accelerometers. Unless otherwise noted, these accelerometers were mounted tangentially on the model with the sensitive axis parallel to the direction of the input force vector. Responses normal to the plane of excitation were also measured at selected locations. A typical accelerometer installation is shown photographically in figure 6. Whenever supplementary data were required, additional measurements were made with a vacuum-mounted movable accelerometer. Accelerometers were also mounted on all engines and on the simulated LM.

Data Acquisition System

The layout of the data acquisition system is shown in figure 7. Data signal cables from the transducers were connected to data group switches in prearranged combinations so that a group of 12 selected channels of information could be monitored or recorded simultaneously. Three data channels were common to all groups: the force-gage output, exciter-oscillator output, and tip-accelerometer signal. Any channel within a given group could be monitored on oscilloscopes, rms meter, or x-y plotter. The data were also recorded on analog tape for subsequent data reduction. The group of instruments designated "Onsite analysis" permitted preliminary, quick-look evaluation of either real-time or tape-recorded data signals.

Data-Reduction Procedure

Recorded data were converted by means of a direct 24-point-per-cycle conversion from analog to digital format suitable for computer-mechanized reduction. Data samples were subjected to quality-control analysis and then used to construct a single cycle of data considered to be representative of the set from which it originated. This constructed cycle was then harmonically analyzed to determine the magnitudes of the fundamental through tenth harmonics and their respective phase angles with reference to that of the input force. The normalized amplitude of the fundamental harmonic, when plotted as a function of the transducer coordinate, yields the normalized deflection at that location.

To obtain damping constants, power to the shaker armature was switched off and the amplitude decay of one or more selected transducer signals was recorded as an

oscillogram. The amplitudes of at least 10 cycles of the resulting decay signal were used to determine the damping value.

Test Procedure

The experimental data were obtained in basically the same manner for all configurations and test conditions. The input-force generator supplied a constant-amplitude sinusoidal force to the model at slowly increasing frequency. Selected transducer outputs were automatically plotted as diagrams of total amplitude versus frequency. These signals were also simultaneously displayed as Lissajous patterns on an oscilloscope, and peak response frequencies and phase shifts were noted. Examination of several diagrams of amplitude versus frequency served to identify individual peak response frequencies, which were then examined by manually tuning the frequency of excitation to obtain peak amplitude and recording the output of all transducers on analog tape for subsequent harmonic analysis. Damping data were then taken as previously discussed.

ANALYSIS

A theoretical investigation was made, in conjunction with the experimental program, to gain insight into the degree of analytical refinement required to produce reasonably accurate calculated mode shapes and natural frequencies. Characteristics calculated for the analytical model, and therefore the correlation achieved between measured and calculated results, depend on both the nature of the mathematical model and the method used to analyze it. Therefore, the subsequent study can be interpreted as a measure of the adequacy of the mathematical model and of the analytical procedure as well. The matrix-Holzer method, which is employed in the calculations, has been used in various forms for many years. Verification of its suitability for analyzing various beam-type structures has been reported (refs. 18 and 19). Nevertheless, few explicit comparisons between measured and calculated characteristics for structures typical of launch vehicles are present in the open literature.

General Method

The development of the transfer matrix method for flexural vibration of beams is presented in chapter 5 of reference 20. The following treatment is similar except that it is stated here in a manner intended to show greater parallel with the classical solution for a beam with distributed mass and distributed stiffness. The development illustrates also that the transfer matrix method is not restricted to discrete systems.

A variable-coefficient partial differential equation is considered which is dependent on a single space variable and a time variable. In addition, the solution must satisfy

given boundary conditions at two separate points. The equation considered is that which describes the lateral displacement of a beam with shear deflection and rotatory inertia effects included:

$$\frac{\partial^4 y}{\partial x^4} + \frac{m(x)}{E(x)I(x)} \frac{\partial^2 y}{\partial t^2} - \left[\frac{\rho(x)}{E(x)} + \frac{\rho(x)}{K(x)G(x)}\right] \frac{\partial^4 y}{\partial x^2 \partial t^2} = 0 \tag{1}$$

Solutions of this equation may be assumed as a product of a space-dependent part and a time-dependent part in the form

$$y(x,t) = X(x)e^{i\omega t} \tag{2}$$

Equation (1) is thus reduced to an ordinary differential equation in the space variable with the frequency ω as a parameter:

$$\frac{d^4X(x)}{dx^4} - \frac{m(x)}{E(x)I(x)} \omega^2 X(x) + \left[\frac{\rho(x)}{E(x)} + \frac{\rho(x)}{K(x)G(x)}\right] \omega^2 \frac{d^2X(x)}{dx^2} = 0 \tag{3}$$

If the coefficients in equation (3) are independent of x, the general solution for $X(x)$ will be of the form

$$X(x) = Ce^{\lambda x} \tag{4}$$

Since the differential equation is of fourth order, the substitution of equation (4) into equation (3) will yield a quartic equation in λ. There will then be four roots of the quartic

$$\lambda_{1,2,3,4} = \pm\sqrt{\frac{m\omega^2}{2EI} \pm \frac{1}{2}\sqrt{\left(\frac{m\omega^2}{EI}\right)^2 + \frac{4\rho\omega^2}{E}\left(1 + \frac{E}{KG}\right)}} \tag{5}$$

and four undetermined coefficients C so that the general solution may be written

$$X(x) = \sum_{s=1}^{4} C_s e^{\lambda_s x} \tag{6}$$

A set of four equations necessary for determining the four constants of integration is formed from derivatives of $X(x)$:

$$X(x) = \sum_{s=1}^{4} C_s e^{\lambda_s x} \tag{7a}$$

$$\frac{dX(x)}{dx} = \sum_{s=1}^{4} \lambda_s C_s e^{\lambda_s x} \tag{7b}$$

$$\frac{d^2X(x)}{dx^2} = \sum_{s=1}^{4} \lambda_s{}^2 C_s e^{\lambda_s x} \tag{7c}$$

$$\frac{d^3X(x)}{dx^3} = \sum_{s=1}^{4} \lambda_s{}^3 C_s e^{\lambda_s x} \tag{7d}$$

These equations may be written in matrix notation as

$$\left\{\frac{d^{p-1}X(x)}{dx^{p-1}}\right\} = \left[\lambda_s{}^{p-1} e^{\lambda_s x}\right]\{C_s\} \qquad (p,s = 1, 2, 3, 4) \tag{8}$$

where, by definition,

$$\frac{d^0X(x)}{dx^0} = X(x)$$

The constants of integration will be determined from the boundary conditions prescribed in this case at the two end points of the beam, $x = 0$ and $x = l$.

A relationship can be found between the dependent variable $X(x)$ and its derivatives at stations $x = 0$ and $x = l$:

$$\left\{\frac{d^{p-1}X(x)}{dx^{p-1}}\right\}_{x=0} = \left[\lambda_s{}^{p-1}\right]\{C_s\} \tag{9}$$

and

$$\left\{\frac{d^{p-1}X(x)}{dx^{p-1}}\right\}_{x=l} = \left[\lambda_s{}^{p-1} e^{\lambda_s l}\right]\{C_s\} \tag{10}$$

Upon eliminating the integration constants, the result is

$$\left\{\frac{d^{p-1}X(x)}{dx^{p-1}}\right\}_{x=l} = \left[\lambda_s{}^{p-1} e^{\lambda_s l}\right]\left[\lambda_s{}^{p-1}\right]^{-1}\left\{\frac{d^{p-1}X(x)}{dx^{p-1}}\right\}_{x=0} \tag{11}$$

We may express this equation in the notation used in reference 20 as follows:

$$\{Z\}_l = \left[U(\lambda_s)\right]\{Z\}_0$$

where $\{Z\} = \{X,\phi,V,M\}^T$. The quantities V and M are proportional to d^3X/dx^3 and d^2X/dx^2, respectively. The quantity $\{Z\}$ is referred to as the state vector because it describes the state of the beam at a given cross section and $\left[U(\lambda_s)\right]$ is the transfer matrix given by

$$\left[U(\lambda_s)\right] = \begin{bmatrix} 1 & 1 & 1 & 1 \\ \lambda_1 & \lambda_2 & \lambda_3 & \lambda_4 \\ \lambda_1^2 EI & \lambda_2^2 EI & \lambda_3^2 EI & \lambda_4^2 EI \\ \lambda_1^3 EI & \lambda_2^3 EI & \lambda_3^3 EI & \lambda_4^3 EI \end{bmatrix} \begin{bmatrix} e^{\lambda_1 l} & & & \\ & e^{\lambda_2 l} & & \\ & & e^{\lambda_3 l} & \\ & & & e^{\lambda_4 l} \end{bmatrix} \begin{bmatrix} 1 & 1 & 1 & 1 \\ \lambda_1 & \lambda_2 & \lambda_3 & \lambda_4 \\ \lambda_1^2 EI & \lambda_2^2 EI & \lambda_3^2 EI & \lambda_4^2 EI \\ \lambda_1^3 EI & \lambda_2^3 EI & \lambda_3^3 EI & \lambda_4^3 EI \end{bmatrix}^{-1} \tag{12}$$

The solution is found by imposing the boundary conditions at $x = 0$ and $x = l$. This leads to a homogeneous equation

$$\{0\}_l = \left[\overline{U}(\lambda_s)\right]\{\overline{Z}\}_0 \tag{13}$$

The matrix $\left[\overline{U}(\lambda_s)\right]$ and the vector $\{\overline{Z}\}_0$ are one-half the order of $\left[U(\lambda_s)\right]$ and $\{Z\}_0$. A nontrivial solution for $\{\overline{Z}\}_0$ from equation (13) exists if and only if the determinant $\left|\overline{U}(\lambda_s)\right| = 0$. The λ_s are functions of ω as given in equation (5); consequently there will be a vector $\{\overline{Z}\}_0$ for each value of ω for which $\left|\overline{U}(\lambda_s)\right| = 0$. The space-dependent function is then formed by combining equations (6) and (9) and using the state vector $\{\overline{Z}\}_0$ related to each natural frequency ω. The result is

$$X(x) = \left[\left[\lambda_s^{p-1}\right]^{-1}\{\overline{Z}\}_0\right]^T \{e^{\lambda_s x}\} \tag{14}$$

The equation $\left|\overline{U}(\lambda_s)\right| = 0$ is the characteristic equation, ω is the eigenvalue, and $\{\overline{Z}\}_0$ is the eigenvector. The function $X(x)$ is the mode shape.

In the foregoing development, the beam was assumed to have uniform mass and stiffness along its length. If these quantities vary with position, the procedure is similar but the transfer matrix must be derived differently. The beam may be assumed piecewise uniform or the physical properties may be lumped at discrete positions on the beam. The lumping approach was applied to the Saturn V model and expressions used in that application are developed next.

Application to Saturn V Model

In the present analysis, the Saturn V model is visualized for mathematical purposes as a flexural beam with lumped mass, distributed stiffness, and attached branch systems. The manner in which the mass of the model is lumped is determined mainly by the actual physical arrangement. Examination of figure 2 shows that some of the mass is naturally lumped, or concentrated, at discrete points along the vehicle. This fact is reflected in the mathematical model shown in figure 8. The first-stage engines; the second- and

third-stage engines, thrust structures, and lox tanks; and the LM are attached as branched discrete systems. The first-stage engines and the LM are attached at the main beam through a rotational spring and a linear spring, respectively. The S-II engines and thrust structure are attached to the main beam at the thrust structure attachment station. The lox tank of the S-II stage is treated as a separate single-degree-of-freedom slosh mass attached to the main beam at the point where the lox tank is tangent to the outer shell. The S-IVB engine, thrust cone, and lox tank are treated as a multielement branched beam attached to the main beam at the S-IVB aft skirt attachment plane. The remainder of the model mass is concentrated at equally spaced points along the beam. The number of mass points used for each configuration is also shown in figure 8. Each mass point is allowed two degrees of freedom, translation and rotation.

The lumping thus idealizes the vehicle into a series of disconnected masses and massless elastic beams in the manner shown in sketch (a) so that the motion of the composite beam results from the elastic beams being described by the static beam equation, and the motion of the masses is governed by the dynamic equations for rigid bodies.

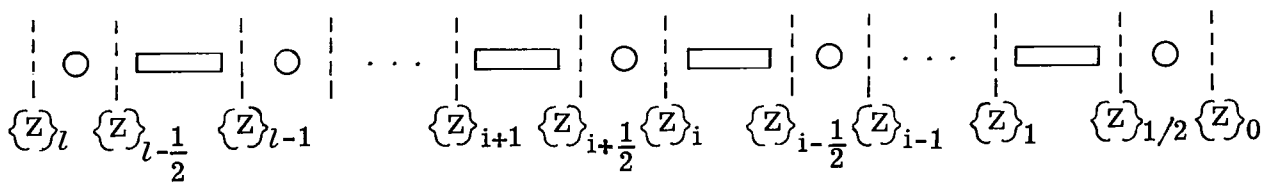

Sketch (a)

Transfer matrix for typical inertial element.- An inertial element is assumed to consist of a rigid body which applies an inertial force and moment to the point on the beam to which it is attached. The inertial forces result from the motion of the beam center line. In most instances the point of attachment will be taken to be the centroid. For the general case, however, the centroid will be assumed to be offset from the attachment point. The element is represented schematically in sketch (b) (small displacements are assumed).

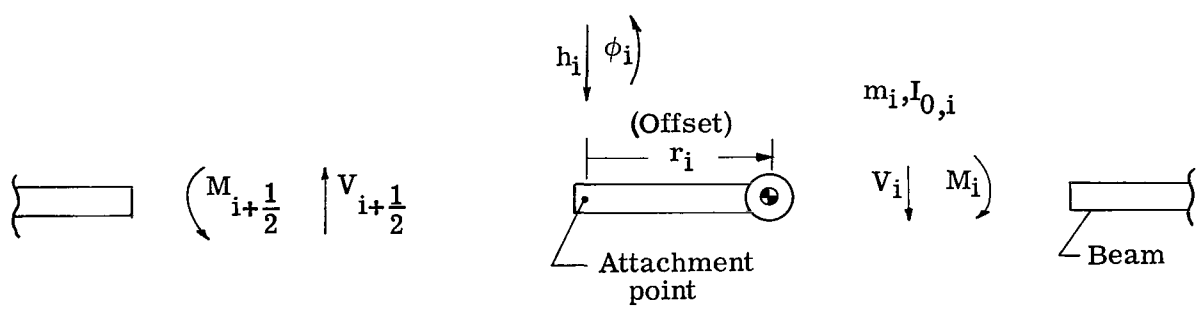

Sketch (b)

Equilibrium of the external forces and moments results in two equations (positive values are indicated in sketch (b)):

$$V_{i+\frac{1}{2}} - V_i + m_i r_i \ddot{\phi} + m\ddot{h}_i = 0 \tag{15}$$

$$M_{i+\frac{1}{2}} - M_i - \left(m_i r_i^2 + I_{0,i}\right)\ddot{\phi} - m_i r_i \ddot{h}_i = 0 \tag{16}$$

Simple harmonic motion is assumed. The equilibrium equations can be rewritten in matrix form as

$$\begin{Bmatrix} V \\ M \\ \phi \\ h \end{Bmatrix}_{i+\frac{1}{2}} = \begin{bmatrix} 1 & 0 & m_i r_i \omega^2 & m_i \omega^2 \\ 0 & 1 & -\left(m_i r_i^2 + I_{0,i}\right)\omega^2 & -m_i r_i \omega^2 \\ 0 & 0 & 1 & 0 \\ 0 & 0 & 0 & 1 \end{bmatrix} \begin{Bmatrix} V \\ M \\ \phi \\ h \end{Bmatrix}_i \tag{17}$$

or

$$\{Z\}_{i+\frac{1}{2}} = \left[m(\omega)\right]_i \{Z\}_i$$

Transfer matrix for typical beam element.- The transfer matrix for the massless elastic beam element is derived from the static beam equations. A beam possessing bending flexibility, which may vary with x, is loaded as shown in sketch (c). The total

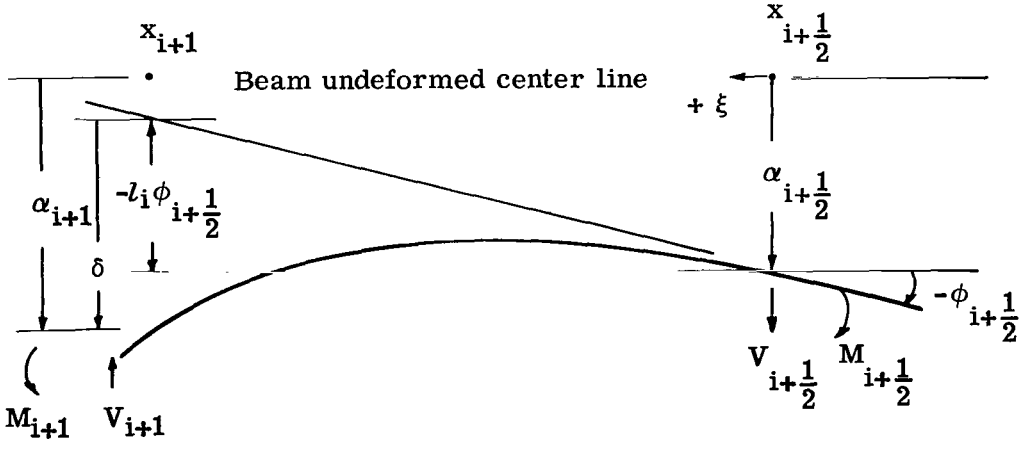

Sketch (c)

lateral deflection of the beam consists of two parts, that due to bending deformation and that due to shear deformation. The bending deflection at station $i + 1$ is denoted α_{i+1} and is equal to

$$\alpha_{i+1} = \alpha_{i+\frac{1}{2}} - \left(-l_i \phi_{i+\frac{1}{2}}\right) + \delta \tag{18}$$

where δ is the tangential deviation and $l_i = x_{i+1} - x_{i+\frac{1}{2}}$. The bending slope at x_{i+1} is obtained from the beam equation

$$\frac{d\phi}{dx} = \frac{M}{EI}$$

by integrating between the $x_{i+\frac{1}{2}}$ and x_{i+1}:

$$\phi_{i+1} - \phi_{i+\frac{1}{2}} = \int_{x_{i+\frac{1}{2}}}^{x_{i+1}} \frac{M(\xi)d\xi}{E(\xi)I(\xi)} \tag{19}$$

The tangential deviation, as given in reference 21, is

$$\delta = \int_{x_{i+\frac{1}{2}}}^{x_{i+1}} \frac{(l_i - \xi)M(\xi)d\xi}{E(\xi)I(\xi)} \tag{20}$$

The moment is

$$M(\xi) = M_i + V_i \xi \tag{21}$$

Equations (18), (19), and (20) are combined and an expression for α_{i+1} results:

$$\alpha_{i+1} = \alpha_{i+\frac{1}{2}} + l_i \phi_{i+\frac{1}{2}} + M_i \int_{x_{i+\frac{1}{2}}}^{x_{i+1}} \frac{(l_i - \xi)d\xi}{E(\xi)I(\xi)} + V_i \int_{x_{i+\frac{1}{2}}}^{x_{i+1}} \frac{\xi(l_i - \xi)d\xi}{E(\xi)I(\xi)} \tag{22}$$

In addition, if the beam can deform in shear, the total deflection will include both bending deflection α_i and shear deflection β_i. As illustrated in sketch (d), the change

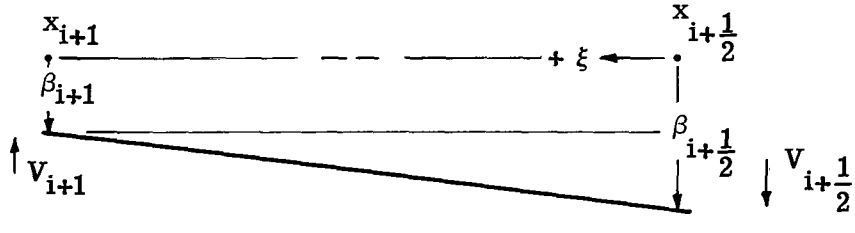

Sketch (d)

in shear deflection is, from reference 21,

$$\frac{d\beta}{d\xi} = -\frac{V}{K(\xi)A(\xi)G(\xi)} \tag{23}$$

Integrating between the limits $x_{i+\frac{1}{2}}$ and x_{i+1} gives the shear deflection:

$$\beta_{i+1} - \beta_{i+\frac{1}{2}} = -V_i \int_{x_{i+\frac{1}{2}}}^{x_{i+1}} \frac{d\xi}{K(\xi)A(\xi)G(\xi)} \tag{24}$$

The total deflection h_i is $\alpha_i + \beta_i$. Equations (22) and (24) are added to obtain

$$h_{i+1} = h_{i+\frac{1}{2}} + l_i\phi_{i+\frac{1}{2}} + M_i \int_{x_{i+\frac{1}{2}}}^{x_{i+1}} \frac{(l_i - \xi)d\xi}{E(\xi)I(\xi)} + V_i \left[\int_{x_{i+\frac{1}{2}}}^{x_{i+1}} \frac{\xi(l_i - \xi)d\xi}{E(\xi)I(\xi)} - \int_{x_{i+\frac{1}{2}}}^{x_{i+1}} \frac{d\xi}{K(\xi)A(\xi)G(\xi)} \right] \tag{25}$$

Equations (19), (21), and (25) may be rewritten in matrix form as

$$\begin{Bmatrix} V \\ M \\ \phi \\ h \end{Bmatrix}_{i+1} = \begin{bmatrix} 1 & 0 & 0 & 0 \\ l_i & 1 & 0 & 0 \\ c_1 & c_2 & 1 & 0 \\ c_3 & c_4 & l_i & 1 \end{bmatrix} \begin{Bmatrix} V \\ M \\ \phi \\ h \end{Bmatrix}_{i+\frac{1}{2}} \tag{26}$$

where

$$c_1 = \int_{x_{i+\frac{1}{2}}}^{x_{i+1}} \frac{\xi\, d\xi}{E(\xi)I(\xi)}$$

$$c_2 = \int_{x_{i+\frac{1}{2}}}^{x_{i+1}} \frac{d\xi}{E(\xi)I(\xi)}$$

$$c_3 = \int_{x_{i+\frac{1}{2}}}^{x_{i+1}} \frac{\xi(l_i - \xi)d\xi}{E(\xi)I(\xi)} - \int_{x_{i+\frac{1}{2}}}^{x_{i+1}} \frac{d\xi}{K(\xi)A(\xi)G(\xi)}$$

$$c_4 = \int_{x_{i+\frac{1}{2}}}^{x_{i+1}} \frac{(l_i - \xi)d\xi}{E(\xi)I(\xi)}$$

The equation may be written in abbreviated form as

$$\{Z\}_{i+1} = [e]_i \{Z\}_{i+\frac{1}{2}}$$

where $[e]_i$ is the transfer matrix for the beam element.

Section properties.- The 1/10-scale Saturn V model was assumed to retain its cross-sectional geometry under deformation. As a result, the sectional area and area moment of inertia of the elastic beams were for the most part based simply on the following:

$$A_e = A_{skin} + A_{str} + A_D \tag{27}$$

$$I = \frac{A_e R^2}{2} \tag{28}$$

where

A_e equivalent area

A_{str} area of stringers

A_D area of doublers

R radius of shell

This procedure, in effect, distributes stringer and doubler area around the circumference and includes the total geometric area. The skirt and interstage sections of the S-II and S-IVB stages, however, employ very thin skin in their construction. For these areas,

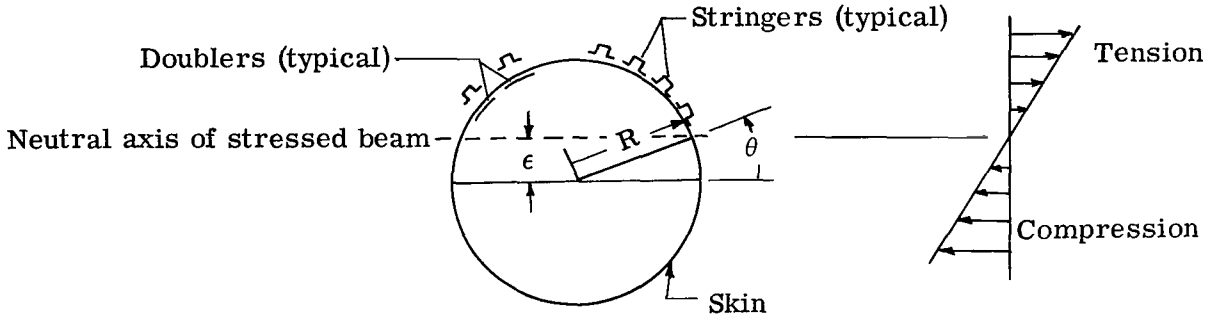

Sketch (e)

shown in figure 3, the area moment of inertia, and thus the bending stiffness, was reduced on the assumption that skin in compression cannot support an axial load. The effect was incorporated in the analysis by using area-moment-of-inertia data based on ϵ, a neutral-axis offset from the geometric center. (See sketch (e).) The magnitude of the offset reflects the assumption that the skin can support tension loads only, whereas the stringers can support both tension and compression. Section properties for the areas treated in this manner were obtained from the following equations:

$$I_{skin} = R^3\tau\left\{\frac{\pi}{2}\left[1 + \left(\frac{\epsilon}{R}\right)^2\right] - \theta\left[1 - 2\left(\frac{\epsilon}{R}\right)^2\right] + \frac{1}{2}\sin\theta - 4\left(\frac{\epsilon}{R}\right)\cos\theta\right\} \tag{29}$$

$$I_{str} = \frac{R^3 A_{str}}{2}\left[1 + 2\left(\frac{\epsilon}{R}\right)^2\right] \tag{30}$$

where

$$\theta = \operatorname{ctn}^{-1}\left(\frac{1}{2} + \frac{A_{str}}{A_{skin}}\pi - \theta\right)$$

$$\frac{\epsilon}{R} = \sin\theta$$

Liquid slosh.- Liquid contained in the model tanks to simulate propellant is represented as a spring-mass system with characteristics calculated by the approximate method described in reference 22. The validity of a spring-mass analogy is substantiated in references 23 and 24. Derivations of the hydrodynamic properties may be found in references 24 and 25. In the present analysis, the amplitude of sloshing may be overestimated since the slosh baffles were not accounted for. Moreover, when the liquid level is near the top of the tank, the slosh mass is low and the frequency high. Consequently, the analytical representations of the S-II and S-IVB stages contain no slosh when these stages are at the 100-percent full condition. Slosh, when included, is represented by a one-mode spring-mass system. The remainder of the liquid mass is uniformly distributed along the tank as rigidly attached masses having no rotatory inertia.

Engine branches.- The first and second stages have five engines each, four outboard and one at the center line. The outboard engines, though gimbaled, are restrained from rotating by push rods designed to simulate the locked valve actuators. The center engine is held relatively rigid. Analytically, the outboard engines were combined into one single-degree-of-freedom system in which the mass is the total mass of four engines. A rotary restraining spring was sized so that the system frequency corresponds to a representative measured engine frequency. The S-IVB engine was treated similarly.

The fuel slosh masses and the engines are treated as branched systems. If the branched system is open – that is, if the branched system is attached to the main beam at a single point – its motion can be found from sketch (f). The column matrices

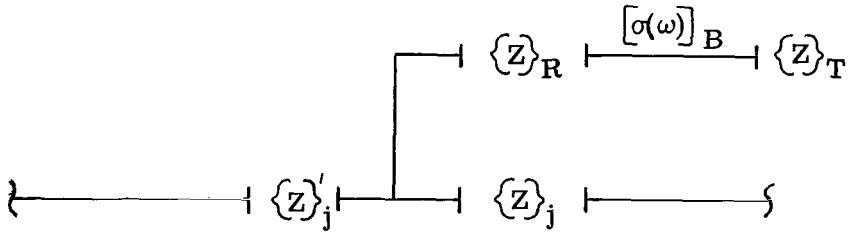

Sketch (f)

$\{Z\}_T$ and $\{Z\}_R$ are the state vectors at the free end and the root of the branch. The column matrices $\{Z\}_j$ and $\{Z\}'_j$ are the state vectors on each side of the connection point. The procedure for developing the transfer matrix $[\sigma(\omega)]_B$ from the elemental matrices $[e]_i$ and $[m]_i$ will be given later in this section. From conditions of equilibrium the internal loads to the left of the connection point are given by

$$\begin{Bmatrix} V \\ M \end{Bmatrix}'_j = \begin{Bmatrix} V \\ M \end{Bmatrix}_j + \begin{Bmatrix} V \\ M \end{Bmatrix}_R \tag{31}$$

Continuity of slope and deflection yield the relationship

$$\begin{Bmatrix} \phi \\ h \end{Bmatrix}'_j = \begin{Bmatrix} \phi \\ h \end{Bmatrix}_j = \begin{Bmatrix} \phi \\ h \end{Bmatrix}_R \tag{32}$$

The state vector $\{Z\}_R$ is found from

$$\{Z\}_R = \left[\begin{array}{c:c} \sigma_{11}(\omega) & \sigma_{12}(\omega) \\ \hdashline \sigma_{21}(\omega) & \sigma_{22}(\omega) \end{array}\right] \left\{\begin{array}{c} V \\ M \\ \hdashline \phi \\ h \end{array}\right\}_T \tag{33}$$

For a free-ended branch, $V_T = M_T = 0$. It follows that

$$\begin{Bmatrix} V \\ M \\ \hline \phi \\ h \end{Bmatrix}_R = \begin{bmatrix} \sigma_{12}(\omega) \\ \hline\hline \sigma_{22}(\omega) \end{bmatrix}_B \begin{Bmatrix} \phi \\ \\ h \end{Bmatrix}_T \tag{34}$$

Equations (32) and (34) are combined with equation (31) to get an expression for the loads on the left of the connection point in terms of the deflections on the right:

$$\begin{Bmatrix} V \\ M \end{Bmatrix}'_j = \begin{Bmatrix} V \\ M \end{Bmatrix}_j + \left[\sigma_{12}(\omega)\right]_R \left[\sigma_{22}(\omega)\right]_B^{-1} \begin{Bmatrix} \phi \\ h \end{Bmatrix}_j \tag{35}$$

In practice the transfer matrices for the beam to the right of the joint are calculated, then the contribution from the branched system is added, and the transfer process is continued. Attention must be given to the sign of the loads to account for the direction in which the branch beam faces with respect to the main beam.

Boundary conditions.- When the frequency-dependent transfer matrices for all beam elements have been obtained, the transfer matrix for the entire beam is constructed by imposing conditions of continuity and equilibrium at the elemental interfaces. Consequently, the state vector at one end of the beam is associated with the state vector at the other end through the product of all the elemental transfer matrices; that is,

$$\{Z\}_l = \left[\sigma(\omega)\right] \{Z\}_0 \tag{36}$$

where

$$\left[\sigma(\omega)\right] = \prod_{i=0}^{l} \left[e\right]_{l-i} \left[m(\omega)\right]_{l-i}$$

The solution must satisfy prescribed boundary conditions at the two end points. The conditions are that any two of the elements of the state vector V, M, ϕ, or h will be identically zero at either end. With these values included, equation (13) becomes

$$\{0\} = \left[\bar{\sigma}(\omega)\right] \{\bar{Z}\}_0 \tag{37}$$

where $\left[\bar{\sigma}(\omega)\right]$ is the reduced transfer matrix obtained by application of the boundary conditions.

As an example of the manner in which the reduction is accomplished, a free-free beam for which $V = M = 0$ at each end is considered. Equation (36) may be partitioned so that

$$\begin{Bmatrix} 0 \\ 0 \\ \hline \phi \\ h \end{Bmatrix}_l = \left[\begin{array}{c|c} \sigma_{11}(\omega) & \sigma_{12}(\omega) \\ \hline \sigma_{21}(\omega) & \sigma_{22}(\omega) \end{array}\right] \begin{Bmatrix} 0 \\ 0 \\ \hline \phi \\ h \end{Bmatrix}_0 \tag{38}$$

From the first two equations of the system,

$$\begin{Bmatrix} 0 \\ 0 \end{Bmatrix} = \left[\bar{\sigma}_{12}(\omega)\right] \begin{Bmatrix} \phi \\ h \end{Bmatrix}_0 \tag{39}$$

which is the desired determinental equation. For other sets of boundary conditions, the transfer matrix will be reduced by a different partitioning.

In this analysis, the model was treated as a free-free beam. Therefore shear V and moment M were set equal to zero at each end. The assumption of zero shear and bending moment at the base of the model does not precisely represent the model in the test stand. However, the model suspension system was designed to impose very small shears and moments at the base. The mass of the suspension-system cradle was included in the analytical model to maintain agreement with the test specimen. The weight of the cables which constitute part of the suspension system was omitted.

A solution of equation (39) other than $\{\bar{Z}\}_0 = \{0\}$ will exist if and only if the determinant

$$\left|\bar{\sigma}_{12}(\omega)\right| = 0 \tag{40}$$

The values of ω for which the determinant vanishes are the eigenvalues ω_c. The state vector components are then

$$\{\bar{Z}\}_0 = \text{adj}\left[\bar{\sigma}(\omega_c)\right]\{I\} \tag{41}$$

where $\text{adj}\left[\bar{\sigma}(\omega_c)\right]$ is the adjoint of $\left[\bar{\sigma}(\omega_c)\right]$ and $\{I\}$ is a column matrix each element of which is unity. The state vector at any location $i = j$ is then

$$\{Z\}_j = \prod_{i=0}^{j} [e]_{j-i} \left[m(\omega_c)\right]_{j-i} \{Z\}_0 \tag{42}$$

where $\{Z\}_0$ now has elements 0, 0, ϕ_0, and h_0.

Values of ω for which $\left|\bar{\sigma}(\omega)\right| = 0$ are found numerically by observing the sign of $\left|\bar{\sigma}(\omega)\right|$ as ω is varied. A change of sign indicates either a zero crossing or an asymptote. An asymptote occurs for a value of ω which corresponds to a fixed-base

resonant frequency of a branch beam – that is, an uncoupled mode. A zero crossing corresponds to a resonant frequency of the coupled system.

RESULTS AND DISCUSSION

Data from analysis and tests of the lateral vibratory characteristics of the 1/10-scale Apollo/Saturn V model are presented in figures 9 to 25, tables 2 to 7, and the appendix. Complete data are shown for three propellant loadings (full, half-full, and empty) in each configuration. Tests were also conducted with other fractional propellant loadings (i.e., 25 percent and 75 percent). A summary of the measured resonant frequencies for each of the three configurations is presented in figure 9. The frequencies are plotted as a function of simulated propellant loading. Other preliminary tests were conducted early in the program which showed that such potential variables as tank ullage pressure, number of shakers, or shaker location had insufficient effect on the model frequencies and response shapes to warrant further consideration in the test program.

The data in figures 10 to 24 follow the same format for each of the three configurations examined: (1) a representative experimental frequency sweep taken in the yaw direction at the 100-percent propellant loading condition, which shows the accelerations of various points on the model structure plotted as a function of the frequency of the input force, and (2) composite plots of calculated and measured normalized response shapes at discrete frequencies. Tabulated on each response-shape plot are the values of the calculated frequency f_a and the measured frequencies in the pitch and yaw directions denoted f_p and f_y, respectively. As discussed previously, the analytical model is assumed to be radially symmetric; consequently, there is no distinction between the calculated pitch and yaw responses.

A check for orthogonality of the measured deflection shapes, including rigid-body translation and rigid-body rotation about the system center of gravity, was made by combining the measured deflection shapes with the calculated mass distributions in the following manner:

$$m_{gh} = \sum_{k=0}^{n} m(k)h_g(k)h_h(k) \tag{43}$$

and normalizing according to the relationship

$$M_{gh} = \frac{m_{gh}}{\sqrt{m_{gg}m_{hh}}} \tag{44}$$

Equivalent mass values $\overline{M}_{gg}$ are then expressed in terms of the total system mass M_t as

$$\overline{M}_{gg} = \frac{m_{gg}}{M_t} \tag{45}$$

where $h_g(k)$ and $h_h(k)$ are the deflection shapes at station k in the gth and hth modes, and $m(k)$ is the analytical concentrated mass at station k (including branch masses). If the deflection shapes are orthogonal, and if the calculated masses are accurate, then the generalized mass matrix having elements m_{gh} will be diagonal. The quality of the measured shapes is indicated by the magnitude of the off-diagonal elements of the matrix M_{gh} relative to unity. No precise criteria exist for good or bad orthogonality correlations and their relationships to errors in the measured deflection shapes. One NASA Space Vehicle Design Criteria document (ref. 26) arbitrarily sets the value of the off-diagonal element magnitude at 0.1 as a demarcation between acceptable and unacceptable shapes.

Configuration I

Data from analysis and tests of configuration I (all stages plus payload) are presented in figures 10 to 13 and in table 2. Numerical values of experimental measurements are also given in the appendix. Figure 10 consists of curves of experimentally determined acceleration as a function of frequency for excitation in the yaw direction with S-IC propellant loading at 100 percent, corresponding to lift-off. Figures 11, 12, and 13 are composite plots of the normalized deflection shapes for the three weight conditions. The calculated mode shapes are indicated by solid curves while the measured deflections are indicated by circular and square symbols for pitch and yaw, respectively. The analytical frequency is denoted by f_a and the pitch and yaw frequencies from experiment are denoted by f_p and f_y, respectively. The various modes are plotted in order of ascending frequency and are denoted mode A, mode B, and so forth. This format and symbol notation are used for subsequent configurations also.

There is generally good agreement between the calculated and measured frequencies and response shapes for the first four bending modes of configuration I for three S-IC stage propellant loading conditions. Table 3 shows the correlation between the calculated frequencies and the measured pitch and yaw frequencies.

The analytically predicted frequencies are higher than either of the measured frequencies and, in general, the measured frequencies are higher in the pitch direction than in the yaw direction. These differences in measured frequency reflect model mass and stiffness asymmetries, some of which are representative of the full-scale structure and others of which may be due to fabrication imperfections. The measured, normalized, pitch and yaw deflection shapes are, however, nearly identical. Small, off-diagonal terms in the orthogonality matrices in table 2 indicate the absence of strong coupling or

TABLE 2.- GENERALIZED MASS MATRIX FOR CONFIGURATION I

(a) Pitch direction

100 percent propellant

						Mode, g	$\overline{M}_{gg}$	f_g, Hz
1.0	0	0.235	-0.029	0.114	-0.059	1	1.0	0
	1.0	-0.109	0.027	0.025	0.078	2	.028	0
		1.0	-0.027	0.395	-0.071	3	.0059	9.1
			1.0	0.165	0.109	4	.00423	16.0
				1.0	-0.210	5	.00224	24.8
					1.0	6	.00206	30.4

50 percent propellant

						Mode, g	$\overline{M}_{gg}$	f_g, Hz
1.0	0	0.0422	-0.077	-0.217	-0.0931	1	1.0	0
	1.0	-0.098	0.056	-0.043	0.103	2	.0364	0
		1.0	-0.075	0.023	-0.138	3	.0069	9.5
			1.0	-0.081	-0.089	4	.0053	18.0
				1.0	-0.26	5	.00264	25.8
					1.0	6	.00354	30.5

0 percent propellant

					Mode, g	$\overline{M}_{gg}$	f_g, Hz
1.0	0	-0.026	-0.072	-0.055	1	1.0	0
	1.0	-0.037	0.007	-0.12	2	.0439	0
		1.0	-0.054	0.089	3	.0149	10.0
			1.0	-0.151	4	.00103	19.3
				1.0	5	.00058	29.0

(b) Yaw direction

100 percent propellant

					Mode, g	$\overline{M}_{gg}$	f_g, Hz
1.0	0	-0.004	-0.003	-0.087	-0.378	1	1.0	0
	1.0	-0.085	0.028	0.040	0.127	2	.0301	0
		1.0	-0.129	0.050	0.340	3	.00628	8.6
			1.0	-0.158	-0.054	4	.00514	15.5
				1.0	0.169	5	.00284	24.7
					1.0	6	.00232	29.8

50 percent propellant

					Mode, g	$\overline{M}_{gg}$	f_g, Hz
1.0	0	0.073	-0.044	-0.072	-0.075	1	1.0	0
	1.0	-0.123	0.044	0.035	0.043	2	.0388	0
		1.0	-0.035	-0.056	-0.047	3	.0074	9.1
			1.0	0.103	0.005	4	.0055	17.9
				1.0	0.003	5	.00227	25.9
					1.0	6	.00352	30.0

0 percent propellant

					Mode, g	$\overline{M}_{gg}$	f_g, Hz
1.0	0	-0.008	0.078	-0.033	1	1.0	0
	1.0	0.007	0.003	0.001	2	.0439	0
		1.0	0.035	0.077	3	.0161	9.7
			1.0	0.088	4	.00335	19.4
				1.0	5	.00035	28.2

TABLE 3.- CONFIGURATION I FREQUENCY SUMMARY

S-IC propellant load, percent	f_a, Hz	$\frac{f_a}{f_p}$	$\frac{f_a}{f_y}$	$\frac{f_p}{f_y}$
100	9.15	1.00	1.06	1.05
	17.30	1.08	1.12	1.03
	26.16	1.05	1.06	1.00
	33.16	1.09	1.11	1.02
50	9.82	1.03	1.08	1.04
	19.07	1.06	1.06	1.00
	27.30	1.05	1.05	1.00
	34.25	1.12	1.14	1.02
0	10.29	1.03	1.06	1.03
	20.31	1.05	1.05	.99
	28.93	1.00	1.02	1.02

branch mass resonances in the frequency range below 30 Hz. S-IC engine resonances occurred in the frequency range between 40 and 43 Hz, both analytically and experimentally. The generalized mass matrix of table 2 combines normalized measured deflection shapes and calculated idealized mass distribution. The off-diagonal elements may be either increased or reduced by variations in the calculated mass distribution, independent of the quality of the measured deflection shapes. In view of the lack of rigorous definition of the correlation between nonzero off-diagonal elements and the lack of orthogonality, results of the orthogonality checks can be used only to estimate the quality of the measured modes. The results are presented for this purpose and for the benefit of future investigators interested in the question of such correlations.

Configuration II

Data from analysis and tests of the model configuration II (S-II, S-IVB, and Apollo payload) are presented in figures 14 to 20 and table 4. Experimental data are also tabulated in the appendix. The format of presentation is identical to that employed for configuration I.

Figures 14 and 15 present the frequency-sweep data and deflection-shape plots for the configuration with 100 percent propellant and LES. The data show a set of three clearly defined, beam-type bending modes in the region between 10 and 60 Hz which agree quite well with the frequencies and mode shapes predicted by analysis. The orthogonality check (table 4) and the measured phase angles given in the appendix are also indicative of

TABLE 4.- GENERALIZED MASS MATRIX FOR CONFIGURATION II

(a) Pitch direction

100 percent propellant + LES

					Mode, g	$\overline{M}_{gg}$	f_g, Hz
1.0	0	0.059	-0.133	-0.063	1	1.0	0
	1.0	-0.016	0.138	0.095	2	.0438	0
		1.0	0.102	-0.028	3	.00969	14.0
			1.0	0.169	4	.00462	27.8
				1.0	5	.269	55.8

100 percent propellant

1.0	0	-0.001	-0.009	0.081	1	1.0	0
	1.0	-0.011	0.005	-0.095	2	.057	0
		1.0	0.019	0.006	3	.0312	16.3
			1.0	0.55	4	.0629	52.6
				1.0	5	.434	98.2

50 percent propellant

1.0	0	0.081	-0.171	-0.114	1	1.0	0
	1.0	-0.129	-0.043	-0.106	2	.0745	0
		1.0	0.138	0.174	3	.0540	17.0
			1.0	0.003	4	.0668	53.0
				1.0	5	.192	100.0

0 percent propellant

1.0	0	-0.035	-0.142	-0.431	1	1.0	0
	1.0	-0.048	0.139	0.283	2	.070	0
		1.0	-0.007	0.023	3	.115	17.9
			1.0	-0.079	4	.145	53.0
				1.0	5	.0353	110.9

(b) Yaw direction

100 percent propellant + LES

					Mode, g	$\overline{M}_{gg}$	f_g, Hz
1.0	0	0.0009	-0.0119	-0.0196	1	1.0	0
	1.0	0.0080	-0.017	0.0175	2	.0438	0
		1.0	0.0917	-0.0601	3	.00846	14.0
			1.0	0.0807	4	.00459	27.1
				1.0	5	.112	55.3

100 percent propellant

1.0	0	-0.001	-0.094	-0.091	1	1.0	0
	1.0	0.000	-0.094	-0.030	2	.0159	0
		1.0	0.005	0.052	3	.0316	16.5
			1.0	0.049	4	.0793	50.4
				1.0	5	.115	87.2

50 percent propellant

1.0	0	0.139	-0.071	-0.043	1	1.0	0
	1.0	-0.156	-0.022	-0.108	2	.0208	0
		1.0	0.166	0.127	3	.0561	17.4
			1.0	-0.038	4	.182	48.2
				1.0	5	.102	97.7

0 percent propellant

1.0	0	0.120	-0.018	-0.567	1	1.0	0
	1.0	0.179	0.015	0.140	2	.0191	0
		1.0	0.134	0.186	3	.067	18.1
			1.0	-0.042	4	.573	48.3
				1.0	5	.0889	100.3

the uncoupled nature of these modes. The resonance at $f \approx 27$ Hz consists primarily of motion of the LES tower. Separate tests, not documented in this paper, showed that the CM-LES assembly, with the base of the CM fixed, has a first lateral bending frequency of 27.5 Hz.

Data from tests and analysis of configuration II with 100 percent propellant loading are shown in figures 16 and 18 and table 4. In this configuration, the model responds as a beam-type structure in only the lowest two modes. The correlation was fair between the analytical and experimental first-mode shapes and frequencies. The selection of the frequencies $f_p = 52.6$ Hz and $f_y = 50.4$ Hz as those of the second bending mode was somewhat arbitrary. As shown by the sweep plot of figure 16, significant vehicle response occurs throughout the frequency band between 45 and 60 Hz. The individual engine resonances shown in table 5 were identified experimentally from free-decay

TABLE 5.- DAMPED NATURAL FREQUENCIES OF UPPER-STAGE ENGINES

S-II engine locations (aft view)

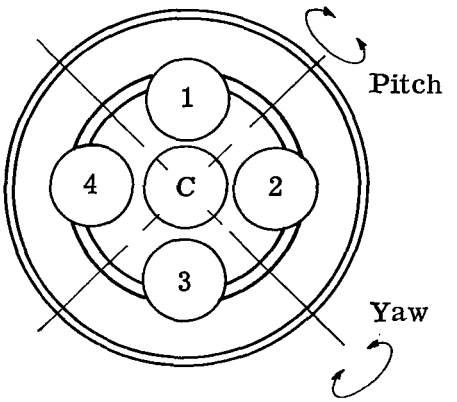

Engine	Damped natural frequency[a] with propellant loading (S-II) of –		
	100 percent	50 percent	0 percent
SII-1	53	53.5	55
SII-2	50	50.5	48
SII-3	53-57	57	58
SII-4	54	54-57	53-57
SII center	70.5	70.5	71
S-IVB	51	50	51

[a]Engine frequencies were determined from observations of the decay time history resulting from a sudden removal of a sinusoidal excitation. The excitation was varied until a decay with minimum beat was obtained. The frequency at which an engine vibrated while decaying was then defined as its damped natural frequency.

oscillograms. The frequency at which an individual engine resonated and decayed most smoothly was considered to be its resonant frequency. The vehicle response shape for each of these resonances has the general appearance of a second beam-type mode. This situation existed for all weight conditions of configuration II, in both pitch and yaw directions. A typical set of these experimental resonant deflection shapes is shown in figure 18 for the 100 percent propellant condition with yaw excitation. Also shown are the individual engine response amplitudes.

The analytical resonance at $f_a = 75.1$ Hz, shown in figure 17(c), is plotted with the yaw resonance at $f_y = 87.2$ Hz purely on the basis of deflection-shape similarity. The measured acceleration amplitudes were extremely small (for example, the amplitude at $x'/L' = 0.856$ was only 0.014g).

The pitch mode at $f_p = 98.2$ Hz shown in figure 17(d) is not a vehicle bending mode; rather, it was found to be a radial or shell mode in the S-II liquid-hydrogen tank. The yaw resonance at $f_y = 117.0$ Hz shown in figure 17(e) is primarily S-II engine motion, as may be seen in the sweep plot for this configuration (fig. 16).

Analytical and experimental dynamic response data for configuration II with 50 percent propellant are shown in figure 19 and in table 4. As in the 100-percent case, the lowest two modes have the classic beam-type shapes. The problem associated with isolation of the second mode from the coupled S-II engine-structure responses is again evident. Localized radial response patterns (discussed in a subsequent section) and component resonances are the chief contributors to the higher modes.

The data of figure 20 and table 4 for configuration II with 0 percent propellant, showed no significant deviations from the trends and patterns discussed for configuration II with 100 percent and 50 percent propellant. The figures show the analysis to be ineffective in predicting either frequency or deflection shape for other than the first two beam-type modes.

Configuration III

Configuration III consists of the model S-IVB stage (including the aft interstage) and the Apollo payload (including the IU, the LM-SLA assembly, and the CM-SM assembly). Data from the analysis and tests of this configuration for pitch and yaw excitation with three simulated propellant loadings are shown in figures 21 to 24 and table 6. For 100 percent propellant (figs. 21 and 22) the data show three distinct response peaks below $f = 115$ Hz. The pitch and yaw responses are similar in shape, but frequency differences of about 5 to 9 percent are shown. For both directions of excitation, the response peak at $f \approx 40$ Hz appears to contain at least two resonant peaks. In previous tests the S-IVB engine was shown to resonate in the neighborhood of $f \approx 50$ Hz. However, for this configuration the model response at $f \approx 40$ Hz is a combined first beam mode

TABLE 6.- GENERALIZED MASS MATRIX FOR CONFIGURATION III

(a) Pitch direction

100 percent propellant

					Mode, g	$\overline{M}_{gg}$	f_g, Hz
1.0	0	-0.098	0.279	-0.077	1	1.0	0
	1.0	0.166	-0.096	-0.132	2	.0682	0
		1.0	-0.190	-0.031	3	.0980	38.0
			1.0	0.674	4	.564	81.2
				1.0	5	.0307	99.0

50 percent propellant

1.0	0	-0.073	0.137	0.045	1	1.0	0
	1.0	0.025	-0.302	0.148	2	.0896	0
		1.0	0.164	-0.659	3	.104	40.4
			1.0	0.108	4	.0548	98.4
				1.0	5	.201	126.9

0 percent propellant

1.0	0	-0.048	-0.431	-0.066	1	1.0	0
	1.0	0.059	-0.018	-0.214	2	.101	0
		1.0	0.513	-0.084	3	.206	41.2
			1.0	0.138	4	.088	96.1
				1.0	5	.196	103.3

(b) Yaw direction

100 percent propellant

						Mode, g	$\overline{M}_{gg}$	f_g, Hz
1.0	0	-0.139	0.305	-0.133	0.256	1	1.0	0
	1.0	0.120	-0.277	0.469	0.070	2	.00614	0
		1.0	0.203	0.256	-0.434	3	.0104	40.4
			1.0	-0.106	0.636	4	.0151	76.3
				1.0	-0.051	5	.00954	100.3
					1.0	6	.0103	114.7

50 percent propellant

1.0	0	-0.083	0.455	0.156	1	1.0	0
	1.0	0.076	-0.272	-0.455	2	.00808	0
		1.0	0.149	-0.200	3	.269	43.3
			1.0	0.827	4	.600	86.1
				1.0	5	.256	91.1

0 percent propellant

1.0	0	-0.016	-0.177	-0.10	1	1.0	0
	1.0	0.020	-0.196	0.38	2	.00906	0
		1.0	-0.036	-0.709	3	.176	43.5
			1.0	0.243	4	.138	99.8
				1.0	5	.595	134.2

and engine resonance. The pitch and yaw response peaks at $f \approx 80$ Hz involve considerable LM motion not noted in the other configurations, the model center-line shape plotted in figure 22(b) being that of a second beam mode. At $f \approx 100$ Hz the second beam mode shape, shown in figure 22(c), again appears with reduced LM response. Consequently, the analytical beam mode calculations were compared with the experimental data at $f \approx 40$ Hz and $f \approx 100$ Hz since the analysis does not, in its present form, permit lateral LM response. In the present analytical representation of the model, the LM is assumed to be rigidly attached at the model center line.

Considering the limitations which the mass distribution imposes on a beam-type analysis (to be discussed in a subsequent section) and the rigid LM assumptions previously mentioned, the analytical frequencies and mode shapes agree reasonably well with experiment in this weight condition.

The test and analysis data for the 50-percent weight condition, shown in figure 23 and table 6, exhibit many of the same characteristics as those discussed for the 100-percent weight condition. The first beam modes in the pitch and yaw directions agree reasonably well with those predicted by the analysis. The LM pitch-response mode at $f = 86.1$ Hz (tabulated in the appendix but not plotted) is superimposed on a second beam-type center-line deflection shape.

The data from tests and analysis of the 0-percent propellant (burnout) condition for model configuration III are presented in figure 24 and table 6. The most significant departure from the trends for the other weight conditions lies in the fact that no LM pitch-response mode was measured in the region $f \approx 80$ Hz. The correlations in both mode shape and frequency plotted in figure 24(b) are poor; the analytically predicted frequency is about 30 percent too high, and the analytical deflections in the S-IVB tank region, $0.1 \leqq x''/L'' \leqq 0.5$, are much lower than those measured. Considerable shell response was noted in the empty tanks, the IU, and the regions of the support cradle and aft interstage at frequencies above 90 Hz. Typical shell response patterns are illustrated in figure 25.

The one-dimensional mathematical model will not predict nonbeam resonances such as the shell responses illustrated in figure 25. This figure shows some of the typical measured radial response patterns from both configurations II and III. The measured nonbeam resonances are identified as S-II tank wall bulge, IU shell distortion, and support-cradle ring modes. Also noted on the figure are the configuration number, the simulated propellant loading, and the excitation frequency associated with each deflection pattern. Since the mathematical model does not permit two-dimensional motion, no calculations are available for comparison with shell and shell-like motion. From the preceding discussion, it would appear that either two- or three-dimensional representations would be required to predict a large number of lateral modes of the model. In most

preliminary analyses for control-system stability, wind loads, or similar applications, only the lower beam-type modes are required. Thus, a one-dimensional analysis of the type presented will be adequate to meet such requirements.

Measured Damping Values

Representative damping values measured on the three configurations during the yaw-plane tests are given in table 7 together with associated resonant frequencies. The damping values are generally in the range of $\frac{1}{2}$ to $1\frac{1}{2}$ percent of critical damping. Similar results were obtained from pitch-plane tests.

TABLE 7.- RESONANT FREQUENCIES AND DAMPING FOR EXCITATION IN YAW DIRECTION

Configuration I						Configuration II								Configuration III					
100%		50%		0%		100% + LES		100%		50%		0%		100%		50%		0%	
f, Hz	g	f, Hz	g	f, Hz	g	f, Hz	g	f, Hz	g	f, Hz	g	f, Hz	g	f, Hz	g	f, Hz	g	f, Hz	g
8.6	0.011	9.1	0.020	9.7	0.017	14.0	0.020	16.5	0.025	17.4	0.020	18.1	0.020	40.4	0.025	43.5	0.025	43.5	0.025
15.5	.011	17.9	.015	19.4	.010	26.9	.020	----	----	----	----	----	----	76.3	.034	86.1	----	----	----
24.7	.018	25.9	.013	---	----	50.0	----	50.4	.020	48.2	.012	48.2	----	100.3	.020	91.2	.035	99.8	.021
29.8	.013	30.0	.013	28.2	.010	----	----	50.8	.12	51.3	.020	50.0	----	114.7	----	----	----	----	----
57.2	.011	51.7	.018	---	----	52.0	----	52.1	.12	52.8	.020	----	----	----	----	132.6	.028	134.2	.024
75.8	.025	72.6	.005	---	----	53.0	----	53.5	----	53.5	.030	53.5	----	----	----	145.4	.020	----	----
---	----	87.2	.017	---	----	56.3	.050	54.4	.005	53.9	----	53.9	----	----	----	----	----	----	----
---	----	---	----	---	----	57.0	----	57.0	----	57.2	----	56.8	----	----	----	----	----	----	----
---	----	---	----	---	----	71.0	----	70.5	.025	70.0	----	70.0	----	----	----	----	----	----	----
---	----	---	----	---	----	---	----	87.2	----	----	----	----	----	----	----	----	----	----	----
---	----	---	----	---	----	98.0	----	99.0	----	97.7	----	100.3	.020	----	----	----	----	----	----
---	----	---	----	---	----	116.0	----	117.0	----	118.3	.023	123.0	----	----	----	----	----	----	----

Applicability of Mathematical Model

Large liquid masses concentrated over short distances along the length of the structure, particularly in the second and third stages, leave the analyst little control over the mathematical mass distribution. Sketch (g) illustrates this natural distribution.

For configuration I, six major mass concentrations exist. They are: S-IC engines and fuel, S-IC lox, S-II lox, S-IVB lox, LM-SLA, and CM-SM. With this type of natural mass lumping, a beam-type analysis would be expected to predict no more than five modes. For configuration II natural lumping produces four major mass concentrations; thus a beam analysis could be expected to predict no more than two modes. In the same context, the analysis would predict only one mode for configuration III. In actuality, the present analysis contains a greater number of mass points than are shown in the sketches; however, because of the relative magnitudes of these masses, the sketched configurations are realistic.

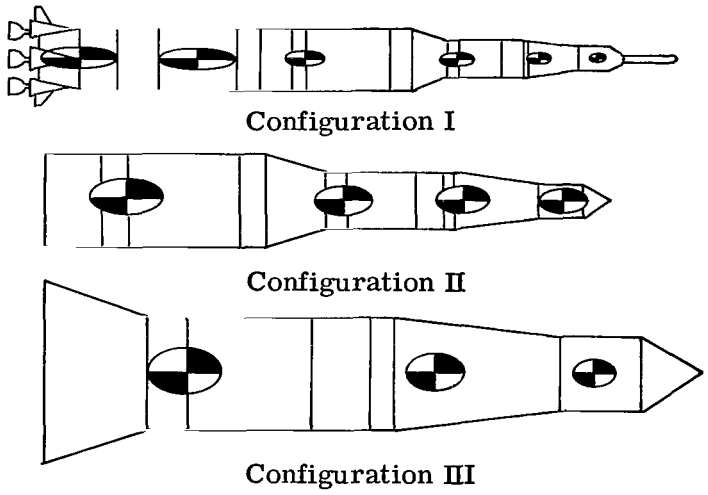

Sketch (g)

Secondary Effects

In the mathematical representation, a number of assumptions were made which were expected to have a second-order effect on the basic beam response. Their importance can be assessed by comparing the measured results and the calculations made with and without the second-order effects.

Engine branches.- Engine resonances for the three stages fall in the range of 40 to 60 Hz. Since the first three beam modes of configuration I are less than 40 Hz, the effect of engine motion on these modes was not studied. In contrast to configuration I, the engine modes for configurations II and III have a decided effect on the interpretation of the beam-mode shapes since the second lateral mode of configuration II occurs in or near the S-II engine frequency band and the first lateral mode and the engine mode of configuration III are at proximate frequencies. The changes in modal frequency resulting from the assumption that the engines are rigidly attached to the model are illustrated in the table shown at right.

Configuration	Calculated frequency, Hz, for –	
	Flexible engine	Rigid engine
II-50%	18.64	18.68
	45.2	-----
	51.71	-----
	58.7	57.2
	87.2	84.8
III-100%	43.1	43.1
	45.3	-----
	106.1	105.8
	135.3	135.2

Liquid slosh.- No provision was made for experimentally measuring liquid motion. Therefore no direct correlation between experimental and analytical slosh-mass amplitude data was possible. Nevertheless, calculations were performed with and without sloshing to assess the magnitude of the effect. Typical results for configuration I with 100 percent propellant and configuration II with 50 percent propellant are given in the following table and show that the inclusion of slosh raises the frequencies of the beam-type modes from 5 to 15 percent over those obtained for the nonsloshing case. The magnitude of the change varies with the particular configuration.

Configuration	Calculated frequency, Hz, with –	
	Slosh	No slosh
I-100%	20.1	19.1
	59.2	58.0
	86.6	82.5
II-50%	9.15	8.92
	17.30	16.85
	26.16	25.92
	33.16	32.42

Ineffective skin.- In order to examine the influence of reduced stiffness due to the assumed inability of thin skin in certain areas to support compression loads, the model structure was analyzed with the assumption and without the assumption according to the methods discussed in the "Analysis" section. Typical results from these calculations are presented in the table at the left for the empty configuration II with rigid engines. The reduction in section stiffness lowers all system natural frequencies, the greatest change being a 2-percent reduction in the first mode.

Calculated frequency, Hz, with –	
Effective skin	Ineffective skin
20.77	19.45
53.84	51.69
87.05	85.31

Shear deformation.- All analytical results shown in this paper include shear deformation effects. One configuration I loading condition (100 percent) was analyzed with shear deformation omitted, and it was found that all calculated beam frequencies were increased by 10 to 20 percent.

SUMMARY OF RESULTS

A 1/10-scale replica model of the Apollo/Saturn V launch vehicle has been tested and analyzed to determine its lateral vibration characteristics while suspended to simulate

free-free boundary restraints. Several propellant loadings were investigated for each of three model configurations simulating first-stage burn (configuration I), second-stage burn (configuration II), and third-stage burn (configuration III). Tests were conducted in both the pitch and yaw directions. A lumped-parameter vibration analysis employing the transfer matrix method was used to calculate the uncoupled natural lateral modes and frequencies of the system. Parameter studies were conducted to investigate analytically the effects of engine flexibility, liquid slosh, decreased stiffness due to ineffective skin, and shear deformation effects on the modal behavior of the system. Salient results of the combined analysis and experiment may be summarized as follows:

1. The model in the first-stage burn configuration responds to lateral excitation primarily as a beam and is therefore amenable to beam analysis. Correlation between predictions of the transfer matrix analysis and the measured response frequencies and shapes is good for model frequencies below 30 Hz.

2. The model in the second-stage burn configuration behaves as a beam only for the lowest two modes. The S-II engine branch-mass resonances which occur at frequencies proximate to the second beam mode tend to obscure the second beam mode. At higher frequencies, shell responses occur in the S-II liquid hydrogen tank and, at still higher frequencies, the payload shell responses predominate. The inclusion of shell modes and engine branch modes in the analysis would be required to predict adequately the behavior of this configuration at frequencies above the fundamental bending mode.

3. In the third-stage burn configuration, the lowest structural mode is a combination of a body beam mode and the S-IVB engine lateral mode. At higher frequencies, radial shell responses of the S-IVB tanks, instrument unit, and Saturn LM adapter preclude the existence of uncoupled beam-type structural modes. The one-dimensional analysis used in the present paper is inadequate for more than one mode of this configuration.

4. In the calculation of beam-bending stiffness properties, stiffness reduction due to loss of skin effectiveness for compression loads in sections having thin-gage skin-stringer construction should be considered. In the present analysis, however, the effect was minor.

5. The inclusion of liquid slosh in the analysis increased system resonant frequencies. This change degraded the correlation between tests and analysis.

6. Measured damping values generally are in the range of $\frac{1}{2}$ to $1\frac{1}{2}$ percent of critical damping.

Langley Research Center,
National Aeronautics and Space Administration,
Langley Station, Hampton, Va., February 10, 1970.

APPENDIX

SUMMARY OF NORMALIZED RESONANT RESPONSES

Numerical data from both pitch and yaw tests of the 1/10-scale Apollo/Saturn V model are given in tables A-1 to A-10. Data are presented for three simulated propellant loadings in each of three model configurations. The data consist of the normalized amplitude of the fundamental harmonic, its phase angle with respect to the input force, and the magnitude of the normalization constant for accelerations measured by individual transducers at discrete resonant frequencies. Also given are the value of each resonant frequency, the peak magnitude of the sinusoidal input force, and the normalized model station at which the transducer was located.

The phase angle tabulated is the angle between the input force vector and the total response vector, measured in the counterclockwise direction. The acceleration amplitudes of the various transducers are normalized for the most part at the tip or forward station of the model. Low tip amplitudes in some modes, however, made alternate normalization stations desirable. The normalization stations are noted in footnotes on each table.

TABLE A-1.- NORMALIZED RESONANT RESPONSE OF CONFIGURATION I WITH 100-PERCENT PROPELLANT LOAD

(a) Pitch direction

Normalized model station, x/L		Frequency = 9.1 Hz Force = 19.1 N a_{ref} = 0.417		Frequency = 16.0 Hz Force = 18.7 N a_{ref} = 0.961		Frequency = 24.8 Hz Force = 18.9 N a_{ref} = 1.118		Frequency = 30.4 Hz Force = 19.6 N a_{ref} = 0.611	
		Normalized amplitude (a)	Phase angle, deg (b)	Normalized amplitude (a)	Phase angle, deg (b)	Normalized amplitude (a)	Phase angle, deg (b)	Normalized amplitude (a)	Phase angle, deg (b)
0.029		0.113	245	-0.086	75	0.037	250	-0.024	59
.078		.091	251	-.059	75	.021	255	-.020	67
.151		.048	249	-.015	90	-.004	48	.005	164
.200		.024	252	.016	247	-.022	62	.015	223
.346		----	---	-----	---	----	---	-----	---
.412		-.045	78	.011	262	.041	243	-.041	47
.432		-.218	65	.002	24	.054	244	-.047	48
.565		-.029	74	-.087	72	.038	247	.008	209
.648		.007	215	-.163	74	-.011	48	.090	245
.734		.105	244	-.172	74	-.090	63	.056	224
.772		.177	245	-.129	74	-.117	65	-.006	20
.868		.458	246	.137	251	-.102	68	-.195	45
.981		1.000	247	1.000	253	1.000	247	1.000	224
S-1C engines									
-0.024	Center	0.144	124	-0.140	75	-0.088	110	-0.090	58
	1	.139	237	-.165	75	.130	253	-.195	67
	2	.125	123	-.139	74	-.089	108	-.094	62
	3	.137	124	-.144	74	-.098	109	-.118	60
	4	.146	124	-.142	75	-.088	109	-.093	59
S-II engines									
0.369	Center	-0.062	56	-0.029	101	-0.052	117	-0.077	48
	1	-.067	56	-.032	100	-.061	116	-.096	50
	2	-.067	60	-.044	90	-.265	68	.244	155
	3	-.057	57	-.031	99	-.148	90	-.101	51
	4	-.067	55	.031	258	.058	244	-.087	51
S-IVB engine									
0.600		0.053	240	-0.202	74	0.021	263		
LM									
0.775		0.170	250	-0.124	75	-0.129	66		
.807		-.240	110	-.062	77	-.140	67		

[a]Normalized with respect to amplitude at forward end of LES.

[b]Phase angle of acceleration relative to input force.

TABLE A-1.- NORMALIZED RESONANT RESPONSE OF CONFIGURATION I

WITH 100-PERCENT PROPELLANT LOAD – Concluded

(b) Yaw direction

Normalized model station, x/L		Frequency = 8.6 Hz Force = 12.0 N a_{ref} = 0.377 g = 0.011		Frequency = 15.5 Hz Force = 9.8 Hz a_{ref} = 0.656 g = 0.011		Frequency = 24.7 Hz Force = 11.4 N a_{ref} = 0.485 g = 0.018		Frequency = 29.8 Hz Force = 11.3 N a_{ref} = 0.370 g = 0.013	
		Normalized amplitude (a)	Phase angle, deg (b)	Normalized amplitude (a)	Phase angle, deg (b)	Normalized amplitude (a)	Phase angle, deg (b)	Normalized amplitude (a)	Phase angle, deg (b)
0.029		0.098	126	-0.091	151	0.344	163	-0.024	161
.078		.074	126	-.062	152	.023	170	-----	---
.151		----	---	-----	---	-.004	290	.005	296
.200		----	---	.018	323	-----	---	-----	---
.346		----	---	.046	334	.002	48	-----	---
.412		----	---	.015	344	.039	150	-----	---
.432		-.064	306	-----	---	.049	152	-.054	149
.565		----	---	-.091	148	.039	153	-----	---
.648		----	---	-.175	150	-.008	276	.100	327
.734		.101	121	-.166	150	-.074	331	.059	332
.772		.180	121	-.139	148	-.109	333	±.008	15
.868		.456	124	.119	326	-.113	337	-.181	145
.981		1.000	126	1.000	329	1.000	153	1.000	324
S-IC engines									
-0.024	Center	0.138	125	-0.152	155	0.082	160	-0.089	160
	1	.133	125	-.145	154	.078	163	-.078	158
	2	.133	124	-.149	154	.089	167	-.097	160
	3	.138	125	-.149	155	.076	161	-.076	163
	4	.138	125	-.151	155	.087	164	-.097	160
S-II engines									
0.369	Center	----	---	-----	---	0.041	144	-0.068	146
	1	----	---	-----	---	-----	---	-----	---
	2	----	---	-----	---	-----	---	-----	---
	3	----	---	-----	---	-----	---	-----	---
	4	----	---	-----	---	-----	---	-----	---
S-IVB engine									
0.600		0.066	128	-0.221	151	0.037	175	0.235	327
LM									
0.775		0.183	122	-0.133	154	-0.122	333	-0.008	83
.807		.252	123	-.082	156	-.138	335	-.054	134

[a]Normalized with respect to amplitude at forward end of LES.

[b]Phase angle of acceleration relative to input force.

TABLE A-2.- NORMALIZED RESONANT RESPONSE OF CONFIGURATION I WITH 50-PERCENT PROPELLANT LOAD

(a) Pitch direction

Normalized model station, x/L		Frequency = 9.5 Hz Force = 14.7 N a_{ref} = 0.685		Frequency = 18.0 Hz Force = 11.1 N a_{ref} = 1.030		Frequency = 25.8 Hz Force = 11.6 N a_{ref} = 0.489		Frequency = 30.5 Hz Force = 16.0 N a_{ref} = 0.811	
		Normalized amplitude (a)	Phase angle, deg (b)	Normalized amplitude (a)	Phase angle, deg (b)	Normalized amplitude (a)	Phase angle, deg (b)	Normalized amplitude (a)	Phase angle, deg (b)
0.029		0.099	342	-0.097	333	0.043	252	-0.031	154
.078		.073	344	-.065	334	.024	270	-.017	164
.151		.033	348	-.014	358	-.014	77	.011	297
.200		.012	352	.019	144	-.037	71	.025	318
.346		-----	---	-----	---	-----	---	-----	---
.412		-.069	159	.045	153	.029	245	-.042	136
.432		-.072	160	.036	153	.041	247	-.050	137
.565		-.063	163	-.052	331	.039	249	.009	292
.648		-.034	169	-.142	332	.004	270	.094	313
.734		.069	336	-.180	333	-.072	68	.057	313
.772		.130	340	-.147	334	-.104	70	-.004	90
.868		.439	341	.072	149	-.119	77	-.197	133
.981		1.000	341	1.000	152	1.000	251	1.000	313
S-IC engines									
-0.024	Center	0.140	17	-0.177	27	-0.127	99	0.117	332
	1	.152	343	-.212	333	.184	264	-.274	161
	2	.136	17	-.176	28	-.127	97	.127	335
	3	.136	18	-.184	28	-.143	98	.158	334
	4	.140	17	-.178	27	-.125	99	.120	332
S-II engines									
0.369	Center	-0.066	160	0.067	153	-0.033	108	0.070	313
	1	-.067	159	.072	153	-.037	107	.088	317
	2	-.082	162	.164	166	.215	14	-.249	68
	3	-.073	162	.087	163	-.041	102	.100	319
	4	-.067	159	.071	153	.035	256	-.079	136
S-IVB engine									
0.600		-0.085	163	-0.180	334	0.049	270	0.245	321
LM									
0.775		0.130	340	-0.147	334	-0.110	79	-0.010	115
.807		.142	340	-.151	333	-.127	79	.068	310

[a]Normalized with respect to amplitude at forward end of LES.

[b]Phase angle of acceleration relative to input force.

TABLE A-2.- NORMALIZED RESONANT RESPONSE OF CONFIGURATION I

WITH 50-PERCENT PROPELLANT LOAD – Concluded

(b) Yaw direction

Normalized model station, x/L		Frequency = 9.1 Hz Force = 12.4 N a_{ref} = 0.531 g = 0.020		Frequency = 17.9 Hz Force = 13.7 N a_{ref} = 0.975 g = 0.015		Frequency = 25.9 Hz Force = 12.9 N a_{ref} = 1.210 g = 0.013		Frequency = 30.0 Hz Force = 13.1 N a_{ref} = 0.649 g = 0.013	
		Normalized amplitude (a)	Phase angle, deg (b)	Normalized amplitude (a)	Phase angle, deg (b)	Normalized amplitude (a)	Phase angle, deg (b)	Normalized amplitude (a)	Phase angle, deg (b)
0.029		0.096	93	-0.103	150	0.050	302	-0.039	258
.078		.072	93	-.070	150	.031	303	-.020	265
.151		.026	98	-----	---	-----	---	.012	54
.200		-----	---	.021	325	-----	---	.034	65
.346		-----	---	.065	320	-----	---	-----	---
.412		-.068	270	.052	322	.015	289	-.052	246
.432		-.072	271	.041	333	.025	292	-.062	245
.565		-.064	274	-.051	144	.039	299	-----	---
.648		-.041	278	-.146	148	-----	---	.106	63
.734		.058	87	-.170	148	-.039	112	.068	66
.772		.126	90	-.159	150	-.080	116	.014	77
.868		.420	92	.046	325	-.135	120	-.185	243
.981		1.000	94	1.000	329	1.000	298	1.000	61
S-IC engines									
-0.024	Center	0.136	94	-0.195	141	0.131	302	-0.139	257
	1	.128	94	-.184	140	.119	302	-.125	256
	2	.128	93	-.189	140	.131	303	-.160	254
	3	.136	95	-.192	141	-.122	122	-.126	255
	4	.132	94	-.195	140	-.136	122	-.157	256
S-II engines									
0.369	Center	0.064	266	0.075	316	0.116	279	-0.072	240
	1	-----	---	-----	---	-----	---	-----	---
	2	-----	---	-----	---	-----	---	-----	---
	3	-----	---	-----	---	-----	---	-----	---
	4	-----	---	-----	---	-----	---	-----	---
S-IVB engine									
0.600		-0.096	274	-0.198	139	-0.901	124	-0.285	244
LM									
0.775		0.137	90	-0.168	140	-0.917	118	0.009	103
.807		.209	92	-.129	140	-.117	119	-.046	236

[a]Normalized with respect to amplitude at forward end of LES.

[b]Phase angle of acceleration relative to input force.

TABLE A-3.- NORMALIZED RESONANT RESPONSE OF CONFIGURATION I WITH 0-PERCENT PROPELLANT LOAD

(a) Pitch direction

Normalized model station, x/L		Frequency = 10.0 Hz, Force = 19.1 N, a_{ref} = 0.717		Frequency = 19.3 Hz, Force = 13.8 N, a_{ref} = 1.198		Frequency = 29.0 Hz, Force = 14.2 N, a_{ref} = 0.690	
		Normalized amplitude (a)	Phase angle, deg (b)	Normalized amplitude (a)	Phase angle, deg (b)	Normalized amplitude (a)	Phase angle, deg (b)
0.029		0.146	36	-0.077	354	0.023	8
.078		.119	36	-.052	357	.016	38
.151		.075	36	-.013	19	-.014	90
.200		.049	38	.013	138	-.017	104
.346		-.006	270	.008	235	-----	---
.412		-.049	212	.060	166	-.019	139
.432		-.054	213	.057	167	-.014	141
.565		-.063	216	-.027	346	.028	317
.648		-.047	218	-.121	346	.068	320
.734		.039	24	-.169	347	.014	336
.772		.102	27	-.160	348	-.039	131
.868		.399	31	.026	156	-.071	138
.981		1.000	32	1.000	167	1.000	318
S-IC engines							
-0.024	Center	0.194	37	-0.148	6	0.070	8
	1	.212	37	-.181	354	.129	12
	2	.192	37	-.146	6	.072	8
	3	.198	36	-.159	6	.088	8
	4	.195	38	-.149	6	.071	8
S-II engines							
0.369	Center	-0.046	148	0.086	166	-0.038	143
	1	-.043	151	.094	167	-.045	145
	2	-.045	153	.204	179	-.151	76
	3	-.051	148	.146	176	-.054	148
	4	-.046	207	.091	167	-.043	144
S-IVB engine							
0.600		-0.092	215	-0.146	350	0.256	324
LM							
0.775		0.107	30	-0.165	346	-0.049	140
.807		.181	31	-.129	12	-.094	143

[a]Normalized with respect to amplitude at forward end of LES.

[b]Phase angle of acceleration relative to input force.

TABLE A-3.- NORMALIZED RESONANT RESPONSE OF CONFIGURATION I

WITH 0-PERCENT PROPELLANT LOAD – Concluded

(b) Yaw direction

Normalized model station, x/L		Frequency = 9.7 Hz Force = 17.8 N a_{ref} = 0.482 g = 0.017		Frequency = 19.4 Hz Force = 10.4 N a_{ref} = 0.892 g = 0.010		Frequency = 28.2 Hz Force = 10.2 N a_{ref} = 0.572 g = 0.010	
		Normalized amplitude (a)	Phase angle, deg (b)	Normalized amplitude (a)	Phase angle, deg (b)	Normalized amplitude (a)	Phase angle, deg (b)
0.029		0.149	154	-0.075	151	0.023	190
.078		.118	155	-.049	152	.016	204
.151		.056	159	-.009	176	-.009	263
.200		.048	162	.016	306	-----	---
.346		-.031	298	.048	322	-.023	325
.412		-.058	314	.061	324	-.017	332
.432		-.058	325	.058	324	-.016	335
.565		-.064	324	-.028	140	.030	148
.648		-.054	336	-----	---	.070	150
.734		.044	145	-.159	144	.012	167
.772		.098	160	-.156	144	-.038	323
.868		.398	151	.012	310	-.163	329
.981		1.000	153	1.000	324	1.000	148
S-IC engines							
-0.024	Center	0.216	147	-0.142	149	0.066	184
	1	.212	142	-.135	148	.061	182
	2	.210	140	-.139	148	.072	184
	3	.214	148	-.138	149	.061	184
	4	.216	144	-.142	148	.073	183
S-II engines							
0.369	Center	-0.050	307	0.081	319	-----	---
	1	-----	---	-----	---	-----	---
	2	-----	---	-----	---	-----	---
	3	-----	---	-----	---	-----	---
	4	-----	---	-----	---	-----	---
S-IVB engine							
0.600		0.114	143	0.298	322	0.175	150
LM							
0.775		0.129	137	-0.157	143	-0.049	325
.807		.210	141	-.131	143	-.089	327

[a]Normalized with respect to amplitude at forward end of LES.

[b]Phase angle of acceleration relative to input force.

TABLE A-4.- NORMALIZED RESONANT RESPONSE OF CONFIGURATION II WITH 100-PERCENT PROPELLANT LOAD PLUS LAUNCH ESCAPE SYSTEM

(a) Pitch direction

Normalized model station, x'/L'	Frequency = 14.0 Hz Force = 16.9 N a_{ref} = 0.597		Frequency = 27.8 Hz Force = 16.0 N a_{ref} = 0.799		Frequency = 55.8 Hz Force = 15.6 N a_{ref} = 0.268	
	Normalized amplitude (a)	Phase angle, deg (b)	Normalized amplitude (a)	Phase angle, deg (b)	Normalized amplitude (a)	Phase angle, deg (b)
0.002	0.085	338	-0.031	303	0.026	288
.077	.047	344	-.015	310	.011	307
.109	.032	345	-.010	323	.007	13
.190	-.003	155	.009	74	-.019	74
.244	-.030	163	.019	97	-.026	90
.317	-.062	164	.028	103	-.022	104
.371	-.089	155	.038	107	-.030	114
.448	-.122	163	.048	110	-.026	133
.581	-.101	165	-.014	270	.067	292
.641	-.057	167	-.061	285	.101	295
.792	.223	341	-.160	289	-.041	125
.970	1.000	336	1.000	110	1.000	300
S-II engines						
0.009 Center	0.080	20	0.426	32	-0.276	69
0.009 1	.084	342	.144	323	-.172	136
0.009 2	.084	338	.180	325	-.597	141
0.009 3	.094	22	.215	35	-1.321	60
0.009 4	.082	340	.084	318	-.601	58
S-IVB engine						
0.372	-0.149	156	0.217	130	0.672	301
LM						
0.647	-0.054	159	-0.073	287	0.127	300
.696	.012	44	.109	71	-.116	59

[a]Normalized with respect to amplitude at forward end of CM.

[b]Phase angle of acceleration relative to input force.

TABLE A-4.- NORMALIZED RESONANT RESPONSE OF CONFIGURATION II WITH 100-PERCENT PROPELLANT LOAD PLUS LAUNCH ESCAPE SYSTEM – Concluded

(b) Yaw direction

Normalized model station, x'/L'	Frequency = 14.0 Hz Force = 16.4 N a_{ref} = 1.040 g = 0.020		Frequency = 26.9 Hz Force = 16.9 N a_{ref} = 1.190 g = 0.020		Frequency = 56.3 Hz Force = 14.2 N a_{ref} = 0.066 g = 0.050	
	Normalized amplitude (a)	Phase angle, deg (b)	Normalized amplitude (a)	Phase angle, deg (b)	Normalized amplitude (a)	Phase angle, deg (b)
0.002	0.074	320	-0.025	298	0.151	265
.077	.041	315	-.013	295	.076	259
.109	.028	313	-.007	291	.030	231
.190	-.009	160	.007	126	-.076	90
.244	-.033	144	.018	122	-.151	90
.317	-.065	143	.029	121	-.182	80
.371	-.092	152	.036	119	-.197	67
.448	-.130	141	.047	120	-.167	130
.496	-.123	155	.029	128	.167	198
.581	-.091	143	-.019	277	.333	264
.641	-.046	134	-.066	290	.485	270
.696	.030	317	-.114	293	.439	274
.763	.145	329	-.162	295	.061	270
.827	.310	318	-.127	298	-.485	100
.970	1.000	330	1.000	113	1.000	277
S-II engines						
0.009 Center	0.072	23	0.029	63	0.591	97
0.009 1	.076	337	-.036	297	2.864	84
0.009 2	.077	338	-.039	298	1.136	79
0.009 3	.074	23	.035	65	6.212	84
0.009 4	.076	23	.035	64	1.606	54
S-IVB engine						
0.372	-0.167	200	-0.127	239	-2.939	305
LM						
0.647	0.040	340	0.077	112	0.636	94
.696	-.019	133	.112	113	.636	96

[a]Normalized with respect to amplitude at forward end of LES.

[b]Phase angle of acceleration relative to input force.

TABLE A-5.- NORMALIZED RESONANT RESPONSE OF CONFIGURATION II WITH 100-PERCENT PROPELLANT LOAD

(a) Pitch direction

Normalized model station, x'/L'	Frequency = 16.4 Hz Force = 12.4 N a_{ref} = 0.520		Frequency = 52.6 Hz Force = 17.8 N a_{ref} = 0.114		Frequency = 98.2 Hz Force = 16.0 N a_{ref} = 0.010	
	Normalized amplitude (a)	Phase angle, deg (b)	Normalized amplitude (a)	Phase angle, deg (b)	Normalized amplitude (a)	Phase angle, deg (b)
0.002	0.154	151	-0.114	181	-7.5	201
.077	.083	148	-.044	187	-3.7	201
.109	.046	148	-.009	235	-.7	201
.190	-.029	334	.088	343	8.0	86
.244	-.083	331	.149	345	10.0	139
.317	-.144	331	.132	340	3.5	0
.371	-.198	332	.158	340	-1.3	314
.448	-.267	331	.202	4	-1.0	313
.581	-.167	332	-.342	175	.1	127
.641	-.037	313	-.596	177	-.1	332
.792	.654	150	.193	351	-.1	270
.856	1.000	152	1.000	358	1.000	136
S-II engines						
0.009 Center	0.158	152	-0.518	158	-6.8	202
0.009 1	-.162	331	1.140	6	-6.4	199
0.009 2	-----	---	-----	---	------	---
0.009 3	.179	151	-2.540	157	7.1	79
0.009 4	.161	151	-1.456	175	6.3	19
S-IVB engine						
0.372	-0.373	340	2.482	156	-1.3	314
LM						
0.647	-0.021	353	-0.754	176	------	---
.696	.150	149	-.711	178	0.1	40

[a]Normalized with respect to amplitude at forward end of CM.

[b]Phase angle of acceleration relative to input force.

TABLE A-5.- NORMALIZED RESONANT RESPONSE OF CONFIGURATION II

WITH 100-PERCENT PROPELLANT LOAD – Concluded

(b) Yaw direction

Normalized model station, x'/L'		Frequency = 16.5 Hz Force = 12.0 N a_{ref} = 0.373 g = 0.025		Frequency = 50.4 Hz Force = 15.6 N a_{ref} = 0.373 g = 0.020		Frequency = 87.2 Hz Force = 20.0 N a_{ref} = 0.014 g = ----		Frequency = 117.0 Hz Force = 17.8 N a_{ref} = 0.192 g = ----	
		Normalized amplitude (a)	Phase angle, deg (b)	Normalized amplitude (a)	Phase angle, deg (b)	Normalized amplitude (a)	Phase angle, deg (b)	Normalized amplitude (c)	Phase angle, deg (b)
0.002		0.147	345	-0.135	263	3.071	360	1.000	95
.077		.078	342	-.056	258	1.285	352	.333	98
.109		.048	346	-.011	269	.357	331	.151	101
.190		-.024	154	.090	80	-1.285	188	-.099	190
.244		-.078	157	.157	76	-2.428	176	-.229	205
.317		-.150	158	.202	76	-3.000	165	-.224	198
.371		-.196	161	.191	79	-2.928	139	-.255	162
.448		-.268	160	.180	105	-.786	131	-.104	151
.496		-.252	161	.101	182	.857	318	.021	354
.581		-.139	161	-.360	256	.357	342	.015	357
.641		-.005	200	-.561	260	.071	32	.010	0
.696		.188	335	-.528	265	-.428	137	0	0
.763		.220	338	-.146	269	-.571	140	-.005	174
.827		.826	339	.596	83	.500	20	.010	33
.856		1.000	339	1.000	82	1.000	338	.005	25
				S-II engines					
0.009	Center	0.153	20	0.292	105	-8.428	176	0.656	83
	1	.163	341	-1.326	261	-3.428	175	-.370	277
	2	.166	340	2.393	43	-2.571	182	.354	279
	3	.161	21	.865	97	-3.357	179	.427	86
	4	.163	20	1.011	93	-4.286	165	.406	85
				S-IVB engine					
0.372		-0.418	165	-3.652	237	2.071	237	0.042	205
				LM					
0.647		-0.016	116	0.708	84	0.071	330	-0.005	180
.696		-.172	156	.685	86	.428	19	.010	0

[a]Normalized with respect to amplitude at forward end of CM.

[b]Phase angle of acceleration relative to input force.

[c]Normalized with respect to amplitude at aft end of S-II.

TABLE A-6.- NORMALIZED RESONANT RESPONSE OF CONFIGURATION II WITH 50-PERCENT PROPELLANT LOAD

(a) Pitch direction

Normalized model station, x'/L'	Frequency = 17.0 Hz Force = 16.0 N a_{ref} = 0.510		Frequency = 53.0 Hz Force = 16.9 N a_{ref} = 0.150		Frequency = 100.0 Hz Force = 14.7 N a_{ref} = 0.013	
	Normalized amplitude (a)	Phase angle, deg (b)	Normalized amplitude (a)	Phase angle, deg (b)	Normalized amplitude (a)	Phase angle, deg (b)
0.002	0.214	160	-0.073	163	7.770	213
.077	.129	158	-.020	161	3.615	209
.109	.084	156	-----	---	.231	198
.190	.008	90	.060	343	±13.77	118
.244	-.055	350	.120	345	9.85	152
.317	-.127	346	.113	339	-4.46	17
.371	-.192	344	.153	344	-3.08	359
.448	-.221	344	.200	7	-9.23	350
.581	-.186	345	-.327	179	±.231	90
.641	-.073	342	-.573	180	±.154	90
.792	.637	162	.193	358	.462	235
.856	1.000	162	1.000	360	1.000	235
S-II engines						
0.009 Center	0.216	159	-0.407	137	7.08	32
0.009 1	.217	158	-.967	165	6.85	31
0.009 2	-----	---	-----	---	------	---
0.009 3	.249	158	-2.053	179	7.15	31
0.009 4	.222	158	-1.227	156	6.62	32
S-IVB engine						
0.372	-0.386	354	-2.006	154	1.000	346
LM						
0.647	-0.047	353	-0.747	179	±0.076	90
.696	.127	157	-.713	179	.076	37

[a]Normalized with respect to amplitude at forward end of CM.

[b]Phase angle of acceleration relative to input force.

TABLE A-6.- NORMALIZED RESONANT RESPONSE OF CONFIGURATION II

WITH 50-PERCENT PROPELLANT LOAD – Concluded

(b) Yaw direction

Normalized model station, x'/L'	Frequency = 17.4 Hz Force = 11.6 N a_{ref} = 0.346 g = 0.020		Frequency = 48.2 Hz Force = 11.6 N a_{ref} = 0.046 g = 0.012		Frequency = 97.7 Hz Force = 16.0 N a_{ref} = 0.100 g = ----		Frequency = 118.3 Hz Force = 16.0 N a_{ref} = 0.387 g = 0.023	
	Normalized amplitude (a)	Phase angle, deg (b)	Normalized amplitude (a)	Phase angle, deg (b)	Normalized amplitude (c)	Phase angle, deg (b)	Normalized amplitude (c)	Phase angle, deg (b)
0.002	0.283	252	-0.174	177	1.000	56	1.000	348
.077	.188	251	-.087	171	.47	54	.351	348
.109	.150	250	-.043	167	.01	353	.147	347
.190	.052	246	.043	14	-.68	233	-.220	161
.244	-.017	90	.109	2	-1.18	226	-.783	162
.317	-.101	76	.174	359	-1.01	221	-.519	150
.371	-.168	81	.174	27	-.73	201	-.465	137
.448	-.277	75	.087	57	-.20	191	-.163	134
.496	-.257	77	-.130	190	.16	26	.054	360
.581	-.159	76	-.391	191	.05	23	.016	291
.641	-.035	97	-.565	190	.01	35	±.008	270
.696	.165	251	-.500	193	-.04	207	.002	244
.763	.471	252	-.109	199	-.03	206	-.002	64
.827	.824	253	.630	6	.04	108	-.008	113
.856	1.000	253	1.000	8	.11	37	-.005	161
S-II engines								
0.009 Center	-0.295	110	±0.413	136	2.12	125	-0.628	169
0.009 1	.315	250	-1.239	179	-.88	253	-.367	169
0.009 2	.329	250	±5.848	286	-.91	237	-.346	170
0.009 3	-.315	110	±.978	127	1.17	125	-.426	167
0.009 4	-.318	110	±1.239	116	1.19	127	-.400	166
S-IVB engine								
0.372	0.410	283	2.022		-0.27	190	-0.096	220
LM								
0.647	0.017	297	0.696		-0.02	210	-0.005	156
.696	-.144	70	.652		.02	90	.002	44

[a]Normalized with respect to amplitude at forward end of CM.

[b]Phase angle of acceleration relative to input force.

[c]Normalized with respect to amplitude at aft end of S-II.

TABLE A-7.- NORMALIZED RESONANT RESPONSE OF CONFIGURATION II WITH 0-PERCENT PROPELLANT LOAD

(a) Pitch direction

Normalized model station, x'/L'	Frequency = 17.9 Hz Force = 14.2 N a_{ref} = 0.396		Frequency = 53.0 Hz Force = 14.2 N a_{ref} = 0.140		Frequency = 110.9 Hz Force = 14.2 N a_{ref} = 0.100	
	Normalized amplitude (a)	Phase angle, deg (b)	Normalized amplitude (a)	Phase angle, deg (b)	Normalized amplitude (a)	Phase angle, deg (b)
0.002	0.409	148	-0.064	140	1.30	115
.077	.295	145	-.021	130	-.59	360
.109	.230	144	-.007	60	-2.09	338
.190	.116	139	.071	345	-10.30	100
.244	.040	124	.121	344	-----	---
.317	-.066	345	.114	339	-6.48	335
.371	-.144	337	.150	345	-4.89	334
.448	-.253	333	.214	360	-1.81	331
.581	-.199	334	-.329	177	.52	212
.641	-.081	343	-.586	180	.27	214
.792	.634	150	.207	360	-.34	99
.856	1.000	150	1.000	2	1.00	207
S-II engines						
0.009 Center	0.429	147	-0.443	128	-0.46	48
0.009 1	.437	147	-.836	149	-.32	68
0.009 2	.444	148	-1.014	146	-.42	48
0.009 3	.492	148	-1.650	163	-.68	30
0.009 4	.442	147	-1.136	140	-.60	323
S-IVB engine						
0.372	-0.323	340	-2.314	158	-0.99	311
LM						
0.647	-0.066	342	-0.757	180	0.26	205
.696	.106	148	-.714	178	.04	10

[a]Normalized with respect to amplitude at forward end of CM.

[b]Phase angle of acceleration relative to input force.

TABLE A-7.- NORMALIZED RESONANT RESPONSE OF CONFIGURATION II WITH 0-PERCENT PROPELLANT LOAD – Concluded

(b) Yaw direction

Normalized model station, x'/L'	Frequency = 18.1 Hz Force = 12.9 N a_{ref} = 0.579 g = 0.020		Frequency = 48.2 Hz Force = 11.1 N a_{ref} = 0.044 g = ----		Frequency = 100.3 Hz Force = 11.1 N a_{ref} = 0.045 g = 0.020	
	Normalized amplitude (a)	Phase angle, deg (b)	Normalized amplitude (a)	Phase angle, deg (b)	Normalized amplitude (a)	Phase angle, deg (b)
0.002	0.181	345	-0.273	251	1.200	250
.077	.130	345	-.159	247	.067	204
.109	.107	345	-.136	241	-.822	86
.190	.052	339	.068	173	-3.27	81
.244	.014	314	.091	131	-4.91	83
.317	-.038	180	.159	103	-4.29	77
.371	-.071	180	.159	103	-3.27	73
.448	-.133	174	.136	157	-.889	80
.496	-.128	177	-.114	237	.711	270
.581	-.088	174	-.386	289	.333	285
.641	-.026	185	-.545	295	.089	296
.696	.069	349	-.500	284	-.120	109
.763	.221	352	-.114	289	-.511	102
.827	.406	350	.614	114	.356	286
.856	1.000	351	1.000	102	1.000	288
S-II engines						
0.009 Center	0.192	7	0.636	129	-2.22	66
0.009 1	.207	354	-1.977	241	-.778	78
0.009 2	.218	354	±6.273	18	-.911	68
0.009 3	.204	6	1.477	117	-1.18	71
0.009 4	.207	7	1.591	116	-1.16	64
S-IVB engine						
0.372	-0.193	183	4.250	192	1.04	300
LM						
0.647	0.016	19	0.704	99	-0.111	79
.696	-.060	168	.659	103	-.067	56

[a]Normalized with respect to amplitude at forward end of CM.

[b]Phase angle of acceleration relative to input force.

TABLE A-8.- NORMALIZED RESONANT RESPONSE OF CONFIGURATION III WITH 100-PERCENT PROPELLANT LOAD

(a) Pitch direction

Normalized model station, x"/L"	Frequency = 38.0 Hz Force = 9.3 N a_{ref} = 0.319		Frequency = 81.2 Hz Force = 8.0 N a_{ref} = 0.310		Frequency = 99.0 Hz Force = 5.8 N a_{ref} = 0.885	
	Normalized amplitude (a)	Phase angle, deg (b)	Normalized amplitude (a)	Phase angle, deg (b)	Normalized amplitude (a)	Phase angle, deg (b)
0.017	0.460	93	-2.74	68	-0.434	180
.172	.100	112	-.203	84	-.052	207
.271	-.272	267	.754	250	.091	348
.361	-.106	251	.912	254	.111	9
.444	-.010	292	.787	255	.080	24
.565	-.498	272	.048	274	-.080	127
.676	-.382	272	-.355	74	-.277	154
.812	.038	94	-.364	78	-.472	158
.872	.010	113	.068	225	-.151	134
.942	.658	93	.510	250	.418	353
1.000	1.000	94	1.000	256	1.000	343
			S-IVB engine			
0.017	±1.777	174	0.516	292	0.063	47
			LM			
0.576	-0.570	275	-0.639	79	-0.064	141
.676	-.436	275	-1.06	116	-.139	166

[a]Normalized with respect to amplitude at forward end of CM.

[b]Phase angle of acceleration relative to input force.

TABLE A-8.- NORMALIZED RESONANT RESPONSE OF CONFIGURATION III

WITH 100-PERCENT PROPELLANT LOAD – Concluded

(b) Yaw direction

Normalized model station, x''/L''	Frequency = 40.0 Hz Force = 13.4 N a_{ref} = 0.465 g = 0.025		Frequency = 76.3 Hz Force = 17.6 N a_{ref} = 0.629 g = 0.034		Frequency = 114.7 Hz Force = 13.3 N a_{ref} = 0.535 g = ----	
	Normalized amplitude (a)	Phase angle, deg (b)	Normalized amplitude (a)	Phase angle, deg (b)	Normalized amplitude (a)	Phase angle, deg (b)
0.017	0.47	108	-0.591	101	-1.18	226
.172	.11	127	-.068	127	-.110	246
.271	-.09	275	.432	289	.308	132
.361	-.27	285	.461	286	.515	108
.444	-.38	290	.279	291	-----	---
.565	-.49	290	-.185	104	.295	97
.676	-.37	293	-.448	111	.060	114
.812	.02	99	-.341	110	-.204	277
.872	.34	113	.073	276	-.069	318
.942	.65	110	.548	235	.257	81
1.000	1.000	112	1.00	239	1.00	95
			S-IVB engine			
0.017	-----	---	-0.205	62	0.278	90
			LM			
0.576	-0.56	292	-0.78	108	0.088	107
.676	-.47	294	-.89	111	-.071	249

[a]Normalized with respect to amplitude at forward end of CM.

[b]Phase angle of acceleration relative to input force.

TABLE A-9.- NORMALIZED RESONANT RESPONSE OF CONFIGURATION III WITH 50-PERCENT PROPELLANT LOAD

(a) Pitch direction

Normalized model station, x''/L''	Frequency = 40.4 Hz Force = 7.5 N a_{ref} = 0.574		Frequency = 98.4 Hz Force = 6.6 N a_{ref} = 1.160	
	Normalized amplitude (a)	Phase angle, deg (b)	Normalized amplitude (a)	Phase angle, deg (b)
0.017	0.554	90	-0.263	134
.172	.153	105	.075	239
.271	-.265	254	.211	293
.361	-.089	225	.203	284
.444	-.423	258	.156	306
.565	-.538	261	-.076	33
.676	-.451	261	-.272	78
.812	-.012	262	-.471	86
.872	.331	82	-.166	91
.942	.641	82	.431	267
1.000	1.000	83	1.000	267
S-IVB engine				
0.017	-0.233	221	-0.147	49
LM				
0.576	-0.632	262	-0.058	52
.676	-.522	305	-.149	91

[a]Normalized with respect to amplitude at forward end of CM.

[b]Phase angle of acceleration relative to input force.

TABLE A-9.- NORMALIZED RESONANT RESPONSE OF CONFIGURATION III WITH 50-PERCENT PROPELLANT LOAD – Concluded

(b) Yaw direction

Normalized model station, x''/L''	Frequency = 43.5 Hz Force = 5.8 N a_{ref} = 0.460 g = 0.025		Frequency = 86.1 Hz Force = 12.0 N a_{ref} = 0.430 g = ----		Frequency = 91.2 Hz Force = 10.7 N a_{ref} = 0.428 g = 0.035	
	Normalized amplitude (a)	Phase angle, deg (b)	Normalized amplitude (a)	Phase angle, deg (b)	Normalized amplitude (a)	Phase angle, deg (b)
0.017	0.56	70	-0.91	130	-2.34	161
.172	.15	78	.45	282	.22	289
.271	-.08	245	1.07	306	1.52	348
.361	-.26	249	1.25	300	1.92	340
.444	---	---	----	---	----	---
.565	-.52	252	.13	330	.13	34
.676	-.42	255	-.31	108	-.69	152
.812	-.04	264	-.37	104	-1.16	151
.872	.30	75	.17	11	-1.31	155
.942	.64	72	.58	313	-.53	136
1.000	1.00	74	1.00	302	1.00	342
S-IVB engine						
0.017	---	---	----	---	----	---
LM						
0.576	0.61	106	-0.55	121	0.60	
.676	-.54	256	-.79	125	.86	

[a]Normalized with respect to amplitude at forward end of CM.

[b]Phase angle of acceleration relative to input force.

TABLE A-10.- NORMALIZED RESONANT RESPONSE OF CONFIGURATION III

WITH 0-PERCENT PROPELLANT LOAD

(a) Pitch direction

Normalized model station, x''/L''	Frequency = 41.2 Hz Force = 5.1 N a_{ref} = 0.841		Frequency = 96.1 Hz Force = 6.0 N a_{ref} = 0.686		Frequency = 103.3 Hz Force = 6.8 N a_{ref} = 1.046	
	Normalized amplitude (a)	Phase angle, deg (b)	Normalized amplitude (a)	Phase angle, deg (b)	Normalized amplitude (a)	Phase angle, deg (b)
0.017	0.511	106	0.183	150	-0.245	118
.172	.116	115	-.192	250	.310	95
.271	-.100	210	-.421	279	.834	230
.361	-.302	279	-.598	286	1.183	237
.444	-.448	281	-.392	284	.608	246
.565	-.562	282	-.271	302	.204	233
.676	-.469	282	-.380	320	-.132	29
.812	-.230	290	-.481	328	-.460	51
.872	.305	102	-.166	320	-.230	61
.942	.041	102	.427	147	.459	97
1.000	1.000	103	1.000	140	1.000	209
S-IVB engine						
0.017	-0.861	245	±0.249	26	0.035	227
LM						
0.576	-0.650	286	-0.139	288	0.157	---
.676	-.542	279	-.088	257	-.152	---

[a]Normalized with respect to amplitude at forward end of CM.

[b]Phase angle of acceleration relative to input force.

TABLE A-10.- NORMALIZED RESONANT RESPONSE OF CONFIGURATION III WITH 0-PERCENT PROPELLANT LOAD – Concluded

(b) Yaw direction

Normalized model station, x''/L''	Frequency = 43.5 Hz Force = 6.7 N a_{ref} = 1.06 g = 0.025		Frequency = 99.8 Hz Force = 8.0 N a_{ref} = 0.690 g = 0.021	
	Normalized amplitude (a)	Phase angle, deg (b)	Normalized amplitude (a)	Phase angle, deg (b)
0.017	0.48	140	-0.34	227
.172	.01	132	±.11	60
.271	-.09	304	.72	287
.361	-.27	309	.87	284
.444	-.38	315	.38	277
.565	-.53	313	.16	265
.676	-.42	316	-.24	167
.812	-.05	321	-.48	161
.872	.28	137	.31	214
.942	.63	134	.51	297
1.000	1.00	136	1.00	325
	S-IVB engine			
0.017	-----	---	-----	---
	LM			
0.576	-0.016	290	0.025	331
.676	.034	50	-.002	140

[a]Normalized with respect to amplitude at forward end of CM.

[b]Phase angle of acceleration relative to input force.

REFERENCES

1. Brooks, George W.: The Application of Models to Helicopter Vibration and Flutter Research. American Helicopter Society, Inc. (Proc. Ninth Annual Forum, Washington, D.C., May 14-17, 1953).

2. Regier, Arthur A.: The Use of Scaled Dynamic Models in Several Aerospace Vehicle Studies. Paper presented at ASME Colloquium on Use of Models and Scaling in Simulation of Shock and Vibration (Philadelphia, Pa.), Nov. 1963.

3. Garrick, I. E.: Some Concepts and Problem Areas in Aircraft Flutter. S.M.F. Fund Paper No. FF-15, Inst. Aero. Sci., Mar. 1957.

4. Runyan, H. L.; Morgan, H. G.; and Mixson, J. S.: Use of Dynamic Models in Launch-Vehicle Development. AGARD Rept. 479, May 1964.

5. Mixson, John S.; Catherine, John J.; and Arman, Ali: Investigation of the Lateral Vibration Characteristics of a 1/5-Scale Model of Saturn SA-1. NASA TN D-1593, 1963.

6. Mixson, John S.; and Catherine, John J.: Experimental Lateral Vibration Characteristics of a 1/5-Scale Model of Saturn SA-1 With an Eight-Cable Suspension System. NASA TN D-2214, 1964.

7. Mixson, John S.; and Catherine, John J.: Comparison of Experimental Vibration Characteristics Obtained From a 1/5-Scale Model and From a Full-Scale Saturn SA-1. NASA TN D-2215, 1964.

8. Catherine, John J.: Torsional Vibration Characteristics of a 1/5-Scale Model of Saturn SA-1. NASA TN D-2745, 1965.

9. Chang, C.: Experimental Damping Studies. HREC/0088-1, LMSC/HREC A712619 (Contract NAS8-20088), Lockheed Missiles and Space Co., Jan. 6, 1966.

10. Thompson, William M., Jr.: An Investigation of the Response of a Scaled Model of a Liquid-Propellant Multistage Launch Vehicle to Longitudinal Excitation. NASA TN D-3975, 1967.

11. Jaszlics, Ivan J.; and Morosow, George: Dynamic Testing of a 20% Scale Model of the Titan III. AIAA Symposium on Structural Dynamics and Aeroelasticity, Aug.-Sept. 1965, pp. 477-485.

12. Catherines, John J.: Experimental Vibration Characteristics of a 1/40-Scale Dynamic Model of the Saturn V—Launch-Umbilical-Tower Configuration. NASA TN D-4870, 1968.

13. Adelman, Howard M.; and Steeves, Earl C.: Vibration Analysis of a 1/40-Scale Dynamic Model of Saturn V—Launch-Platform—Umbilical-Tower Configuration. NASA TN D-4871, 1968.

14. Steeves, Earl C.; and Catherines, John J.: Lateral Vibration Characteristics of a 1/40-Scale Dynamic Model of Apollo-Saturn V Launch Vehicle. NASA TN D-4872, 1968.

15. Pinson, Larry D.; and Leonard, H. Wayne: Longitudinal Vibration Characteristics of 1/10-Scale Apollo/Saturn V Replica Model. NASA TN D-5159, 1969.

16. Leadbetter, Sumner A.; Leonard, H. Wayne; and Brock, E. John, Jr.: Design and Fabrication Considerations for a 1/10-Scale Replica Model of the Apollo/Saturn V. NASA TN D-4138, 1967.

17. Herr, Robert W.; and Carden, Huey D.: Support Systems and Excitation Techniques for Dynamic Models of Space Vehicle Structures. Proceedings of Symposium on Aeroelastic & Dynamic Modeling Technology. RTD-TDR-63-4197, Pt. I, U.S. Air Force, Mar. 1964, pp. 249-277.

18. Bisplinghoff, Raymond L.; Ashley, Holt; and Halfman, Robert L.: Aeroelasticity. Addison-Wesley Pub. Co., Inc., c.1955.

19. Loewy, Robert G.; and Joglekar, Mukund M.: Matrix Holzer Analyses for Fully-Coupled Vibrations of Clustered Launch-Vehicle Configurations Including Applications to the Titan IIIC and Uncoupled Saturn I Cases. NASA CR-592, 1966.

20. Pestel, Edward C.; and Leckie, Frederick A.: Matrix Methods in Elastomechanics. McGraw-Hill Book Co., Inc., c.1963.

21. Timoshenko, S.; and Young, D. H.: Elements of Strength of Materials. Fifth ed., D. Van Nostrand Co., Inc., c.1968.

22. Hieatt, J. L.; and Riley, J. D.: Digital Program for Fluid Sloshing in Tanks With Axial Symmetry. TM-59-0000-00389, Space Technol. Lab., Inc., Sept. 30, 1959.

23. Bauer, Helmut F.: Fluid Oscillations in the Containers of a Space Vehicle and Their Influence Upon Stability. NASA TR R-187, 1964.

24. Stephens, David G.; and Leonard, H. Wayne: The Coupled Dynamic Response of a Tank Partially Filled With a Liquid and Undergoing Free and Forced Planar Oscillations. NASA TN D-1945, 1963.

25. Abramson, H. Norman, ed.: The Dynamic Behavior of Liquids in Moving Containers. NASA SP-106, 1966.

26. Anon.: Propellant Slosh Loads. NASA Space Vehicle Design Criteria (Structures). NASA SP-8009, 1968.

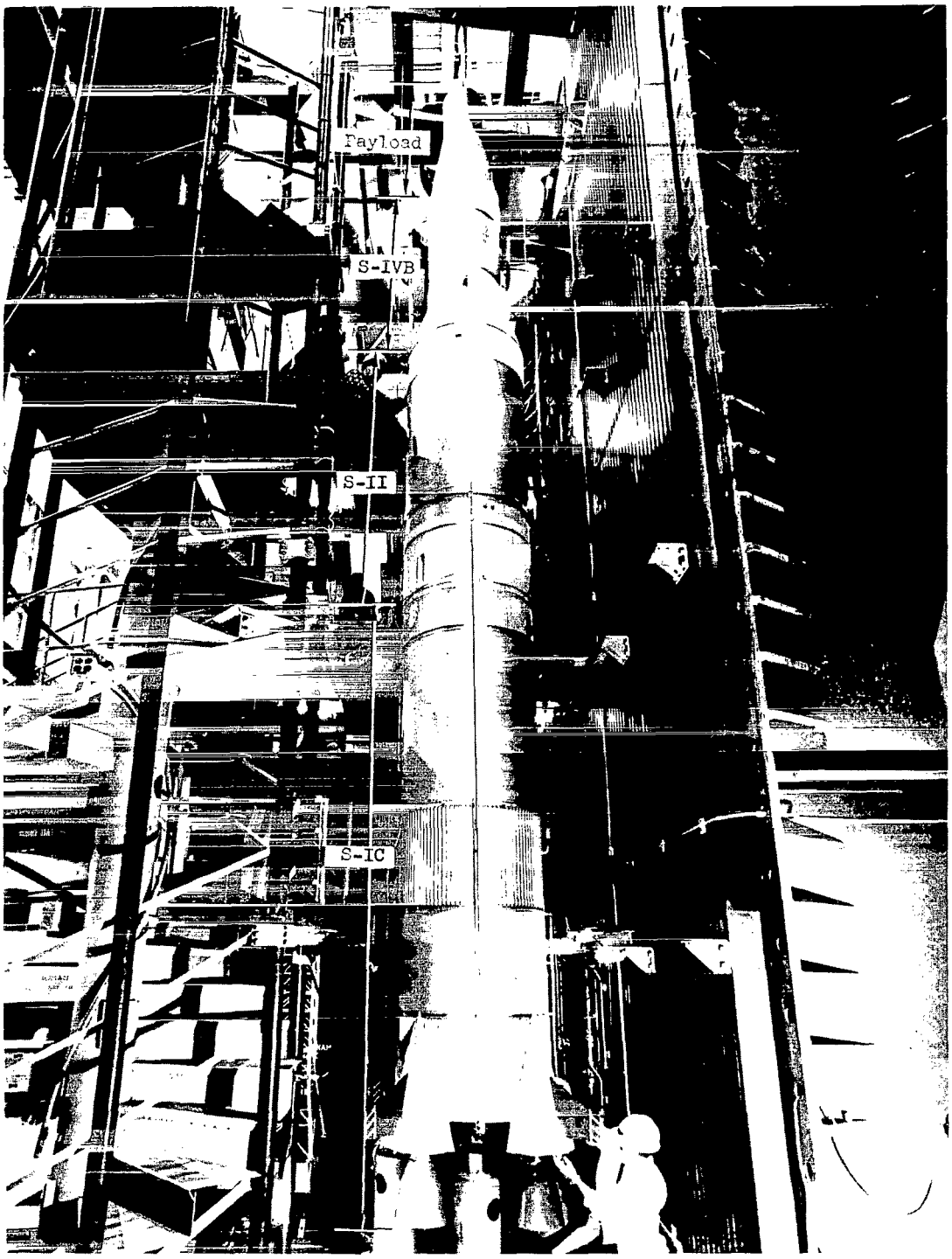

Figure 1.- 1/10-scale model of Apollo/Saturn V launch vehicle. L-69-1221

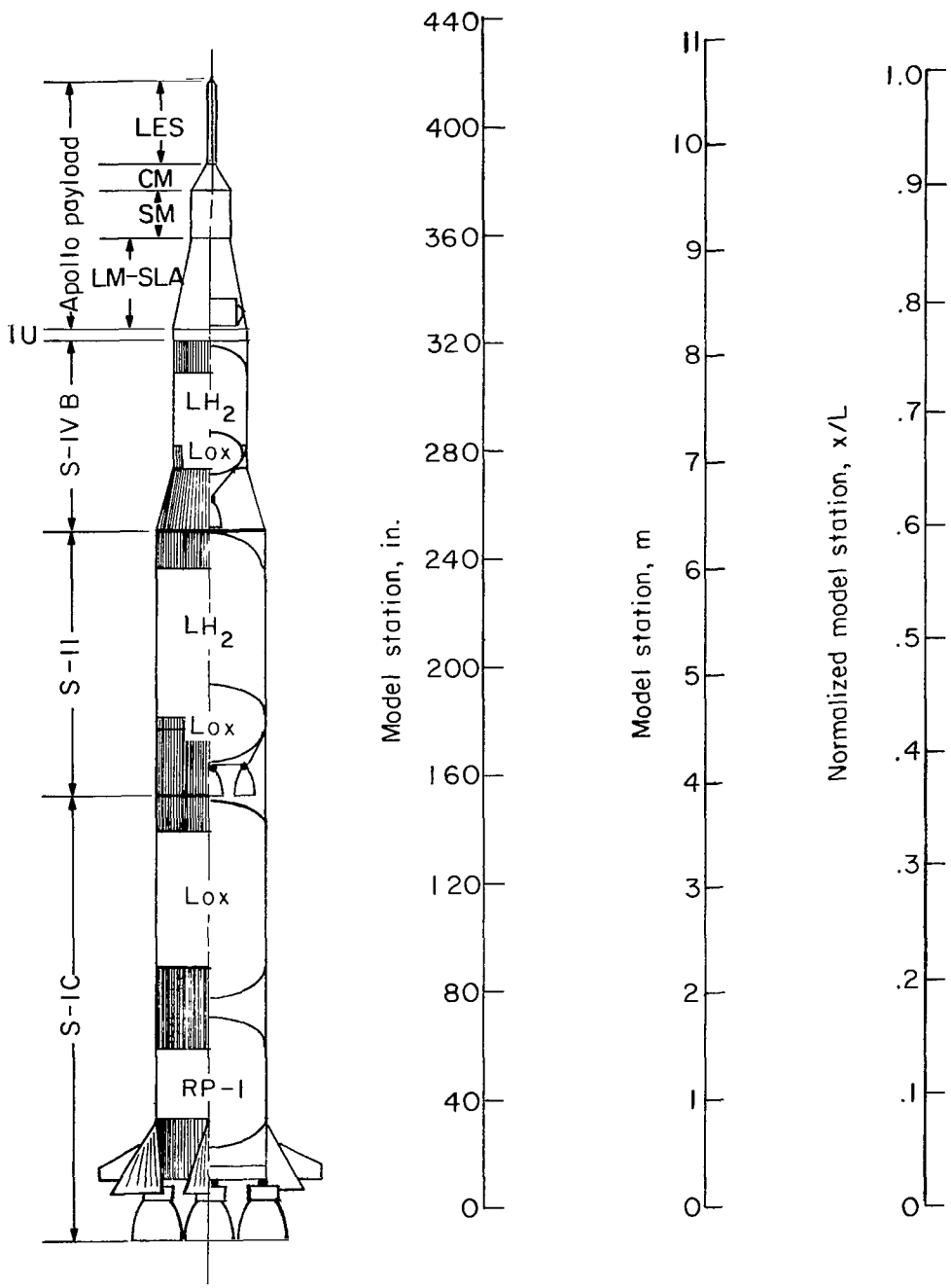

Figure 2.- Schematic of 1/10-scale Apollo/Saturn V model.

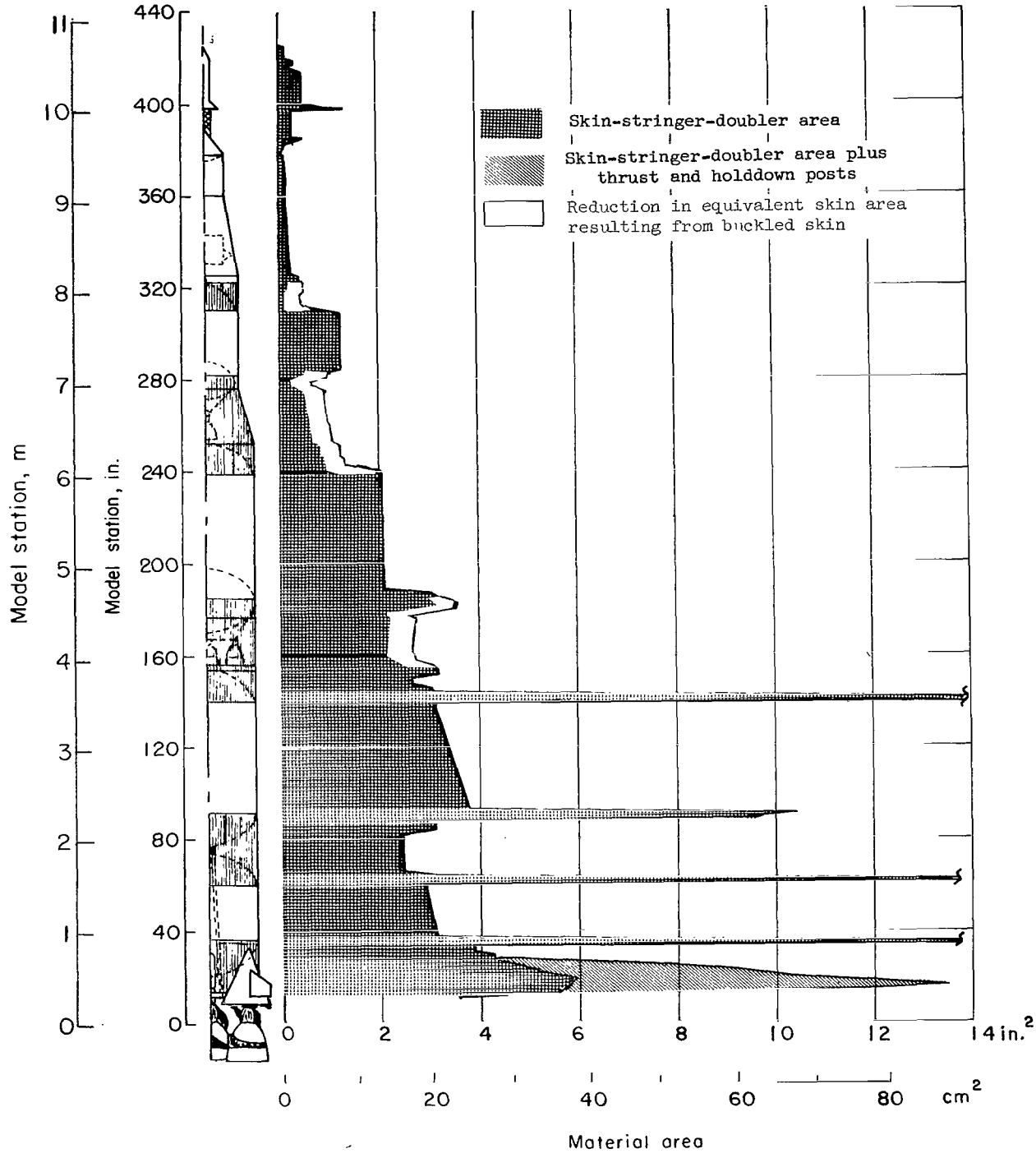

Figure 3.- Cross-sectional area of main structure.

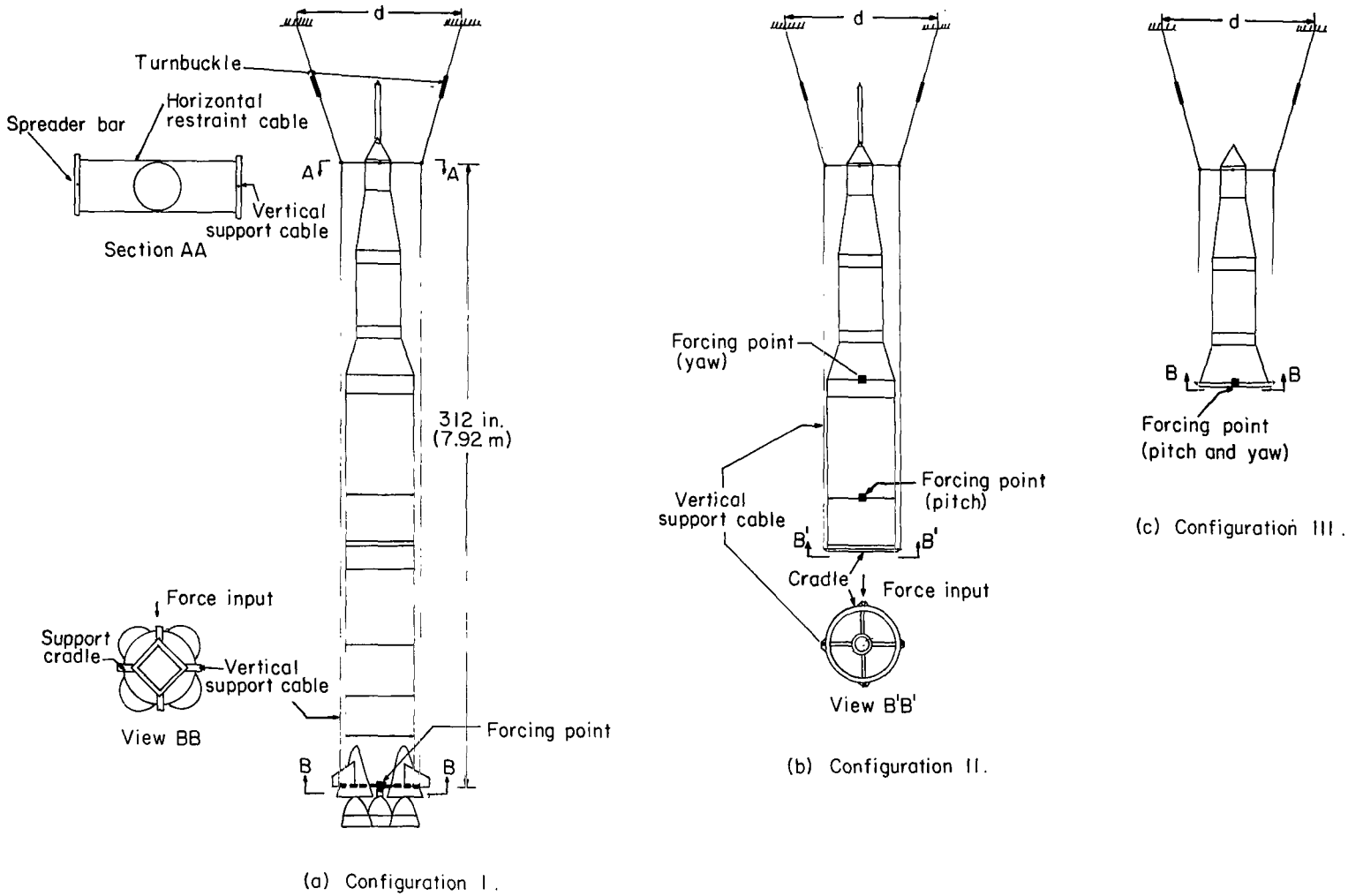

Figure 4.- Suspension system.

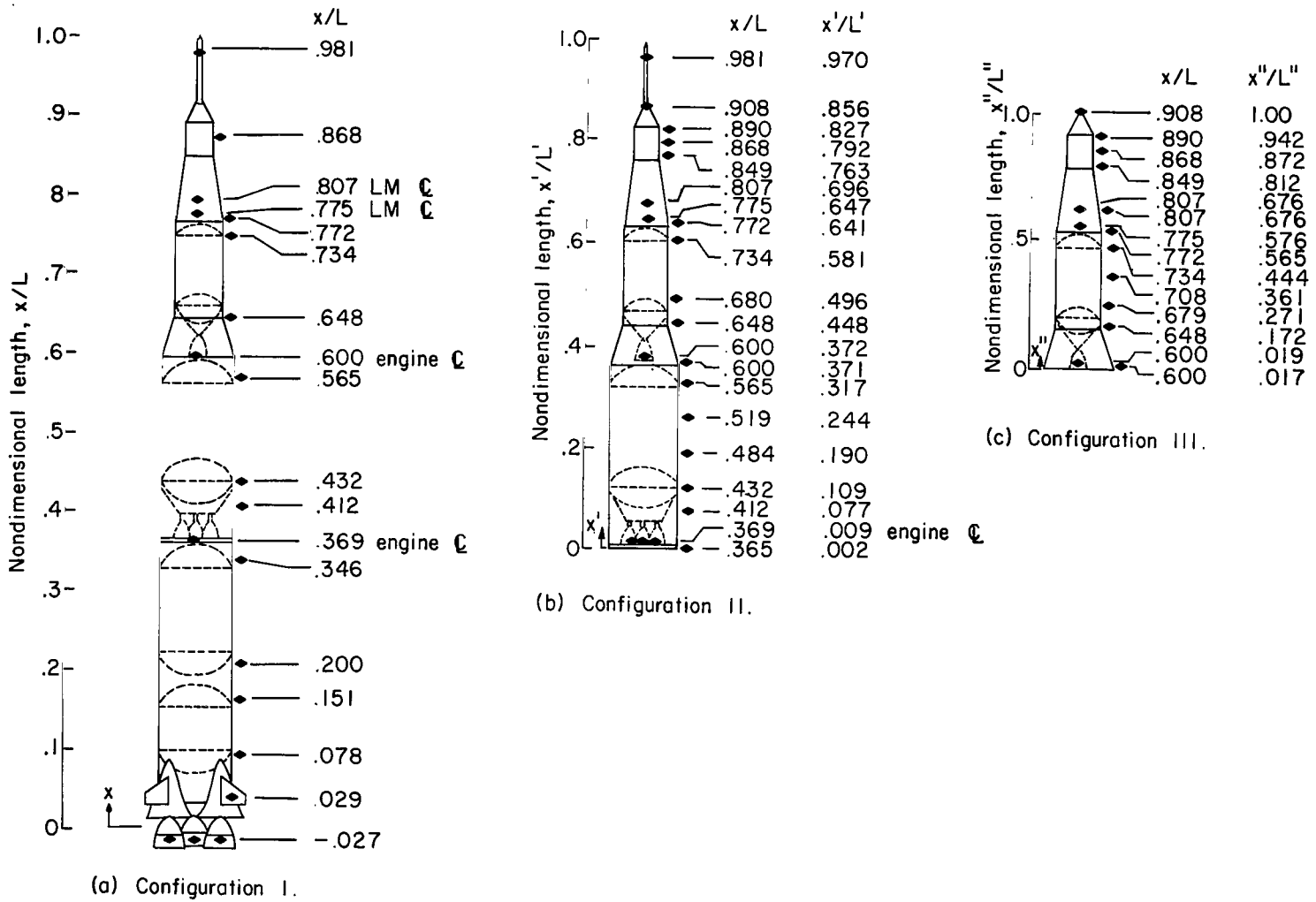

Figure 5.- Locations of primary transducers.

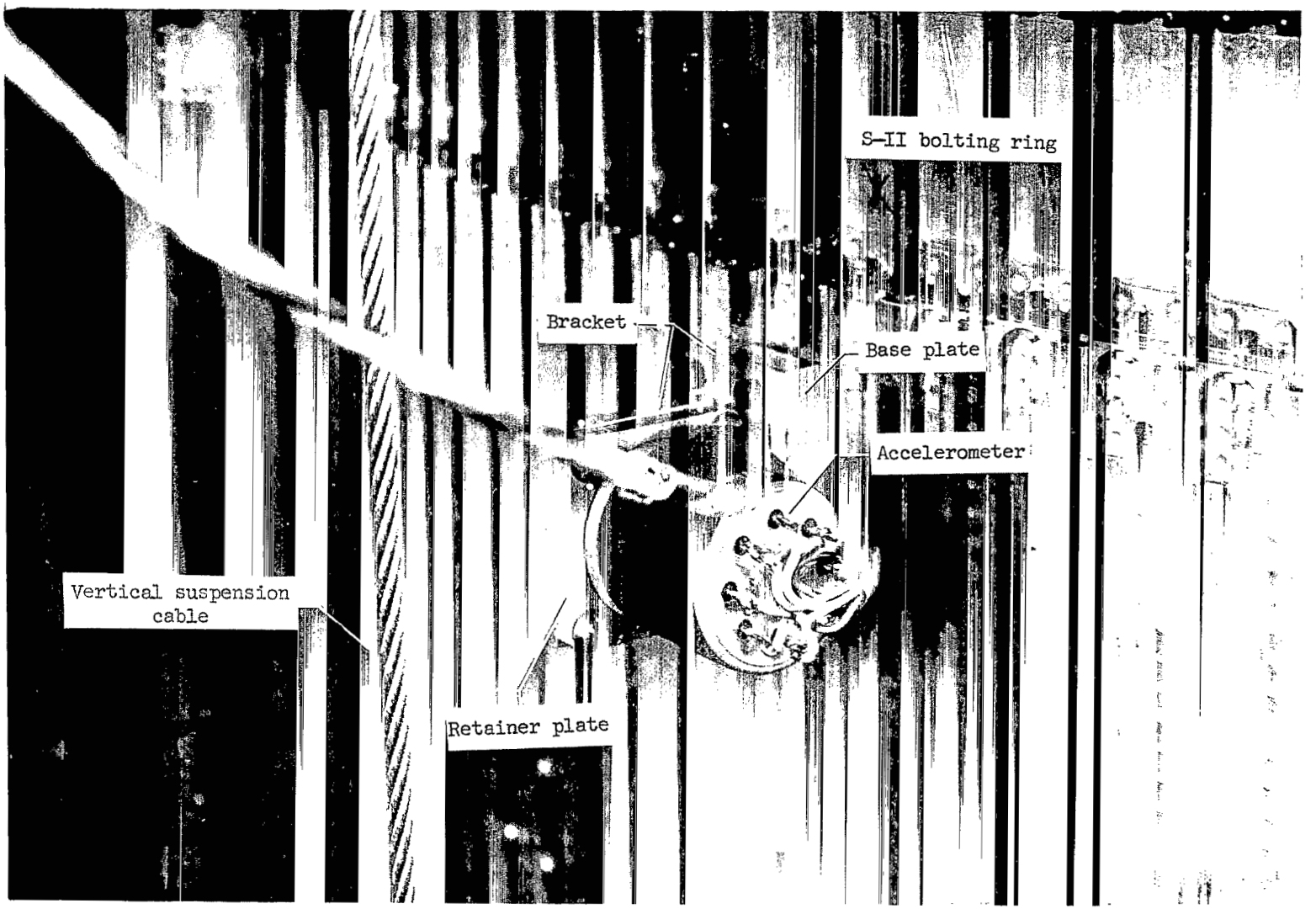

Figure 6.- Typical transducer installation.

L-65-1860.1

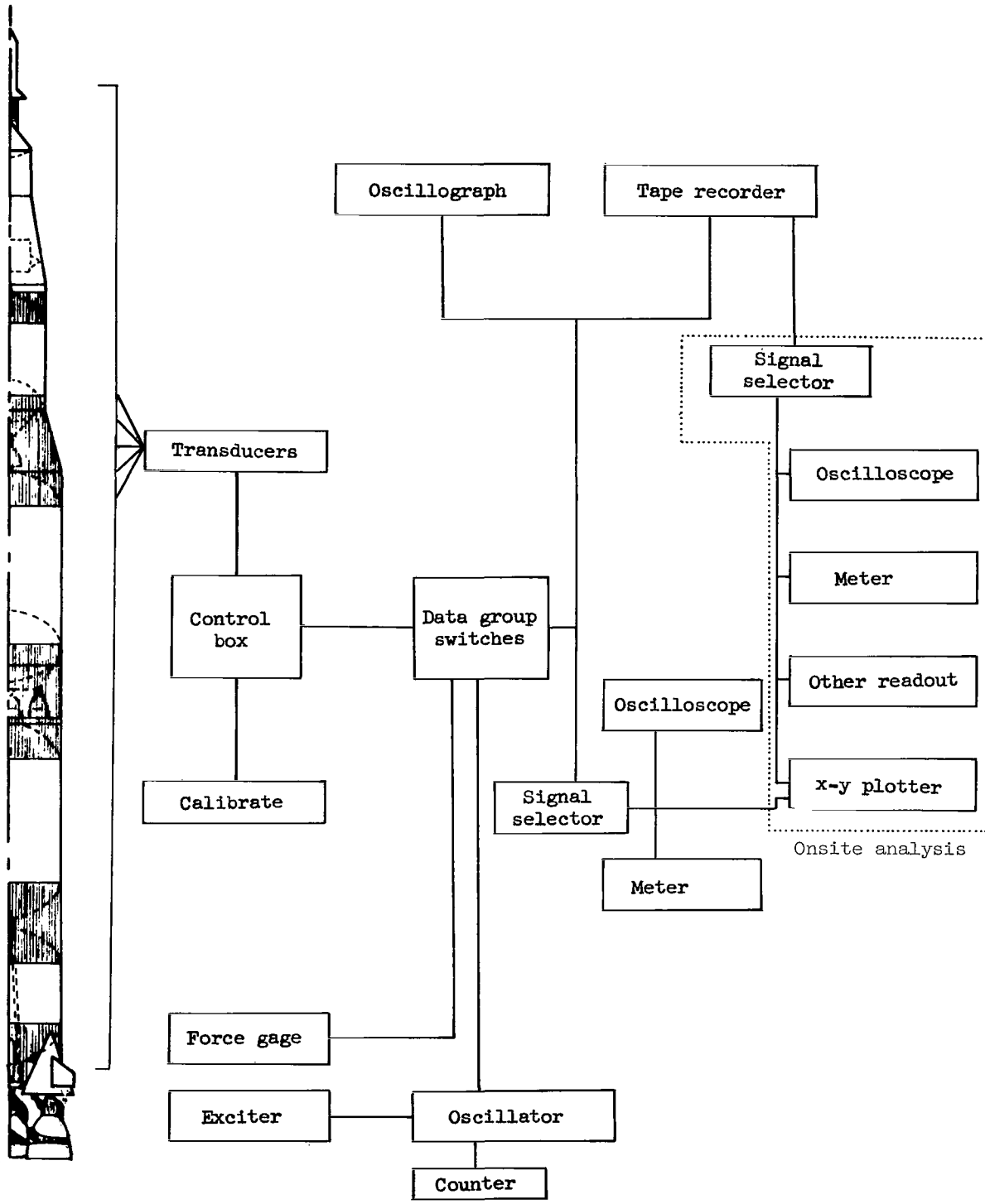

Figure 7.- Schematic diagram of instrumentation.

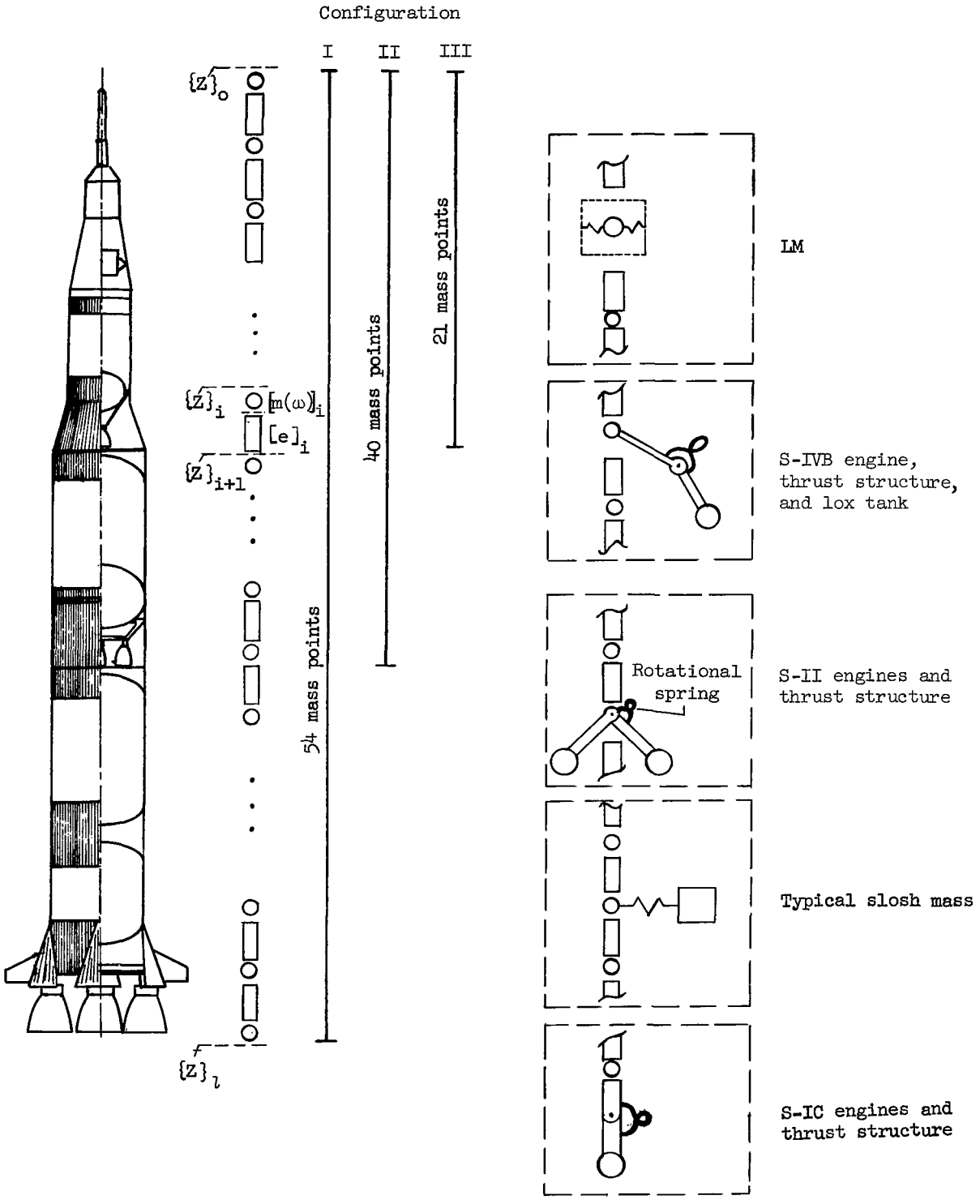

Figure 8.- Mathematical representation.

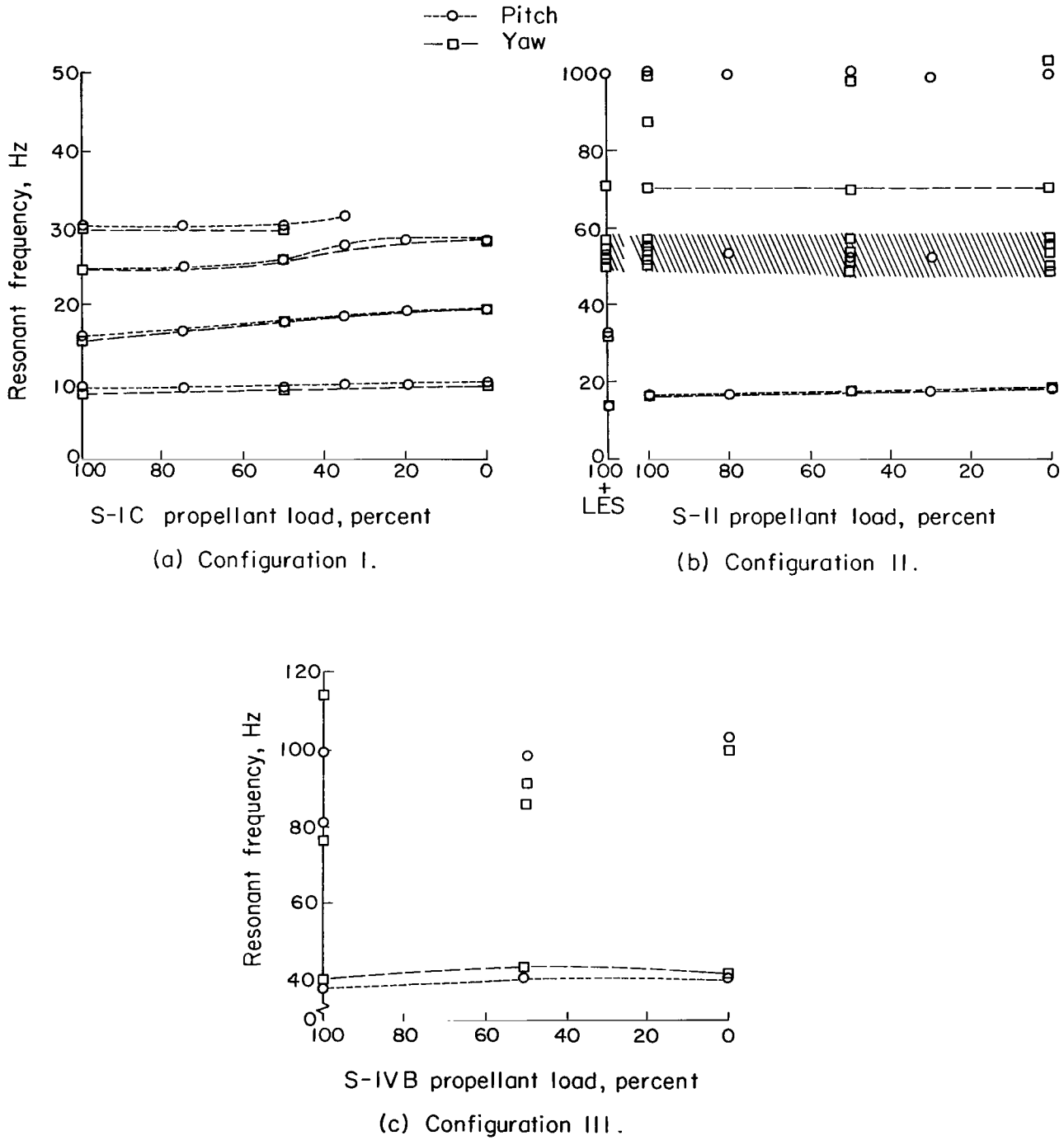

Figure 9.- Summary of measured resonant frequencies as a function of simulated propellant loading.

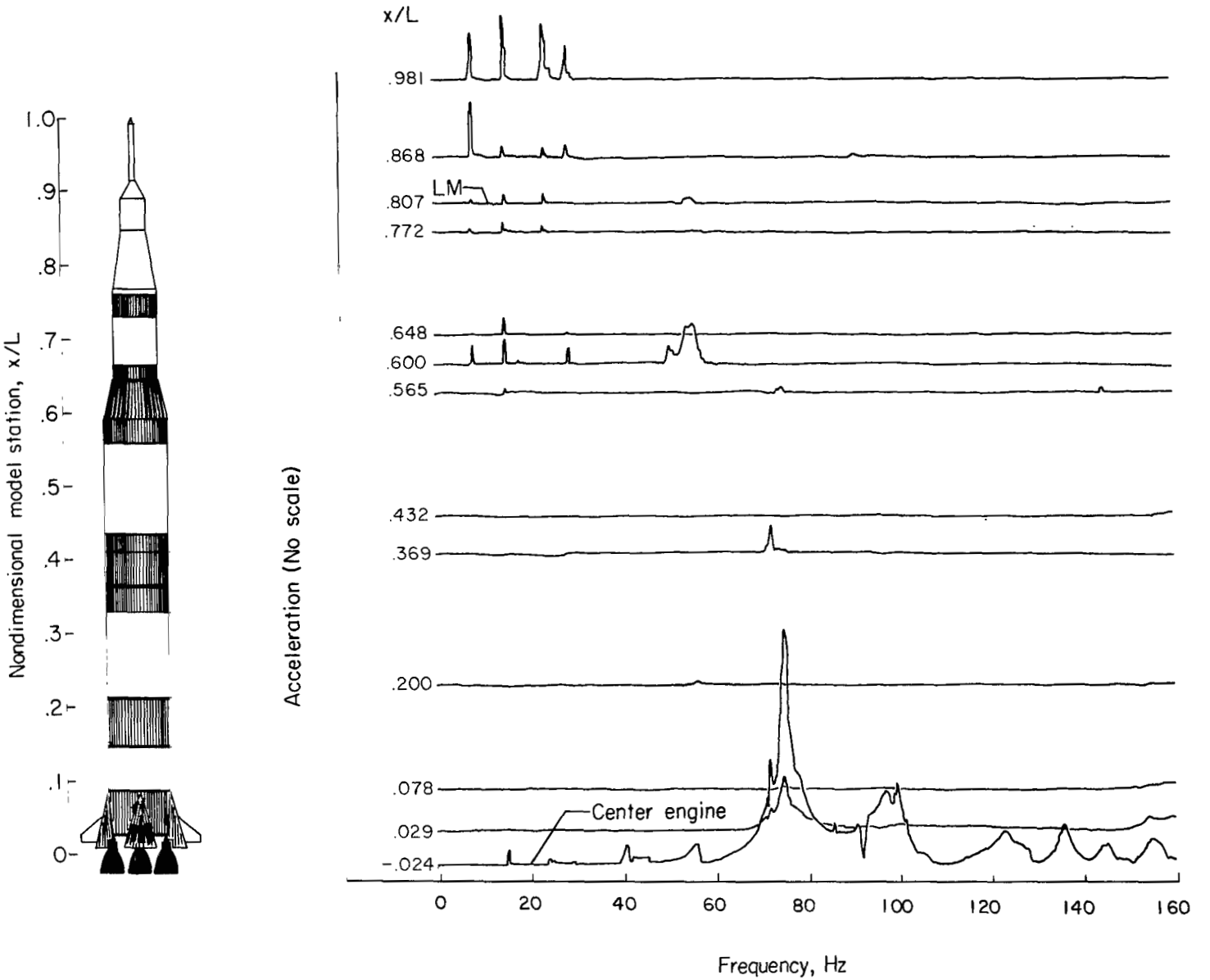

Figure 10.- Accelerations of configuration I with 100 percent propellant as a function of frequency for excitation in the yaw direction.

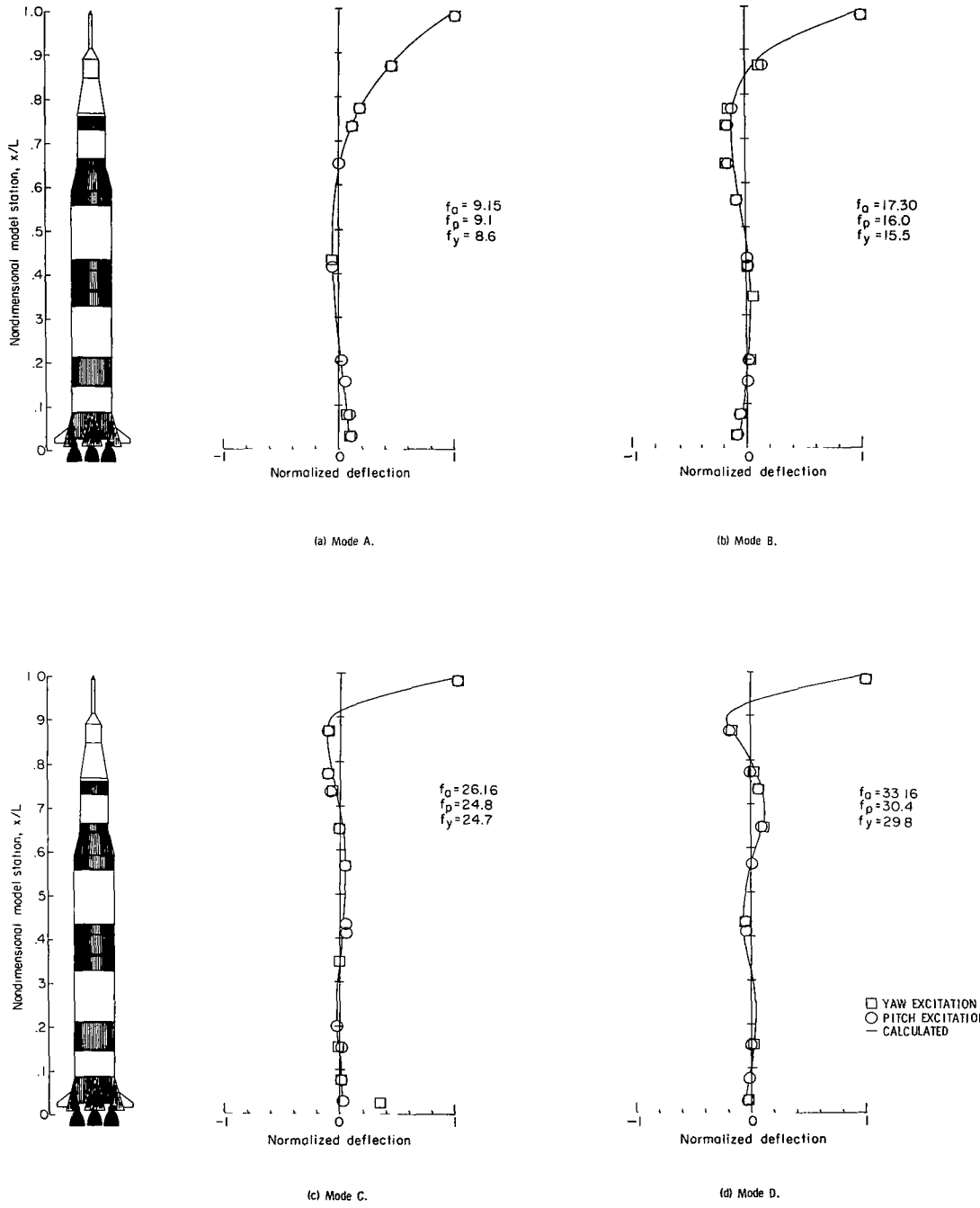

Figure 11.- Measured and calculated deflection shapes for configuration I with 100 percent propellant.

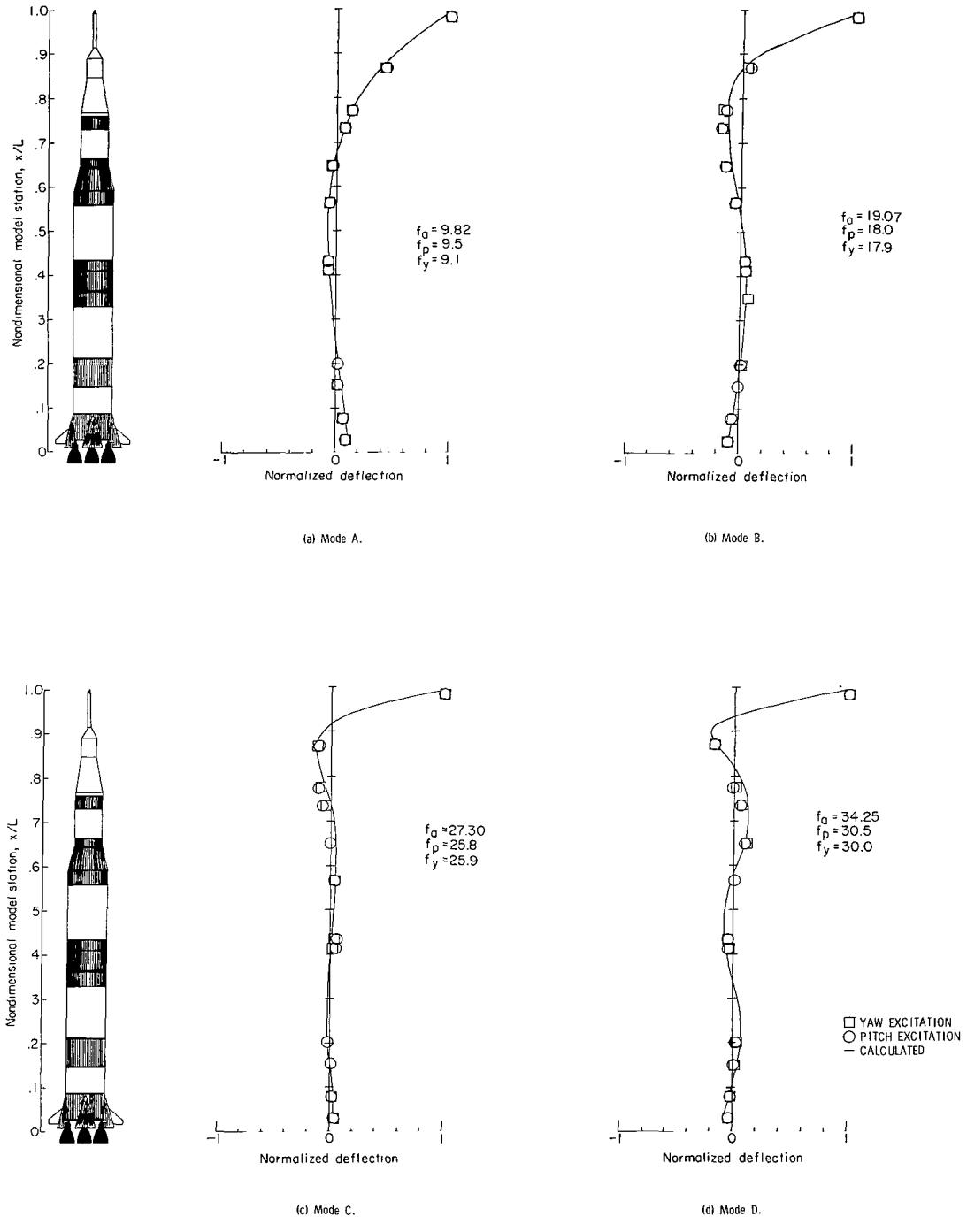

Figure 12.- Measured and calculated deflection shapes for configuration I with 50 percent propellant.

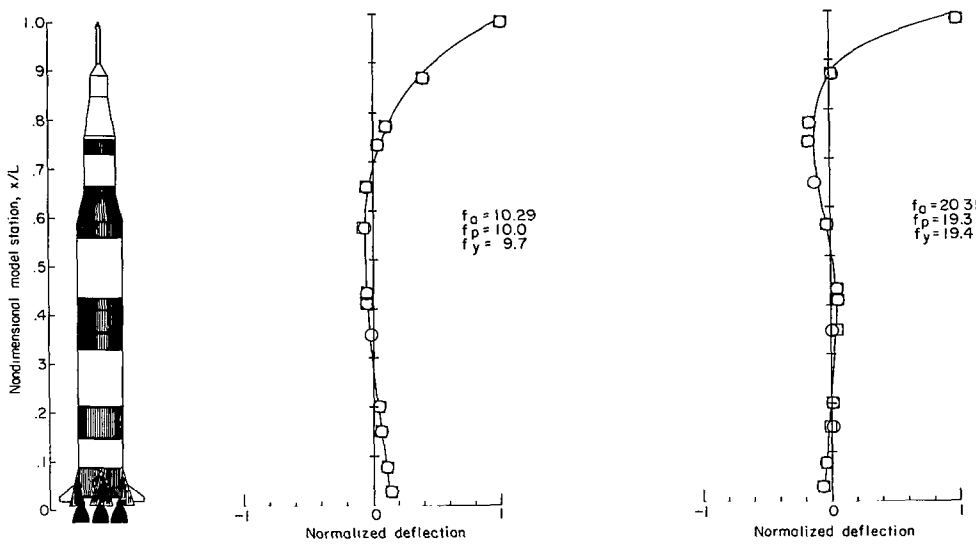

(a) Mode A.

(b) Mode B.

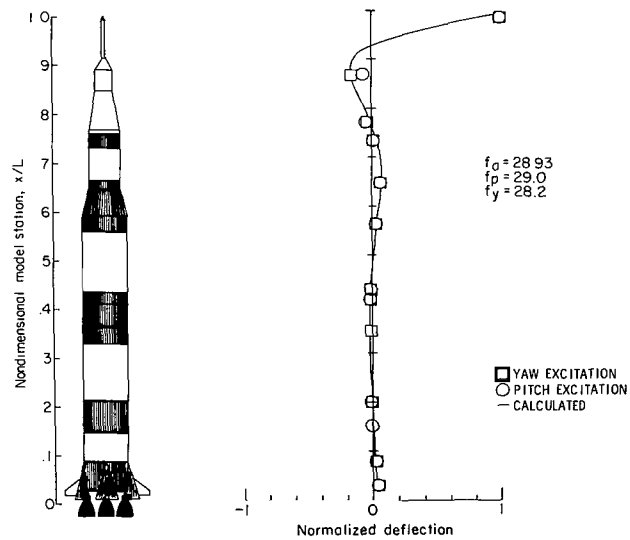

(c) Mode C.

Figure 13.- Measured and calculated deflection shapes for configuration I with 0 percent propellant.

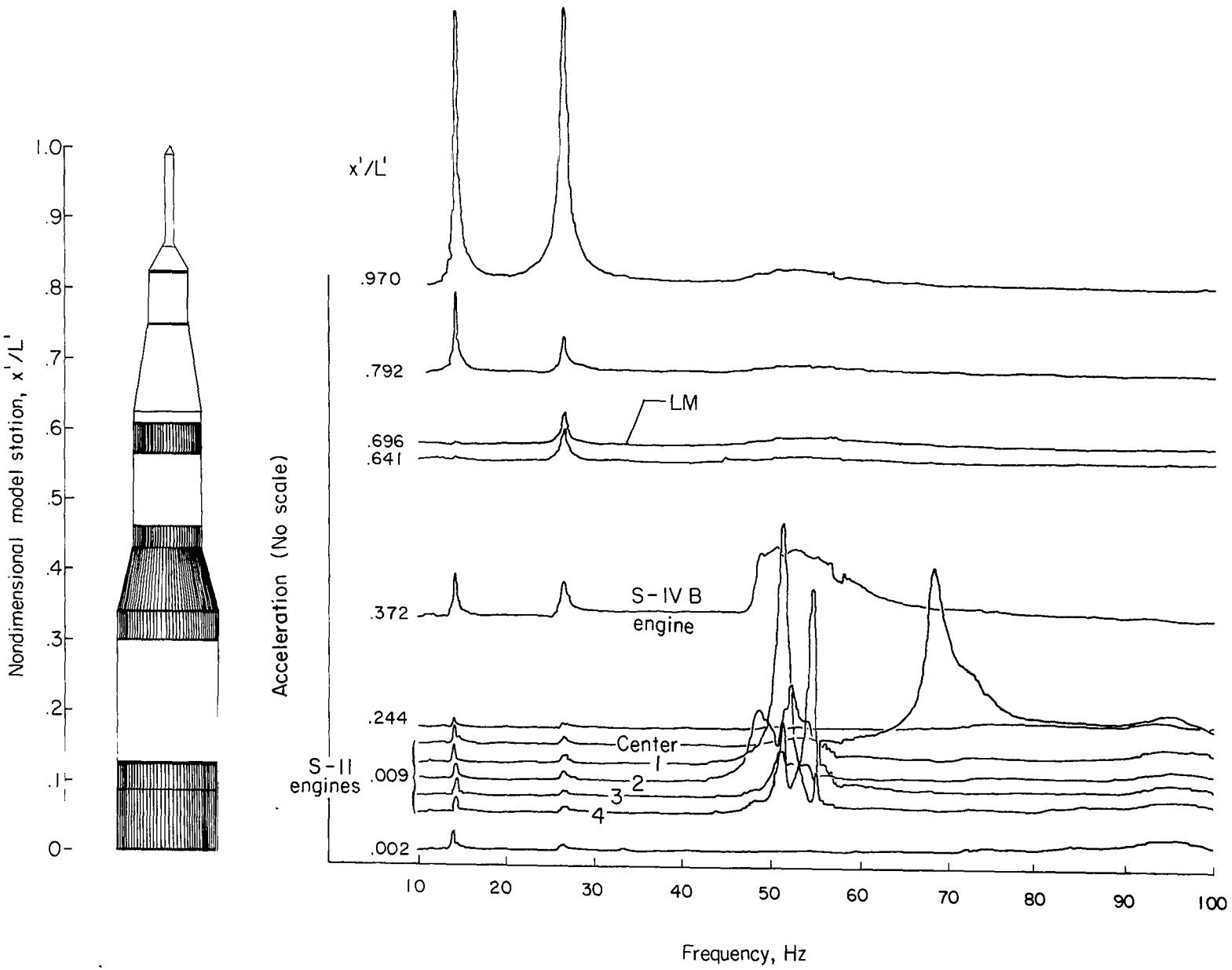

Figure 14.- Accelerations of configuration 11 with 100 percent propellant plus LES as a function of frequency in the yaw direction.

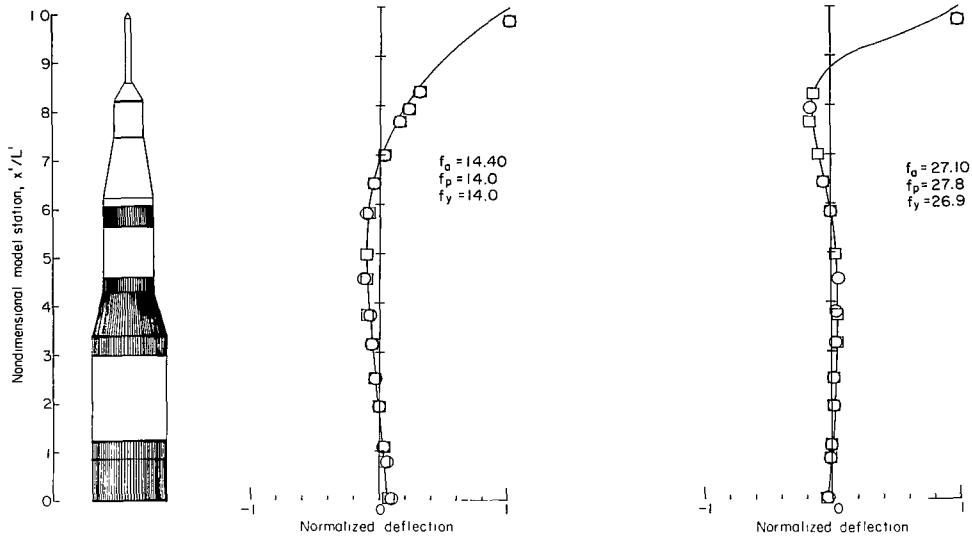

(a) Mode A.

(b) Mode B.

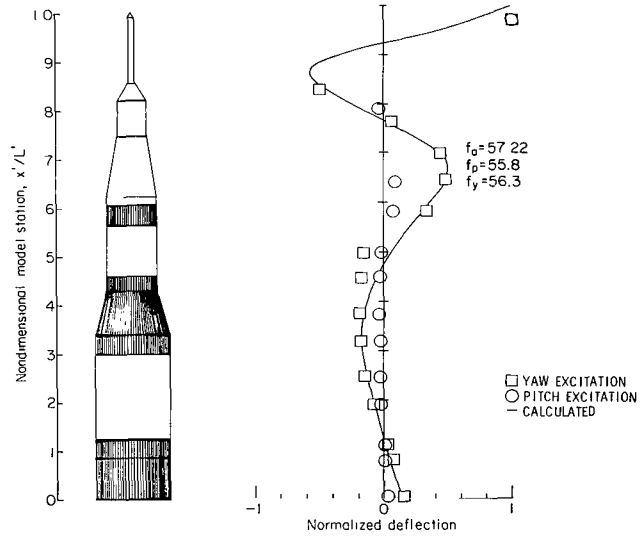

(c) Mode C.

Figure 15.- Measured and calculated deflection shapes for configuration II with 100 percent propellant plus LES.

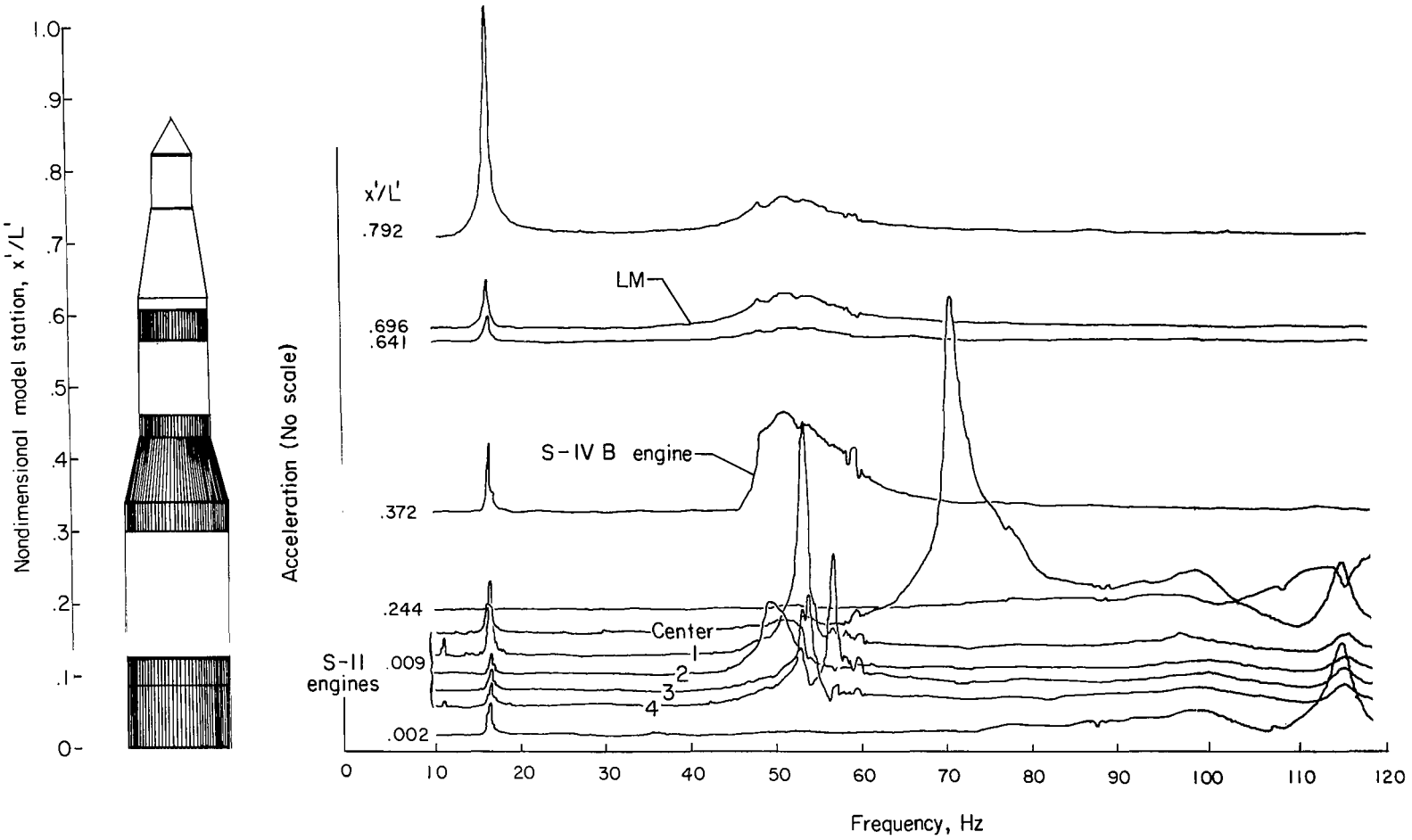

Figure 16.- Accelerations of configuration II with 100 percent propellant as a function of frequency in the yaw direction.

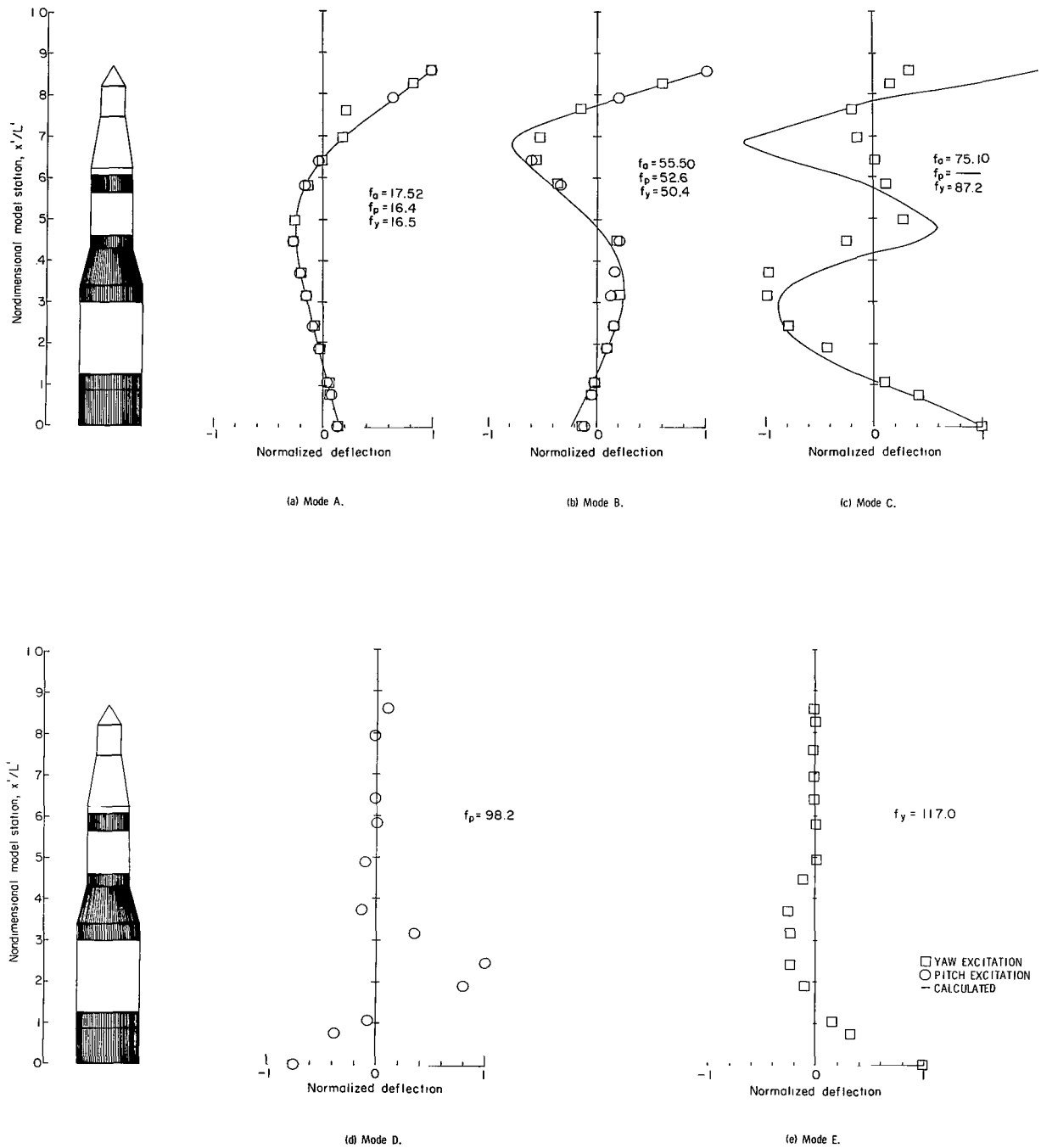

Figure 17.- Measured and calculated deflection shapes for configuration II with 100 percent propellant.

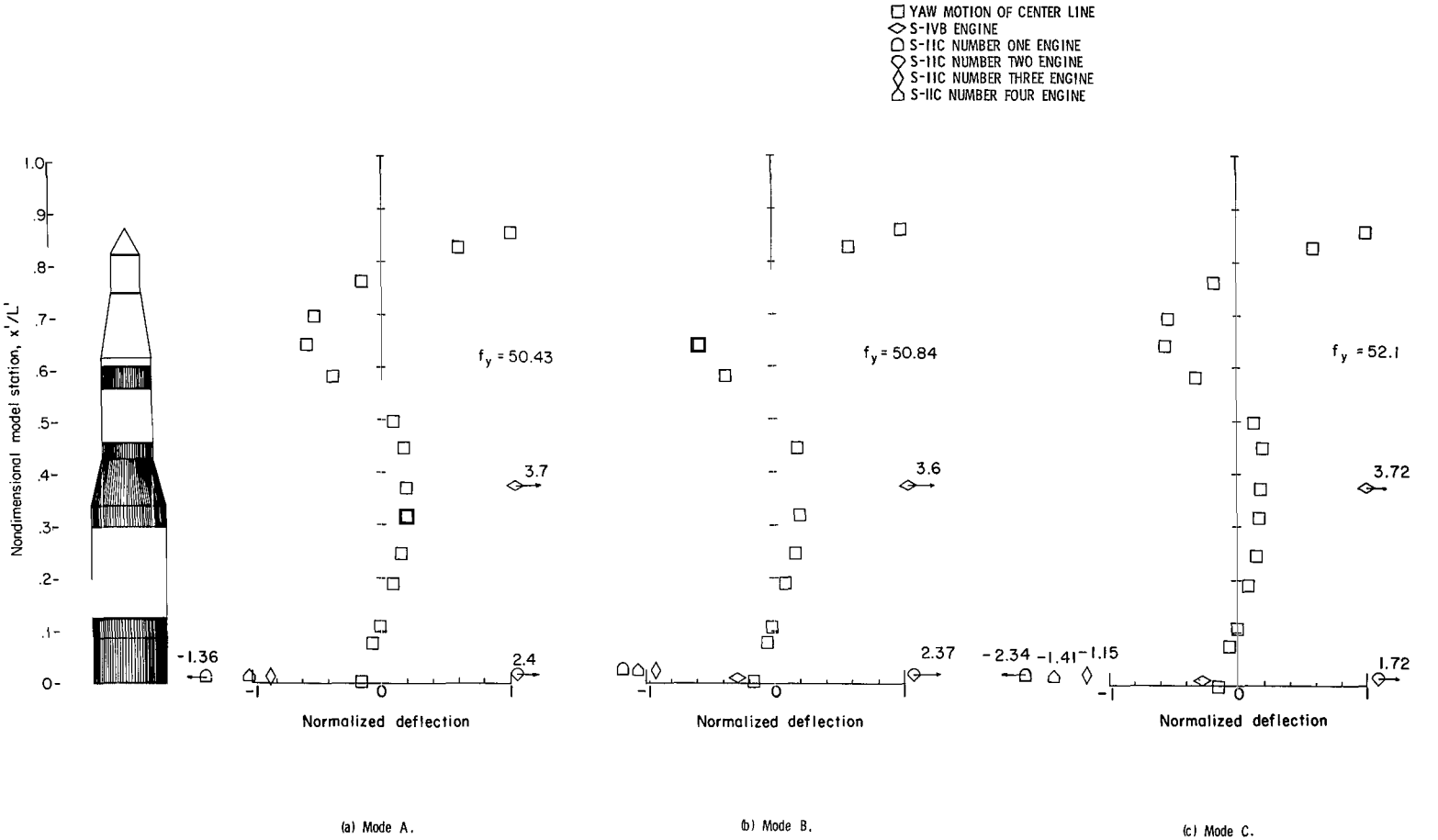

Figure 18.- Measured engine resonance deflection shapes for configuration II with 100 percent propellant.

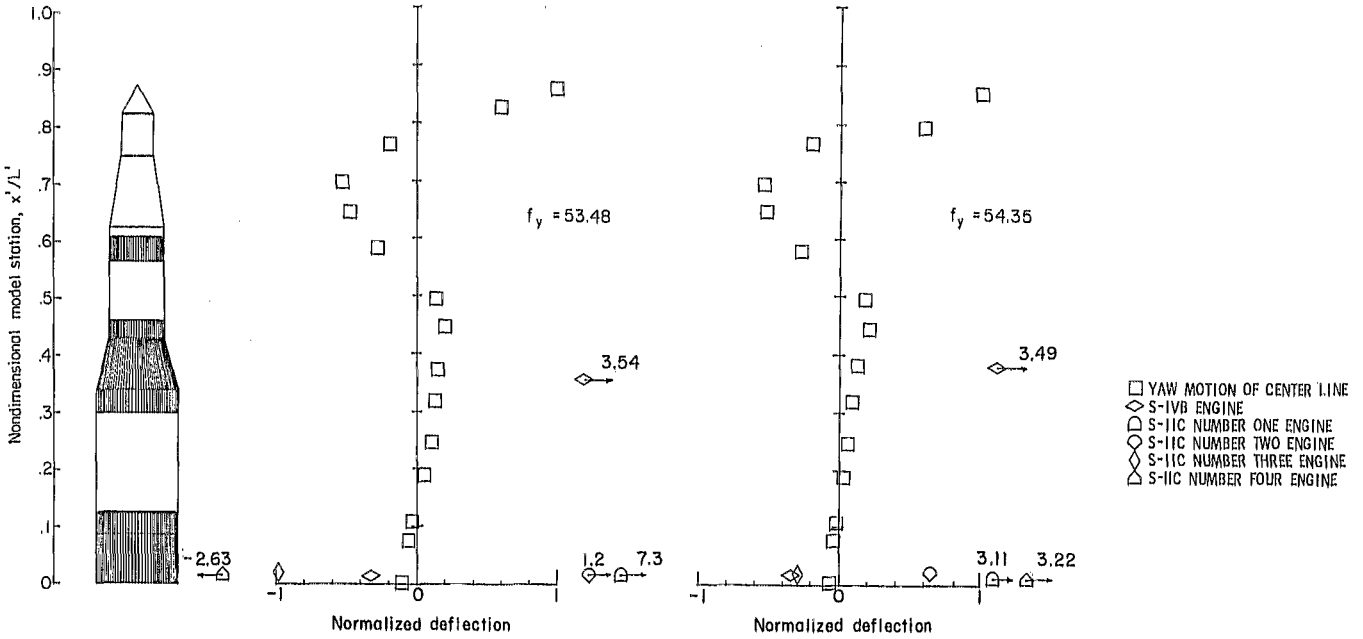

(d) Mode D.

(e) Mode E.

Figure 18.- Concluded.

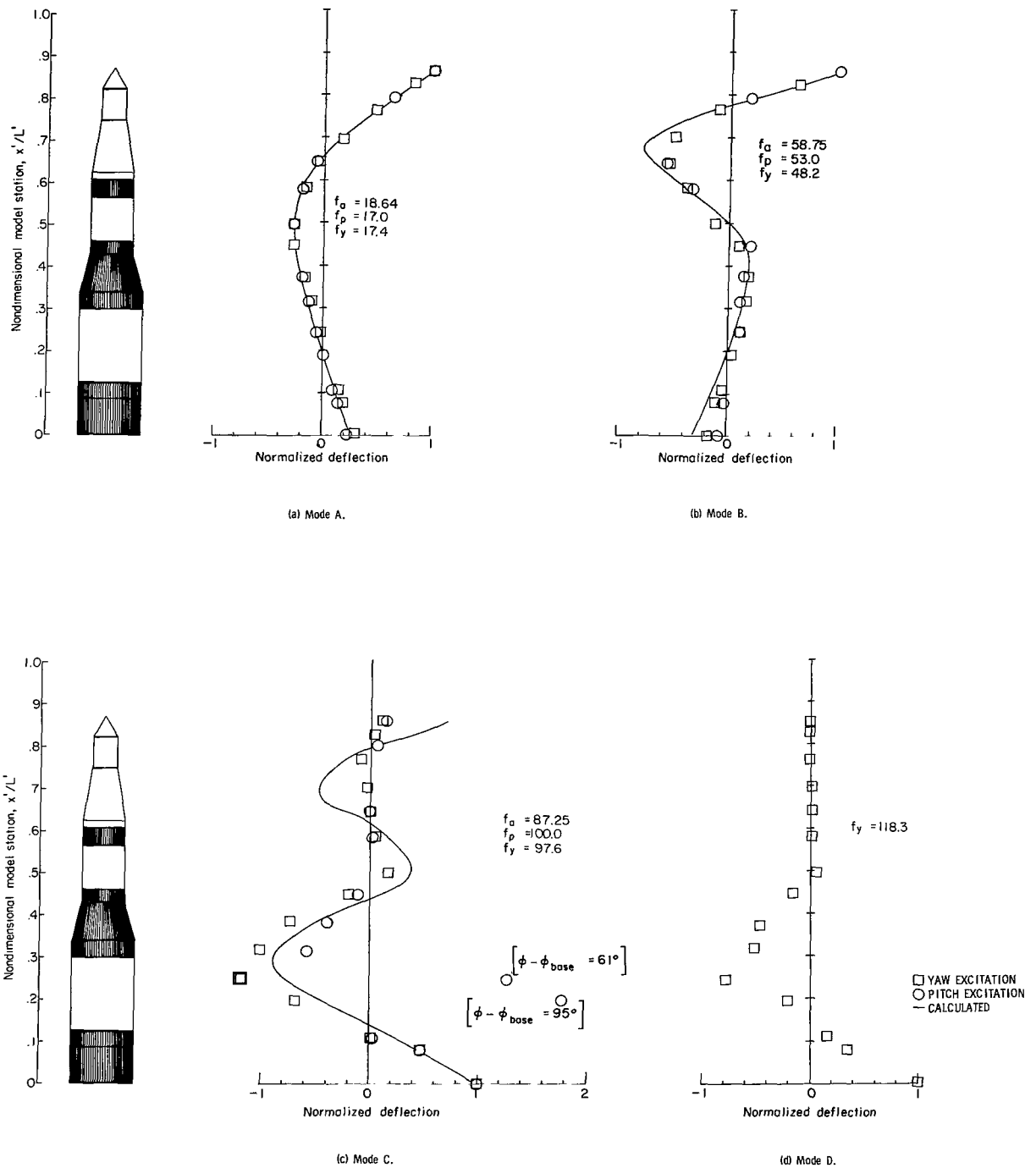

Figure 19.- Measured and calculated deflection shapes for configuration II with 50 percent propellant.

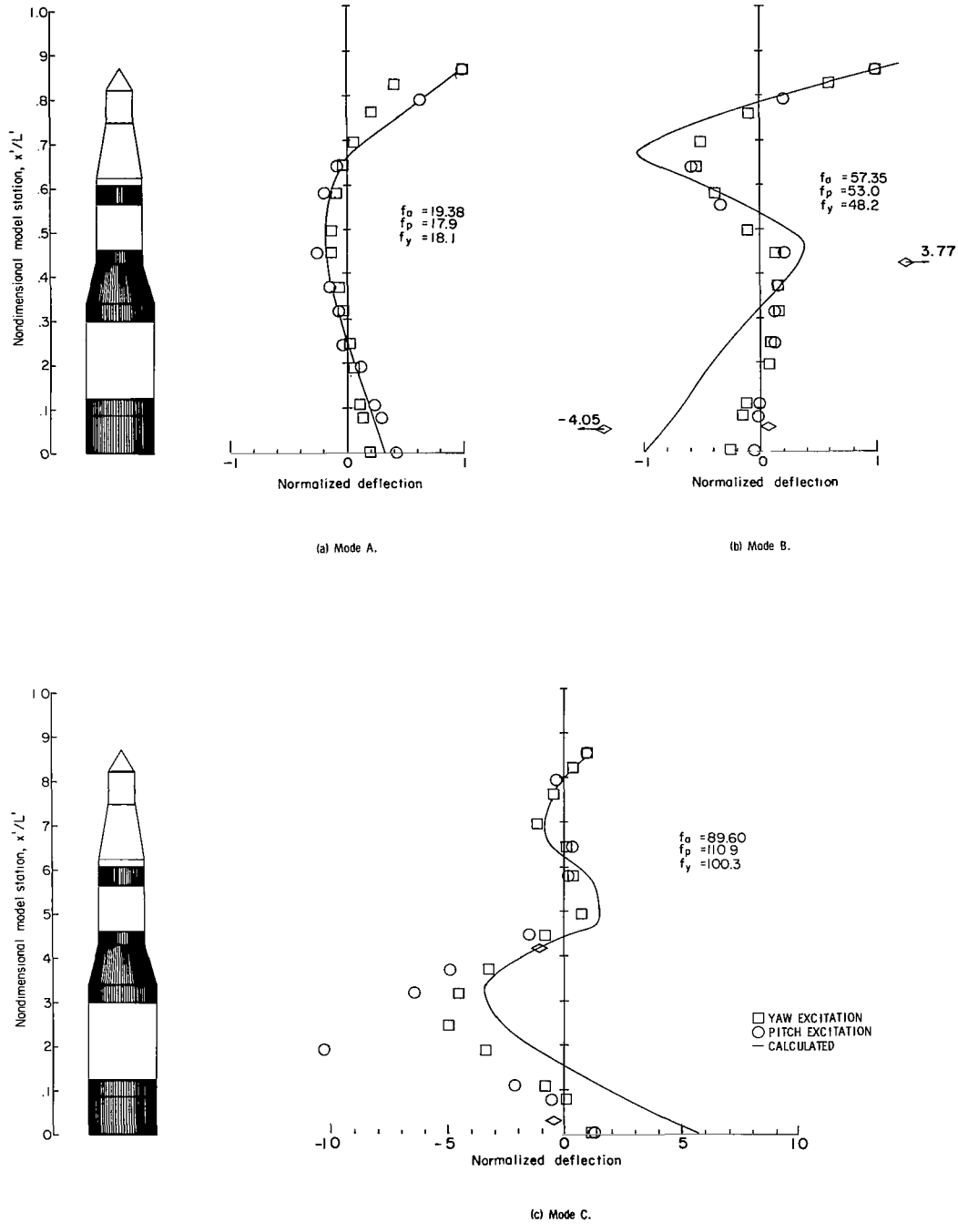

Figure 20.- Measured and calculated deflection shapes for configuration II with 0 percent propellant.

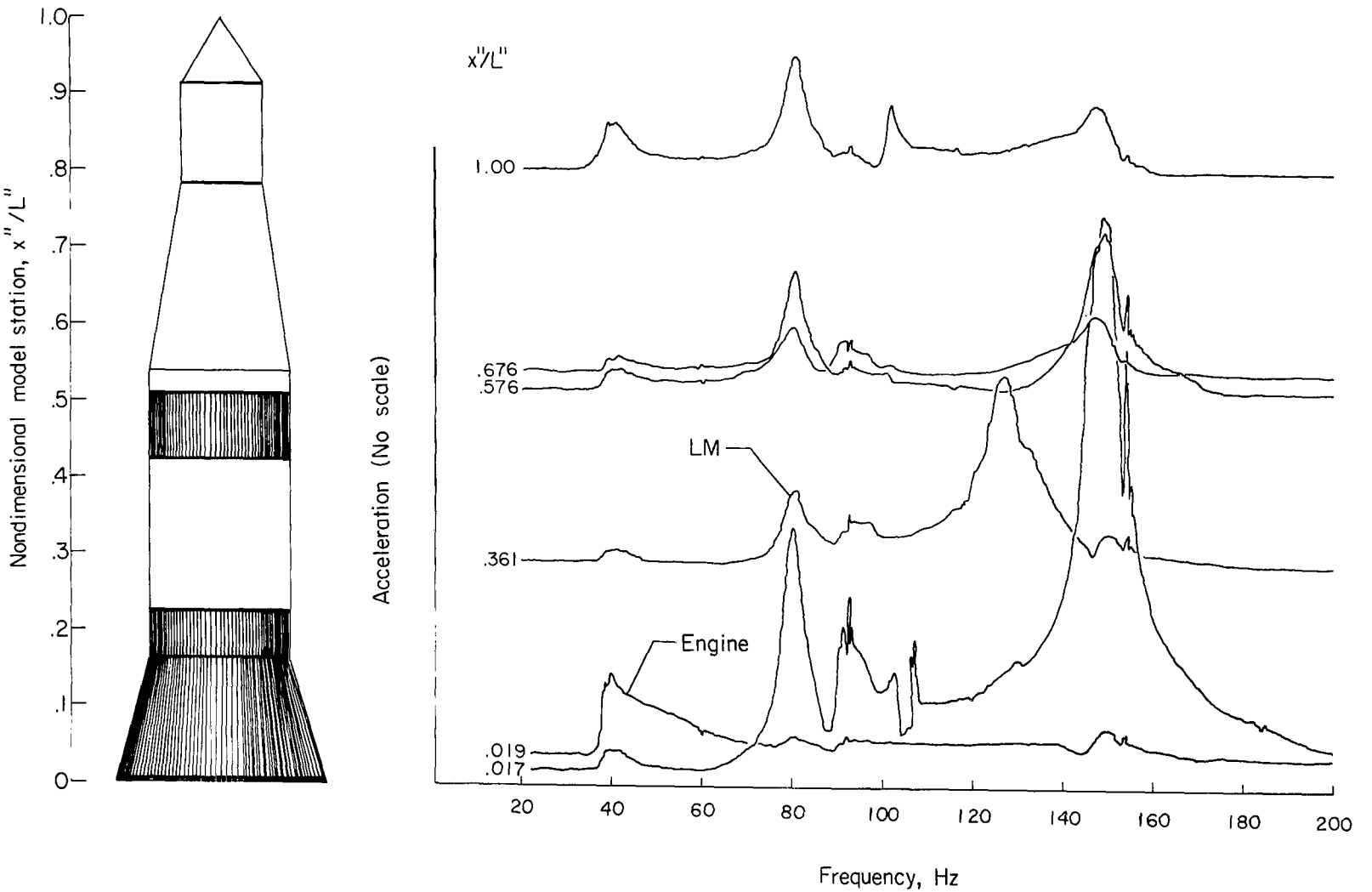

Figure 21.- Accelerations of configuration III with 100 percent propellant as a function of frequency for excitation in the yaw direction.

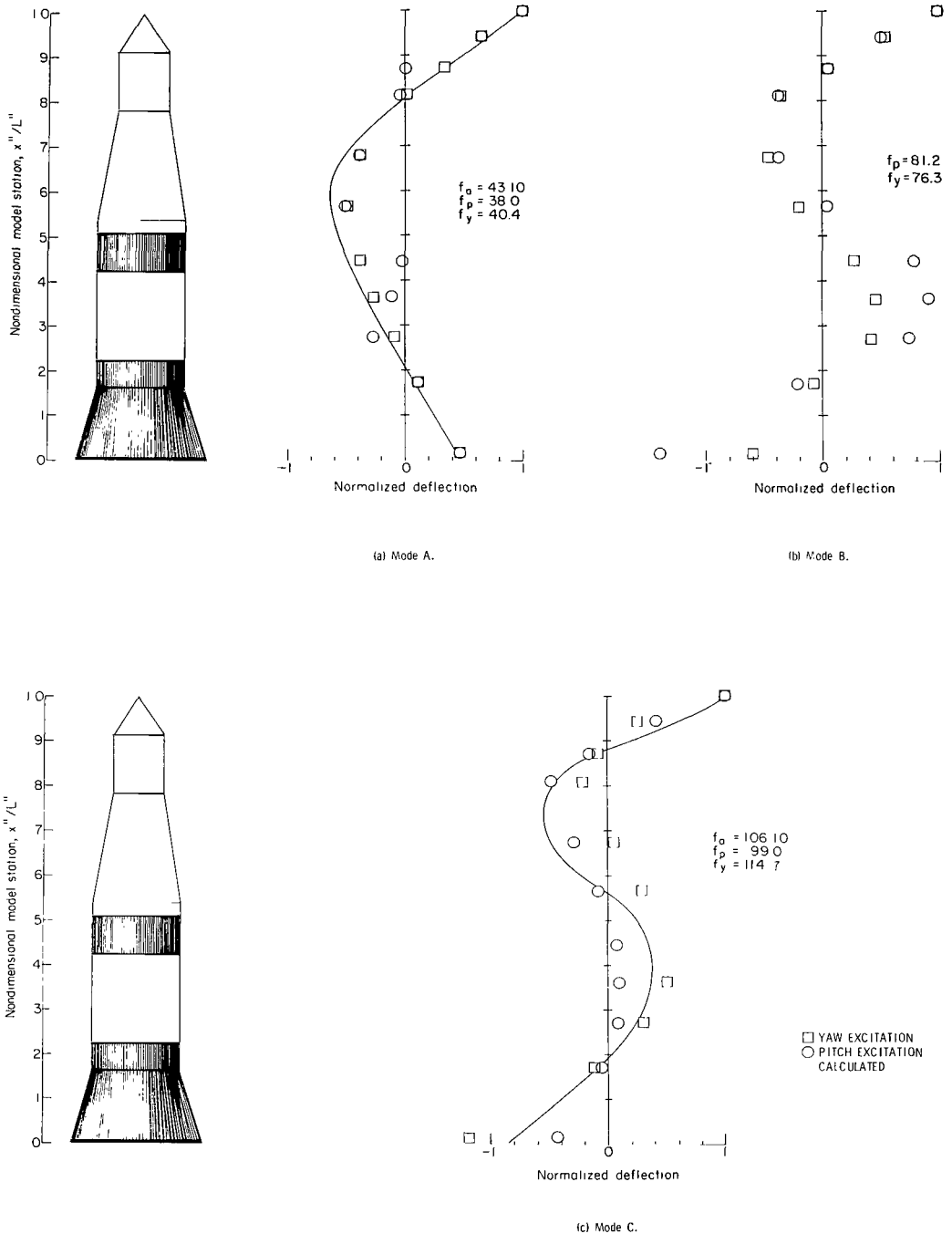

Figure 22.- Measured and calculated deflection shapes for configuration III with 100 percent propellant.

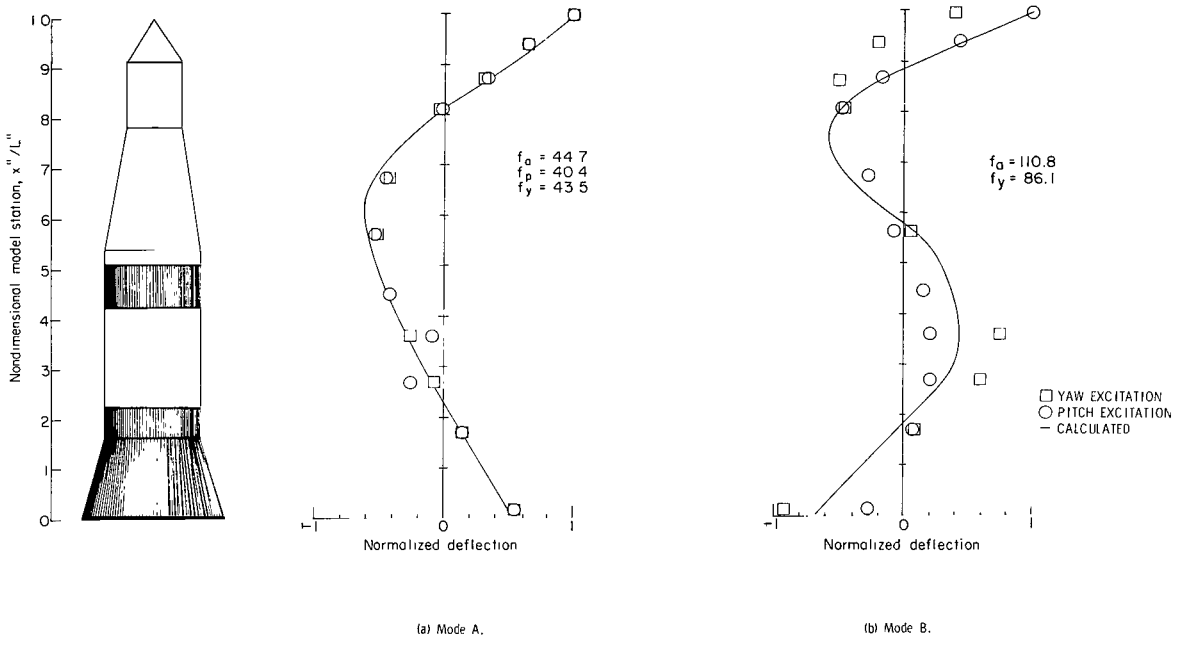

Figure 23.- Measured and calculated deflection shapes for configuration III with 50 percent propellant.

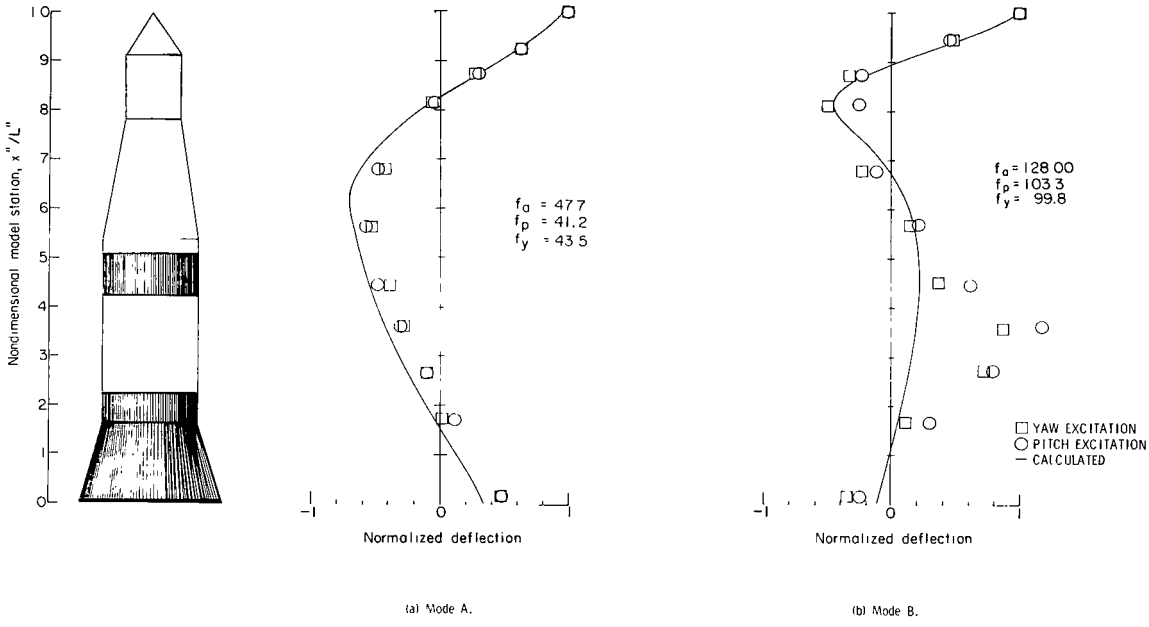

Figure 24.- Measured and calculated deflection shapes for configuration III with 0 percent propellant.

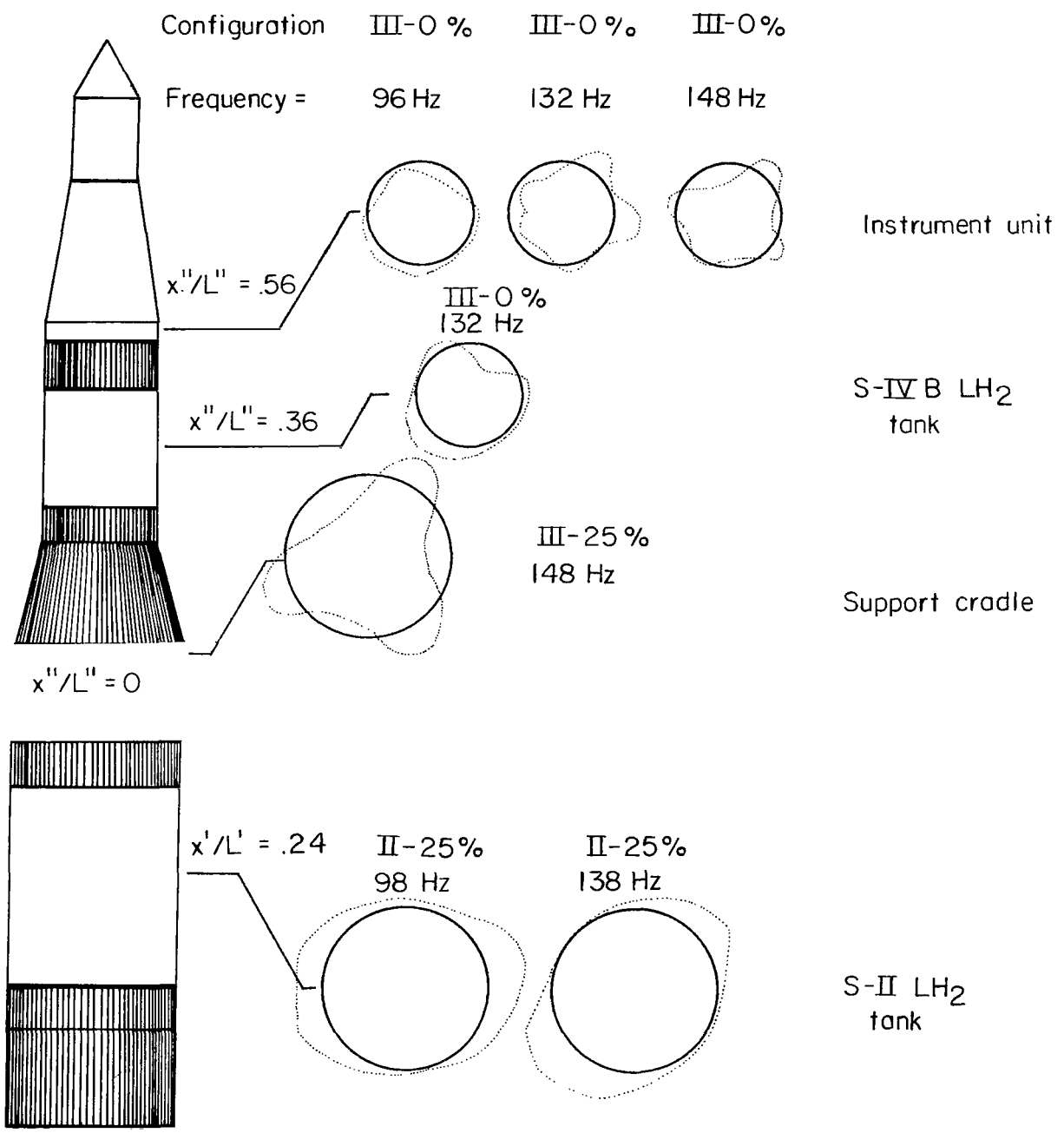

Figure 25.- Typical measured shell deformations.

NASA-Langley, 1970 —— 32 L-6736

"The aeronautical and space activities of the United States shall be conducted so as to contribute . . . to the expansion of human knowledge of phenomena in the atmosphere and space. The Administration shall provide for the widest practicable and appropriate dissemination of information concerning its activities and the results thereof."

—NATIONAL AERONAUTICS AND SPACE ACT OF 1958

NASA SCIENTIFIC AND TECHNICAL PUBLICATIONS

TECHNICAL REPORTS: Scientific and technical information considered important, complete, and a lasting contribution to existing knowledge.

TECHNICAL NOTES: Information less broad in scope but nevertheless of importance as a contribution to existing knowledge.

TECHNICAL MEMORANDUMS: Information receiving limited distribution because of preliminary data, security classification, or other reasons.

CONTRACTOR REPORTS: Scientific and technical information generated under a NASA contract or grant and considered an important contribution to existing knowledge.

TECHNICAL TRANSLATIONS: Information published in a foreign language considered to merit NASA distribution in English.

SPECIAL PUBLICATIONS: Information derived from or of value to NASA activities. Publications include conference proceedings, monographs, data compilations, handbooks, sourcebooks, and special bibliographies.

TECHNOLOGY UTILIZATION PUBLICATIONS: Information on technology used by NASA that may be of particular interest in commercial and other non-aerospace applications. Publications include Tech Briefs, Technology Utilization Reports and Notes, and Technology Surveys.

Details on the availability of these publications may be obtained from:

SCIENTIFIC AND TECHNICAL INFORMATION DIVISION

NATIONAL AERONAUTICS AND SPACE ADMINISTRATION

Washington, D.C. 20546